T.C.
ANTALYA BILIM UNIVERSITY INSTITUTE OF POSTGRADUATE EDUCATION

GRADUATE SCHOOL OF ELECTRICAL AND COMPUTER ENGINEERING

MASTER THESIS

INVESTIGATING THE USE OF IMPEDANCE PLETHYSMOGRAPHY FOR DETECTING DECREASED BLOOD FLOW IN DIABETIC PATIENT LIMBS

Mirza Taimoor Sultan BAIG

JANUAR 2023
ANTALYA

T.C.
ANTALYA BILIM UNIVERSITY
INSTITUTE OF POSTGRADUATE EDUCATION

GRADUATE SCHOOL OF ELECTRICAL AND COMPUTER ENGINEERING

MASTER THESIS

INVESTIGATING THE USE OF IMPEDANCE PLETHYSMOGRAPHY FOR DETECTING DECREASED BLOOD FLOW IN DIABETIC PATIENT LIMBS

Mirza Taimoor Sultan BAIG

JANUARY 2023
ANTALYA

T.C.
ANTALYA BILIM UNIVERSITY
INSTITUTE OF POSTGRADUATE EDUCATION

INVESTIGATING THE USE OF IMPEDANCE PLETHYSMOGRAPHY FOR DETECTING DECREASED BLOOD FLOW IN DIABETIC PATIENT LIMBS

Mirza Taimoor Sultan BAIG

Mirza Taimoor Sultan BAIG, an M.Sc. student of Antalya Bılım University, Institute of Post Graduate Education, Electrical and Computer Engineering owning student ID 2031227, successfully defended the thesis/dissertation entitled "Investigatingthe use of Impedance Plethysmography for Detecting Decrease Blood Flow in Diabetics Patient Limbs", which he prepared after fulfilling the requirements specified in the associated legislations, before the jury whose signatures are below.

Doç. Dr. Mustafa İlker Beyaz (Supervisor) [ ]

Dr. Öğr. Üy. Yusuf Öztürk [ ]

Dr. Öğr. Üy. Deniz Kaya [ ]

Director of The Institute
Dr. İbrahim Sani MERT [ ]

Thesis Submission Date: 13/02/2023

DEDICATION

Master Thesis of this study named “Investigating the use of Impedance Plethysmography for Detecting Decrease Blood Flow in Diabetic Patient Limbs” which I presented, I declare that scientific moral principles were followed in the preparation of this study, in case of benefiting from the works of others, reference is made following scientific norms, no falsification has been made in the data used, and that any part of this s study is not presented as another academic study.

13/02/2023
Mirza Taimoor Sultan BAIG

TABLE OF CONTENTS

ABSTRACT

INVESTIGATING THE USE OF IMPEDANCE PLETHYSMOGRAPHY FOR DETECTING DECREASED BLOOD FLOW IN DIABETICS PATIENT LIMBS

Mirza Taimoor Sultan BAIG

MSc Thesis in Electrical and Computer Engineering

Supervisor: Assoc. Prof. Dr. Mustafa Ilker BEYAZ

December 2022; 73 Pages

The amount of blood flow into a body tissue is very critical and can be evaluated by monitoring the distention of the blood vessel (artery) feeding that tissue. Several techniques for artery distention monitoring have been reported in the literature. In this study, the impedance plethysmography (IPG) technique has been used as a non-invasive method with multiple electrodes to find the impedance across a finger, and therefore, monitor the existence of blood flow. Simulations have been performed on COMSOL finite element analysis software, and experiments have been carried out to obtain the optimum parameters forthis technique. The simulations use 4 electrodes in different positions with a current of 10mA applied throughout a variety of frequencies up to 100 GHz. The resultant data clearly show the advantage of using multiple electrodes to enhance the total information received from the signals, while also indicating that 100Hz can be the optimum frequency for applying IPG. This study demonstrates that IPG with multiple electrodes can be applied to detect the existence of blood flow into body limbs, which is vitally crucial specifically for diabetic patients.

KEYWORDS: Impedance Plethysmography (IPG), COMSOL Multiphysics 5.6,noninvasive, Electrode, Forefinger

COMMITTEE: Doç. Dr. Mustafa İlker Beyaz (Supervisor)
Dr. Öğr. Üy. Yusuf Öztürk
Dr. Öğr. Üy. Deniz Kaya

ÖZET

DIYABETIK HASTA EKSTREMITELERINDE AZALMIŞ KAN AKIŞINI SAPTAMAK IÇIN EMPEDANS PLETISMOGRAFISININ KULLANIMININ ARAŞTIRILMASI

Mirza Taimoor Sultan BAIG

Elektrik ve Bilgisayar Mühendisliği Yüksek Lisans Tezi

Danışman: Assoc. Prof. Dr. Mustafa Ilker BEYAZ

Aralık 2022; 73 Sayfa

Bir vücut dokusuna akan kan miktarı çok önemlidir ve bu dokuyu besleyen kan damarının (arter) şişmesi izlenerek değerlendirilebilir. Literatürde arter distansiyonu izleme için çeşitli teknikler bildirilmiştir. Bu çalışmada empedans pletismografi (IPG) tekniği, bir parmak boyunca empedansı bulmak ve dolayısıyla kan akışının varlığını izlemek için çoklu elektrotlarla invazif olmayan bir yöntem olarak kullanılmıştır. COMSOL sonlu elemanlar analiz yazılımı üzerinde simülasyonlar yapılmış ve bu teknik için optimum parametrelerin elde edilmesi için deneyler yapılmıştır. Simülasyonlar, 100 GHz'e kadar çeşitli frekanslarda uygulanan 10mA akım ile farklı konumlarda 4 elektrot kullanır. Ortaya çıkan veriler, sinyallerden alınan toplam bilgiyi geliştirmek için birden fazla elektrot kullanmanın avantajını açıkça gösterirken, aynı zamanda IPG'yi uygulamak için en uygun frekansın 100 Hz olabileceğini de gösteriyor. Bu çalışma, çoklu elektrotlu IPG'nin, özellikle diyabetik hastalar için hayati önem taşıyan vücut uzuvlarına kan akışının varlığını tespit etmek için uygulanabileceğini göstermektedir.

ANAHTAR KELİMELER: Empedans Pletismografisi (IPG), COMSOL Multifizik 5.6, noninvaziv, Elektrot, İşaret parmağı

JÜRİ: Doç. Dr. Mustafa İlker Beyaz (Supervisor)
Dr. Öğr. Üy. Yusuf Öztürk

Dr. Öğr. Üy. Deniz Kaya

ABBREVIATIONS

DM	: Diabetes mellitus
T2DM	: Type 2 Diabetes mellitus
IFG	: Impaired fasting glycaemia
MEMS	: Micro-electromechanical systems
IGT	: Impaired glucose tolerance
ECG	: Electrocardiogram
AGE	: Aorta abdomen's aneurysm
LDs	: Laser diodes
PDs	: Photodiodes
MSK	: Musculoskeletal
DKA	: Diabetic ketoacidosis
BMI	: Body Mass Index
PTT	: Pulse transit time
PAT	: Pulse arrival time
CW	: Flexible continuous wave
IPG	: Impedance plethysmography
DBP	: Diastolic blood pressure
SBP	: Systolic blood pressure
DBUD	: Double-beam Doppler ultrasound

PPG : Photoplethysmography
PPTT : Peripheral pulse transit time
NCBP : Non-invasive continuous blood pressure
PD : Peak delay
HR : Heart rate
RMSE : Root mean squared relative error
AF : Atrial fibrillation
R-PTT : Reflective pulse-transition time.
rPPG : Remote photoplethysmography
HRV : Heart rate variability
BIA : Bioelectrical impedance analysis
EIS : Electrical impedance spectroscopy
ICG : Impedance cardiography
PWV : Pulse Wave Velocity
EIT : Electrical impedance tomography
FSR : Force sensing resistor
REB : Radial electrical bioimpedance
SBP : Systolic blood pressure
DBP : Diastolic blood pressure
PWV : Pulse wave velocity
EIS : Electrical impedance spectroscopy
CI : Cardiac Index
SV : Stroke Volume stroke volume
ABI : Ankle-brachial index

PAD : Peripheral arterial disease

CT : Crest time

CW : Crest width

ABF : Alternating blood flow

MEIP : Multiple Electrode Impedance Plethysmography

LIST OF FIGURES

LIST OF TABLES

PREFACE

First of All, thanks to Allah Almighty who gave me the strength and resources to complete my master's thesis in a better manner.

To my supervisor – Assoc. Prof. Dr. Mustafa Ilker BEYAZ – I cannot thank you enough for your ongoing mentorship, support, insightful comments, and advice over the past few months. Without your support, the research, learning, and effort that went into this thesis would not have been possible. I appreciate that you shared your knowledge with me and assisting me in realizing my full potential, exploring new opportunities, and overcoming obstacles.

Mom, Dad, and my family since I can remember, you have been a loving family that has motivated me to pursue my goals regardless of what they are. You gave me the resources I needed to achieve my goals. I appreciate you always being there for me and supporting me as I put my effort to complete my thesis.

1. INTRODUCTION

In the world of fast-moving technology, everything around us is changing dramatically. This leads to variations in the number of reactions emitted by the human body as well. One of the prominent changes we see is the change in diets. This includes high amounts of sugar intake and glucose content in many food products which is becoming a prime issue of diabetes. We are tryingour best to find the blood flow of the upper limb by the proposed MEIP (Multiple Electrode Impedance Plethysmography) technique, which we will discuss below.

1.1 What Causes Diabetes?

When the pancreas does not create enough insulin, a hormone that controls blood sugar, or when the body can not properly utilize the insulin that is produced, a dangerous, chronic illnessis developed called diabetes. Uncontrolled diabetes frequently causes raised blood glucose levels,which can eventually cause major harm to the heart, blood vessels, eyes, kidneys, nerves, and other parts of the human body (World Health Organization, 2016). The types of diabetes are as follows.

1.1.1 Type 1: (Childhood-onset Diabetes)

Type 1 diabetes has no specific recognized cause. However, in this type, the body doesn't produce sufficient insulin. Type 1 patients require daily insulin to control their blood sugar levels. In order to maintain the glucose level of the body, insulin is provided on a daily basis according to the body's requirements (World Health Organization, 2016). The symptoms to catch if someoneis going through this stage are.

- Excessive urination
- Urging for food
- Loss of inches from the body
- Loss of overall weight and fat
- Sight issues
- Getting exhausted quickly

Type 1 does not show any specific or identified cause. Since these are commonly found in kids and teenagers of a specific age it is also called child-onset diabetes. After much scientific research have seen that it is coming from complexities between inherited genes issues and environmental variables (World Health Organization, 2016).

1.1.2 Type 2: (Adult-onset Diabetes)

Type 2 is categorized under that type when insulin is not utilized by the body correctly. This is a common and major type found in people suffering worldwide. If compare this with type 1 then the symptoms are less obvious and not prominent to consider. Due to this unidentification of the type 2 causes, it is highly possible for these people to stay undiagnosed. Later, when the body is damaged at the vessel level, the signs start to appear. Type 2 diabetes used to mainly affect adults, but it has now also started to affect children as well. Impaired glucose tolerance (IGT) and impaired fasting

glycaemia (IFG) are intermediary states which can convert from normal blood glucose levels to diabetes (particularly type 2). The risk of heart attacks and strokes is higher in people with IGT or IFG (World Health Organization, 2016).

One of the most frequently discussed criteria is the presence of carried forward genes as well as the metabolic rates of the human body. According to scientific researchers, if one has old age, high body fat percentage, and a sedentary lifestyle, it is for sure he/she will get type 2 diabetes. This also can be further elaborated that poor eating habits, having no mobility, or physical activeness can cause this type inside the human body. Also, continuous consumption of alcohol and indulging in smoking make type 2 symptoms arise in the body. Furthermore, it is also mentioned that gestational diabetes, family background, and ethnicity have now become various factors of diabetes. The biggest and the most common factor is said to be excess body fat which is a byproduct of various unhealthy lifestyle food products and less physical fitness. A high number of percentages of the burden of diabetes globally is thought to be caused by overweight and obesity as well as physical inactivity. Consequently, this causes a lot of fat stored on the waist and hence increases the volume of the stomach side. This also deals with body mass index (BMI), cumulatively increasing type 2. Comparison of European ancestry with communities in South-East Asia, for instance, acquire diabetes at a lower BMI level. Excessive consumption of saturated fatty acids, high total fat intake, and insufficient consumption of dietary fiber are some dietary habits that are connected to unhealthy body weight and/or risk of type 2 diabetes. The chance of being overweight or obese, especially among youngsters is caused due to consumption of sweetened drinks and high-fat dairy drinks since they contain a lot of artificial sweeteners which fascinate young taste buds. The importance of checking on our diet and what consume in our early teenage years is highly a reason for our adult lifestyle. Poor fetal development, low birth weight (especially when it is quickly followed by postnatal catch-up growth), and high birth weight are factors that seem to raise risk (World Health Organization, 2016).

1.1.3 Pregnancy Diabetes

This type of diabetes is arising during pregnancy which has room to develop type 2 diabetes in the future. Unlike type 1 diabetes, the conditions and symptoms are evident when there is an increase in the levels of glucose which is beyond the average level, but lower than the indicated diabetes. Pregnancy and delivery difficulties for both the mother and the baby are more likely in people with gestational diabetes. Prenatal screening rather than the symptoms described are how gestational diabetes is identified (World Health Organization, 2016).

Risk factors and risk indicators for GDM include age-related overweight or obesity, excessive prenatal weight gain, a family history of diabetes, prior GDM pregnancies, a history of stillbirth or giving birth to a child with a congenital abnormality, and an excess of glucose in urine during pregnancy. GDM and pregnancy related diabetes raises the likelihood of childhood obesity and type 2 diabetes (World Health Organization, 2016)

1.2 How Diabetes Affects Your Body?

Diabetes can cause problems that increase the danger to one's health and life when it is not properly controlled. Acute complications have a significant role in mortality, expenditures, and poor quality of life. Extremely high blood sugar levels that result in situations like diabetic ketoacidosis (DKA) in persons with types 1 and 2 and hyperosmolar coma in those with type 2 can be deadly. All varieties of diabetes can be ultra-controlled and then it can produce abnormal low blood glucose levels, which can cause blockage of thinking capability or unconsciousness. This could be a reason due to skipping proper meals and giving in the body more than required mobility. It could also be because of taking too much dosage of anti-diabetic medicines including metformin which is a commonly taken and suggested dose (World Health Organization, 2016).

The damage caused by diabetes starts from weakening blood vessels. These vessels take in and take out blood from/ through the heart. Diabetes leads to a high percentage of mutilating of cardiovascular muscles. As the damage increases without the body taking any action against it and produces a sudden heart stroke Furthermore, it could be paired with nerve damage (neuropathy) in the feet, such damage can limit blood flow, increasing the risk of foot ulcers, infections, and the eventual requirement for limb cut-off. It can significantly contribute to blindness, and diabetic retinopathy results from cumulative long-term damage to the retina's tiny blood vessels. Last, it could lead to kidney failure. Pregnant women with uncontrolled diabetes run a significant risk of fetal loss, congenital defects, stillbirth, perinatal death, obstetric difficulties, and maternal morbidity and mortality, which can have severe effects on both mother and child. During pregnancy, labor, and the first few weeks following delivery, gestational diabetes raises the risk of various negative consequences for the mother and children. The percentage of obstructed pregnancies, maternal fatalities, or perinatal deaths that can be directly linked to hyperglycemia is unknown (World Health Organization, 2016).

In many countries with diabetes, the combination of rising diabetes prevalence and extended life expectancies may be modifying the range of morbidities that accompany diabetes. Being malignant is also one of the high-rate diseases that can be produced through diabetes. In addition to these physical and cognitive handicap characteristics are developed if being diabetic. This diversity of problems and the lengthening of the time individuals live with diabetes points to the necessity of improving the monitoring of the quality of life of people with diabetes and determining how therapies affect the quality of life. According to research, there are more than 400 million people suffering from diabetes (World Health Organization, 2016).

1.3 Difficulties With The Body Limbs' Blood Supply

1.3.1 Lower Limb

- Amputation - The part of the body extending from the gluteal region to the foot is said to be the lower limb also referred to as the legs. It is also referred to as both the human legs. Foot ulcers in diabetes are mentioned as complicated, prolonged, and difficult care since it is also implied that it gets created through

anxiety, and eventually amputation is required. This means removing that particular part of the limb which is diseased. Extreme amputations happen to serious foot ulcer patients. These patients are seriously medically challenged. It has been shown that physical amputation is much worse than psychological amputation. The consequences of extreme amputations destroy the quality of life and could lead to serious mental illness. Cutting off or removing a limb is a serious patient handicap challenge bringing the patient into a psychological disorder. Even before the amputation, the patient needs to go through certain mental challenges and make the patient ready for limb removal. Studies and research have shown that amputations or predisposing of the limb have given anxiety and depression to patients. Moreover, it is said that although sadness and anxiety are high in the first two years following amputation, they then appear to return to normal levels for the general population.

- Recovery - Imagine cutting off a limb from the body, this is consciously a very strong decision made by the patients or their immediate family members. This leaves the patient in sadness, low self-esteem, social isolation, and greater dependency on other humans. The prevalence of phantom and stump pain perceived social support, prosthesis adaption, amputation type, self-esteem, and body image concerns are among the elements documented to have a substantial impact on quality of life and psychosocial functionality throughout the postamputation period.

It has been observed that post-amputation patients are taken through a series of tests, medications, sessions, and therapies to cope with the mental stillness and adaptation of what has happened. Various coping mechanisms and strategies are applied to get quick results. According to the study, emotion-focused, and passive tactics aren't that helpful whereas problem-focused tactics and active mechanisms have led to better and quicker results. In order to give the best results to patients, therapists, and tactic managers need to really focus on what makes the person's thoughts negative and how they can get controlled by it. This will lead to proper rehabilitation procedures. The presumption at the start was that factors affecting the quality of life would include the amount and kind of prosthesis, any extra medical conditions, the presence of stump and phantom pain, and any more medical conditions. Then it was predicted that parameters related to the quality of life would include depression and anxiety scores, body image, self-esteem, coping mechanisms, perceived social support, post-prosthetic activity limitation, and prosthesis satisfaction. All these parameters were checked and then given a final hypothesis that these really affect the quality of life. The quality of life of people having lower extremity amputations is a result of diabetic foot ulcers because they are a homogeneous group with similar characteristics and a lower quality of life than in the general population due to the nature of the disease (World Health Organization, 2016).

1.3.2 Upper Limb

- Complications- Many well-known and well-understood complications of diabetes are said to be presently checked for at routine checkups, following be different types.

a) Diabetic retinopathy
b) Diabetic nephropathy
c) Diabetic polyneuropathy

However, the kind of upper limb diabetes such as Diabetes Mellitus (DM) is still not taken as a condition that could be examined like the ones above. This is also linked to an increased prevalence of a number of musculoskeletal (MSK) conditions, including shoulder, hand, and lower extremity diseases which are not presently examined for. Although the pathophysiological mechanism behind MSK diseases is not completely understood. The points of evidence to a critical role for advanced glycation end-products (AGEs) buildup. In chronic hyperglycemia, this process is accelerated or sped up, resulting in the formation of AGEs from the non-enzymatic condensation of metabolic intermediates and glucose. Tendons, joint capsules, ligaments, and nerves are all harmed by AGE buildup in connective tissue, which distorts their structural and functional compliance. Damage to the periarticular connective tissue results from AGE production, which causes collagen distribution (World Health Organization, 2016), (Alabdali et al., 2021).

According to several findings conducted worldwide skeletal or say MSK abnormalities are more common in T2DM (type 2 diabetes mellitus). To mention this as a proof of example, individuals with DM have a 5% to 30% incidence of frozen shoulder, while those without DM have a 2% to 5% predominance. The considerable fluctuation in noted prevalence in DM patients may be due to different research methods. Furthermore, people with T2DM have a greater risk of having MSK problems than those without the condition, and age appears to be related to this risk: people with DM who are older than 60 have a larger odd ratio than people without DM who are older than 60 (World Health Organization, 2016)

1.4 Importance of Blood Flow Management

Lack of controlling blood pressure is sometimes also referred to as a silent killer. The reason is that it doesn't show prominent or frequently occurring symptoms inside our body. The high level of blood pressure inside the body is hypertension. (The Importance of Monitoring Your Blood Pressure Readings at Home - Sun Sentinel, n.d.) Unrestrained or unchecked high blood pressure can cause organ damage in a span of time and increase the risk of the following.

- Heart attacks
- Heart strokes
- Angina (Chest pains)
- Dizziness
- Headaches
- Other serious illness

Experts advise those who are at risk of developing high blood pressure or who already have it to monitor it at home because blood pressure fluctuates continuously depending upon eat, think, and do daily activities (The Importance of Monitoring Your Blood Pressure Readings at Home - Sun Sentinel, n.d.). A stroke, coronary heart

disease, congestive heart failure, diabetes, chronic renal disease, or hypertension affects about 60% of adults (Why You Need to Check Your Blood Pressure Regularly - TODAY, n.d.).

1.5 Modern Methods of Measuring Blood Flow

There are many modern and convenient gadgets that measure the blood flow, pressure, and heart activity. Some of them are enlisted below, and later discussed in detail with corresponding images to have a better understanding.

- Ultracompact Wearable Blood Flow Sensor
- Sphygmomanometer
- Digital Sphygmomanometer
- PPG Wristwatch
- Pulse oximeter
- Electrocardiogram (ECG)
- Holter Monitor

1.5.1 Ultracompact wearable blood flow sensor

This system is made up of an app specifically designed for smartphones and a sensor gadget. In the sensor device, there are two parts: a core unit and a sensor head. Figure 1 shows the illustrations. Sensor heads are equipped with two light-sensitive components: laser diodes and photodiodes. When the laser emits infrared light, the photo diode picks up any light that is reflected (Kuwabara et al., 2015).

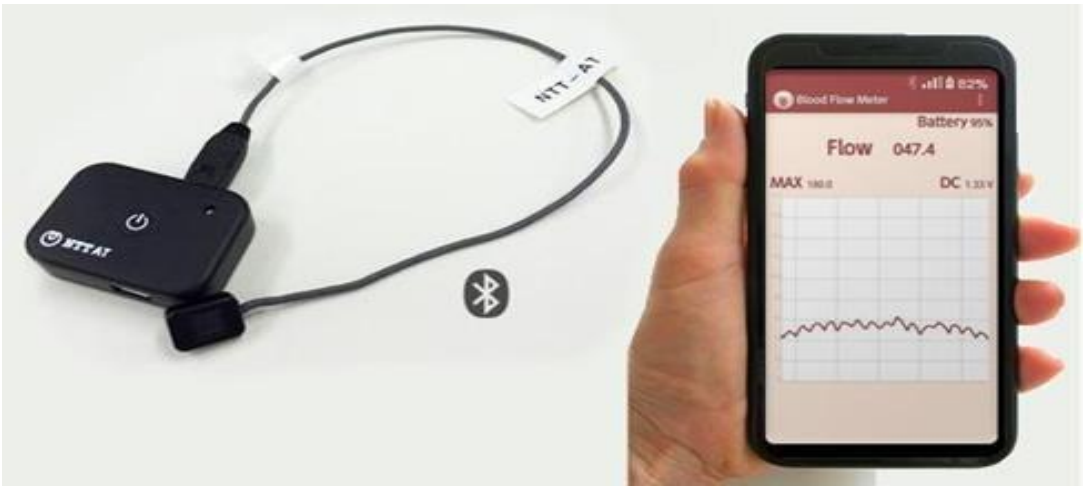

Figure 1. Ultrasound transducer
Source: (Wearable Compact Blood Flow Sensor _ MEMS_Microfabricated Products _ NTT-AT Advanced Technology Product Introduction Site, n.d.)

The skin is exposed to infrared light from the laser, and the photo diode picks up any light that is reflected. By examining the frequency spectrum of the detected signal, it is possible to learn information about the flow of blood. Light that strikes and is scattered by red blood cells moving within blood capillaries causes a frequency

shift that is proportional to the velocity of the flowing red blood cells. With this data, the smartphone offers visualizations like a graph of the volume of blood flow or animations of the heartbeat. (Kuwabara et al., 2015).

1.5.2 Sphygmomanometer

Sphygmomanometers sometimes called blood pressure cuffs. It is used to measure blood pressure. The pressure meter's scale ranges from 0 to 300 mmHg. The pressure meter contains a valve for releasing the air and a rubber pump for pumping air into the cuff. Cuffs are used to stop blood flow in arteries by wrapping them around the upper arm and inflating them. The doctor uses a stethoscope to listen to the blood rushing through the artery as the cuff gradually deflates. A connected gauge to the cuff records these pumping noises. The doctor will note the systolic pressure (when the heart is pumping condition) and diastolic pressures (when the heart is at rest condition) as the first and final pumping sounds, respectively (Blood Pressure Check_ MedlinePlus Medical Encyclopedia Image, n.d.). It shows in the illustration on right in Figure 2.

Figure 2. Sphygmomanometer
Source: (Aneroid Vérnyomásmérő És Sztetoszkópkészlet Egészségügyi Kézi Otthoni Vérnyomásmérő Széria Mandzsetta És Sztetoszkóp _ Wish, n.d.)

1.5.3 Digital Sphygmomanometer

A partially and/or completely automated digital blood pressure monitor is straightforward, used to measure blood pressure. It is portable, easy to use, and rapidly and accurately detects blood pressure and pulse. Each brand in the market features various designs but every device has the same battery-powered digital blood pressure

monitor including a casing with an on/off switch, a start button, and in some models, a pre-set switch and memory button. According to the oscillatory device's working theory, as blood passes through an artery between the systolic (When the heart is pumping condition) and diastolic (When the heart is at rest condition) pressures, it causes vibrations in the arterial wall that may be seen and translated into electrical signals. A screen on the device will show the pulse, systolic blood pressure, and diastolic blood pressure. As seen in Figure 3, the machine's arm cuff has an air tube and air jack to connect it to the machine ((13) A Study on Sphygmomanometers _ LinkedIn, n.d.).

Figure 3. Digital Sphygmomanometer
Source: (Buy Saint Health Arm Automatic Blood Pressure Monitor BP Sphygmomanometer Pressure Meter Tonometer for Measuring Arterial Pressure at Affordable Prices — Free Shipping,Real Reviews Wi, n.d.)

1.5.4 Wristwatch

Wristwatch is a wearable technology easily available for daily convenience. It can be worn on the wrist. It is a continuous, non-invasive method for precisely calculating blood pressure using a photo plethysmography (PPG) technique. PPG measures the volumetric pulsations of blood in tissue; these pulsations are connected to the pulse of arterial pressure. Figure 4 displays the device outlook and how the chip installed inside works. PPG signals may be combined with other functionalities, such as electrocardiograms, to fetch the characteristics for blood pressure measurements, such as pulse wave velocity, pulse transit time (PTT), and pulse arrival time (PAT) (Hosanee et al., 2020).

Figure 4. Wristwatch
Source: (Reader, 2022)

1.5.5 Pulse Oximeter

Oxygen is necessary for the survival of every system and organ in the body. Without O_2, cells start to malfunction and finally diminish. In usual circumstances, cell death will cause organ death, which can produce severe symptoms. By filtering it through the lungs, the body delivers oxygen to the organs. Hemoglobin proteins of the red blood cells allow the lungs to release oxygeninto the circulation of the body's blood, the rest of the body takes in the oxygen from these proteins. Oxygen saturation, which is measured by pulse oximetry, is the proportion of oxygen in hemoglobin proteins. The level of oxygen saturation often reflects how much oxygen is reaching the organs. Measured from a pulse oximeter, it radiates light through a section of skin that is comparatively transparent, meanwhile, the detector receives the light through the skin. One side of a pulse oximeter clip, for instance, beams light while the other detects it when it is attached to a finger. A pulse oximeter estimates the precise amount by using complicated calculations and other information (New Research Backs Use of Pulse Oximeters for Assessing Blood Pressure - UBC Faculty of Medicine, n.d.; Sjoding et al., 2020).

Oximeters are tiny, non-invasive gadgets that may connect to a finger or toe. The instrument monitors the blood's oxygen content or oxygen saturation level. It can tell how well the heart is supplying blood to the hands and feet. By passing a cold light through the finger, thegadget operates. After that, the proportion of oxygen in the blood is calculated by reading the light passing through the finger. Figure 5 illustrates on the right a normal and commonly available oximeter. Between 95 to 100% O_2, saturation is considered normal, if its lower than 90% oxygen saturation values then it is said to be called a clinical emergency (Sjoding et al., 2020).

Figure 5. Pulse Oximeter
Source: (SPO2 Finger Pulse Oximeter Fom a Reputed Online Medical Supply Store _HealthConnection, n.d.)

The foundation of pulse oximetry is the idea that red, and near-infrared (IR) light are differentially absorbed by O_2Hb and HHb. Since red and near-IR light enter tissues well whereas water and non-vascular tissues absorb a substantial amount of blue, green, and far-IR light, it is fortunate that O_2Hb and HHb exhibit significant variances in absorption at these two wavelengths. O_2Hb scatters more red light than HHb, therefore it absorbs less red light and more IR light than HHb, which is compatible with the observation that well-oxygenated blood appears brilliant red to the eye due to its higher concentrations of O_2Hb. While HHb appears less red due to its greater ability to absorb red light. Pulse oximeters use a pair of tiny light-emitting diodes in one arm of the finger probe to emit two wavelengths of light, red at 660 nm and near-IR at 940 nm, to measure O_2Hb and HHb levels in the blood. The light that passes through the finger is subsequently picked up by a photodiode on the probe's opposite arm; hence, the pulse oximeter uses the ratio of red and IR light absorption to calculate the quantity of Hb that is oxygen-bound (Chan et al., 2013)

1.5.6 Electrocardiogram (ECG)

At an early age of minor cardiovascular issues and signs of initial heart malfunction, an electrocardiogram or ECG or EKG is a simple, fast, and common test used to diagnose and catch an overview of the problem. It is a safe procedure that captures the electrical activity of the heart, providing information that clinicians may utilize to identify, diagnose, and assess current or historical issues (Conditions We Help With - Modern Heart and Vascular, n.d.; Electrocardiogram - Modern Heart and Vascular, n.d.).

ECG device gathers information on electrical cardiac signals. It comprises electrodes which are said to be sticky patches with wires attached. The electrodes are subsequently affixed to the patient's limbs and chest skin by the physician. Only the body's normal electrical impulses are captured by EKGs. There is no danger of shock or

electrocution because they do not create electrical impulses. Typically, the procedure takes ten minutes. Figure 6 depicts an example of how this may be set up.

Figure 6: Electrocardiogram ECG
Source: (USA Medical and Surgical Supplies, 2018)

It has 12-lead ten electrodes are positioned on the patient's limbs and on the surface of the chest. After that, 12 distinct angles (or "leads") are used to assess the overall magnitude of the heart's electrical potential, which is then recorded over time (usually ten seconds). Thus, at each instant of the cardiac cycle, the total amplitude and direction of the heart's electrical depolarization are recorded.(Atkielski, 2007; Conditions We Help With - Modern Heart and Vascular, n.d.; Electrocardiogram - Modern Heart and Vascular, n.d.)

1.5.7 Holter Meter

Holter monitors use a few electrodes affixed to the chest to capture electrical cardiac signals. To reduce traces of muscular activity, electrodes are implanted over the bones. For the most part, Holter monitors use between three and eight electrodes, however, the number and placement vary according on the device. These electrodes are linked to a small piece of apparatus that is hung around the patient's neck or attached to their belt and records the electrical activity of their hearts throughout the recording session (Holter Monitor - Wikipedia, n.d.). A Holter blood pressure device is worn by the patient for twenty-four hours. During these hours, the device measures and records the blood flow and pressure of the impulse. The patient’s activities are monitored within the premises of the clinic or hospital. If the increase in blood pressure readings is to rule out or confirm the diagnosis of hypertension and to assess the effectiveness of previously identified hypertension's treatment, an inquiry is required (Holter Monitoring of Blood Pressure _ Medicum, n.d.).

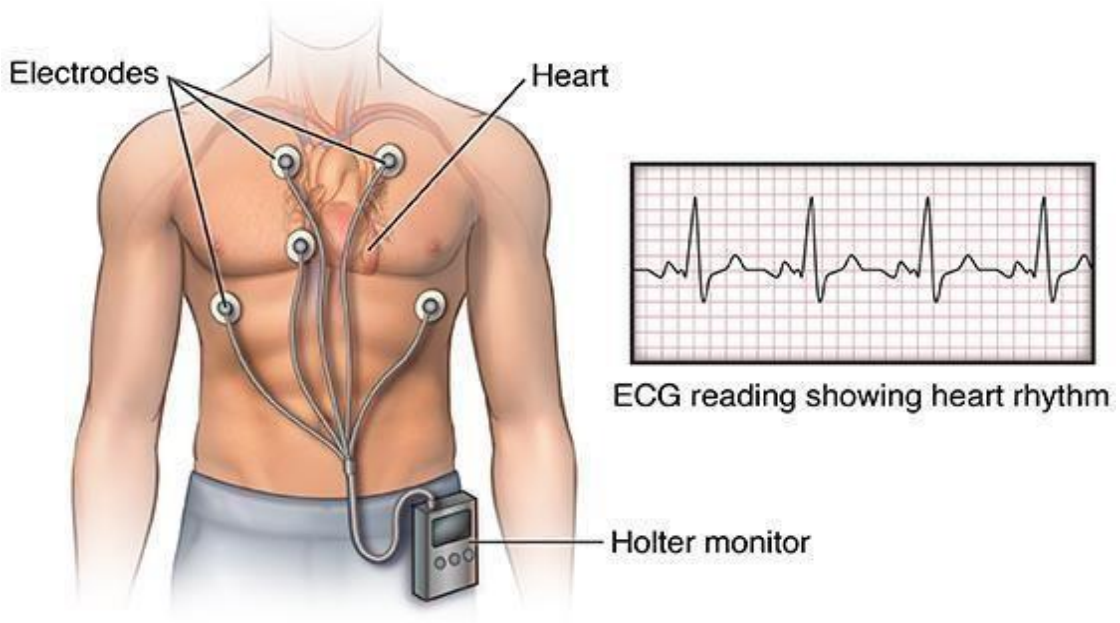

Figure 7. Holter Meter
Source: (Johns Hopkins Medicine, 2019)

As shown in Figure 7, a recorder is placed to the hip level and a blood pressure cuff is affixed to the upper arm during the study. Blood pressure is typically recorded by the recorder every 30 minutes during the day and every 2 hours at night. The inquiry is generally highly received. Patients with especially high blood pressure readings may experience an uncomfortable pressure feeling because of automatic cuff inflation. It is not advised to move your arm significantly when it is wearing a cuff, go to sleep, or become wet (take a bath or shower, etc.) (Holter Monitoring of Blood Pressure _ Medicum, n.d.)

1.6 Motivation (Moving Towards Self-Monitoring)

The main motivation behind our proposed technique is the reason that not everyone can afford the highly expensive Blood flow monitoring devices. Monitoring must be done precisely which increases the price of such devices. Globally, underprivileged communities do not have the significant resources to afford these devices, thus they must travel all the way to hospitals in the cities and get their medication and monitoring done. Beyond the scope of existing approaches, MEIP (Multiple Electrode Impedance Plethysmography) can offer additional information on the overall health of a vast volume of tissues and blood circulation. Additionally, the proposed method has been shown to be helpful in academic and clinical practice.

A device of this nature ought to, in theory, be easy to use, secure for patients, and maybe portable for usage in areas with limited resources. The employment of an impedance plethysmography device, which has the ability to satisfy the requirements once again, is a novel approach in this thesis. This makes it possible to employ this approach at home or at any other remote location without access to many instruments. The outcomes of the experimental study emphasize a portable, non-invasive, useful, and

potentially affordable tool and point the way ahead for distinguishing alterations in arterial and venous circulation through waveform analysis. This project's major goal is to employ impedance plethysmography waveforms to spot tissue with reduced blood flow brought on by circulatory obstructions along the limbs. For this, changes in the blood circulation via a vast volume of tissue are identified using the basal impedance signal. To capture the waveforms within the common impedance range of the finger, a bioelectrical impedance device must be designed and put into use. It is possible to use the device securely and easily at home or in low-resource settings to continually monitor blood changes (Ansari, 2013).

Some of the many techniques that work parallel with impedance as blood flow monitoring have been discussed and listed below. After that a summary table (Table 1) (Ansari, 2013) of different techniques advantages and disadvantages are grouped, visibly, researchers can see that impedance stands out, and stay above among other techniques.

1.7 Emerging Techniques in Monitoring Blood Flow

1.7.1 Photoplethysmography

While discussing this technique above in the different devices section, the author Mejía-Mejía mentioned that it is a continuous, non-invasive method of estimating blood pressure that may be included in wearable technology and has been presented as photoplethysmography (PPG). PPG measures the volumetric pulsations of blood in tissue, which are linked to the pulse of arterial pressure. PPG signals may be combined with other modalities, such as electrocardiograms, to produce characteristics for blood pressure measurements, such as pulse wave velocity, pulse transit time (PTT), and pulse arrival time (PAT). This work, however, focuses on single-source PPG measurements from various anatomical regions due to its higher application in wearable technologies (Hosanee et al., 2020; Mejía-Mejía et al., 2021).

As per the concept of using the Peáz principle for the volume-clamped method to equalize artery and external cuff pressure, this is done for estimating the blood pressure. The amplitude of the PPG signal, which measures blood volume, is usually compared to a set-point constant while the cuff pressure is continually changed so that the PPG amplitude is equal to the set point. This enables the finger cuff, whose pressure is assumed to be equal to the systolic BP, to maintain the blood volume in the finger (SBP). This method, although still needs a cuff, could not be compatible with wearable technologies (Hosanee et al., 2020).

Figure 8 displays several non-invasive methods for determining BP together with the sites examined in prominent research done between January 2010 and January 2019. Various PPG waveform characteristics from a single PPG measurement have been used in studies between 2010 and 2019 to enhance BP estimates. The amplitude, frequency, slope, area under the curve, significant locations along the PPG curve, and derivatives of the PPG waveform are some of the often-retrieved PPG curve properties. The precision or closer to accurate responses of PPG's blood pressure readings is essential for its usage in clinical practice to diagnose hypertension. Particularly in underdeveloped

nations with more restricted access to medical interventions, this device that uses PPG for blood pressure measurement might be a useful medical tool (Hosanee et al., 2020; Mejía-Mejía et al., 2021).

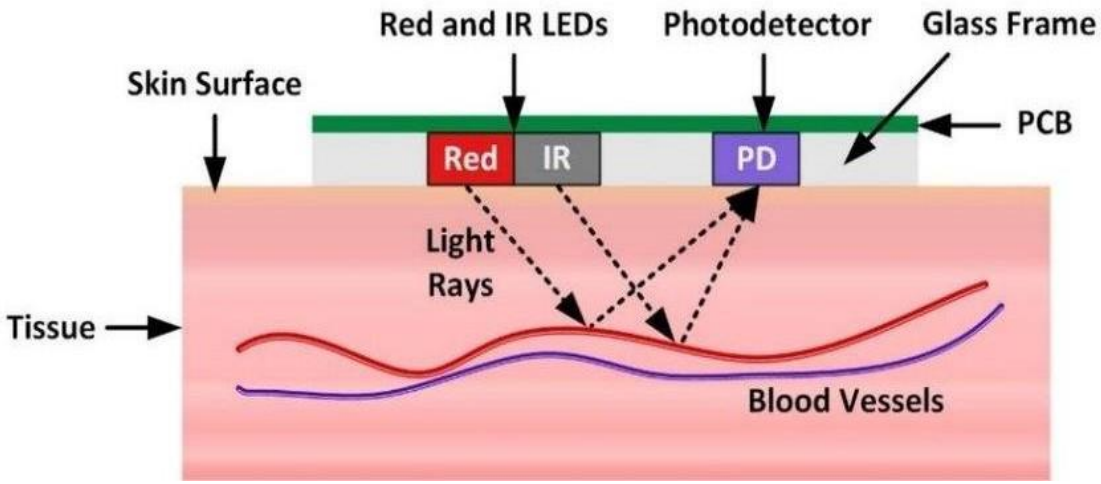

Figure 8. Photoplethysmography Technique
Source: (Kumar et al., 2020)

Due to its low cost and non-intrusiveness, the photoplethysmography (PPG) signal is often employed in clinical and consumer devices. It has traditionally been used largely to check patients' resting heart rates and assess blood oxygen saturation. Today, PPG signal processing is a significant and expanding area of study. The design of signal processing algorithms is complicated by this environment in a number of ways, not the least of which is how to handle motion artefacts. Additionally, the PPG signal carries important data on the respiratory, autonomic, and cardiovascular systems that are not frequently or easily detected in the human body. Together, these elements present a chance to use the PPG to discreetly disseminate thorough medical information in daily life. To advance in this field of technology, one must become proficient in creating various algorithms (Hosanee et al., 2020; M.Sc. Cheriyedath, 2019).

1.7.2 Doppler Ultrasound

Changes in blood flow over time and space reveal much about a person's cardiovascular status. Due to the irregular heartbeat, the blood flow in the arteries is pulsatile and slows down near the walls of the vessel than in the middle of the vessel. Hemodynamics occurring in different types of blood vessels are affected, among other things, by vessel compliance and size. Flow measurements can reveal thrombi, arterial stenoses, stiffness, occlusions, and other disorders (F. Wang et al., 2021).

Some vascular disorders may benefit from long-term continuous blood flow velocity monitoring for diagnosis and prognosis. For example, an ischemic stroke occurs when a carotid artery narrows and a blood clot develops, blocking a blood vessel leading to the brain. A blood clot can block the carotid artery (thrombosis) or break and travel into the vessel. Although carotid endarterectomy is an accepted and reliable

procedure for preventing stroke due to carotid artery stenosis, acute thrombosis can occur at the endarterectomy and pinch sites within 72 hours, it can lead to increased post-stroke and postoperative morbidity and mortality (F. Wang et al., 2021).

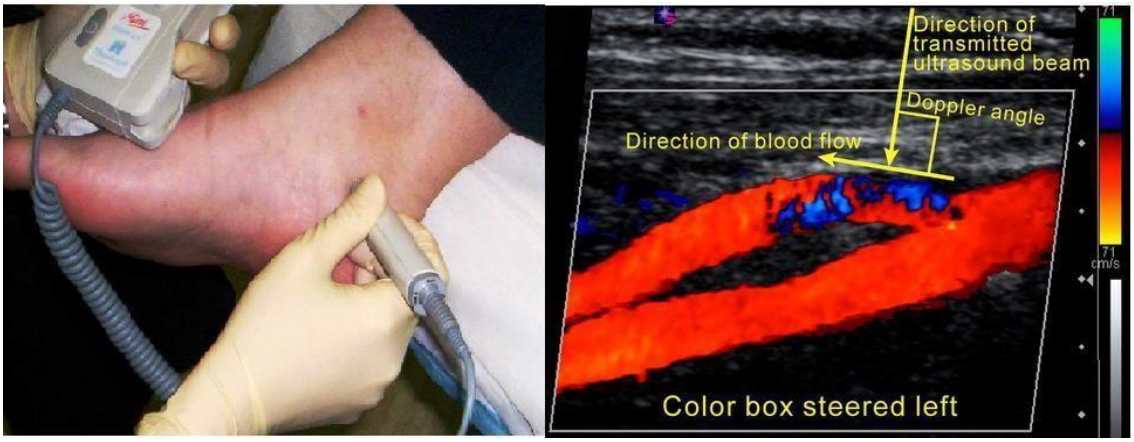

Figure 9. (Left) Operation of Doppler Ultrasound, (Right)Result of Doppler Ultrasound
Source: (Doppler Ultrasound _ The Fresh Foot Centre, n.d.), (Tahmasebpour et al., 2005)

Postoperative intimal hyperplasia or progression of underlying atherosclerosis can lead to restenosis even within a year. Rapid identification of the problem and immediate treatment is critical. However, patients are often examined only after the recurrence of ischemic symptoms, requiring urgent reoperation. In addition to angioplasty, stenting, and reimplantation surgery, postoperative thrombosis can also occur after other revascularization treatments. Standard evaluation after reimplantation surgery is an hourly physical examination for capillary filling and skin tone to prevent thrombosis at the vascular anastomosis site. Post-discharge testing is seldom or never performed, as patients are only able to undergo a limited number of tests during hospitalization and miss the opportunity to preserve tissue/grafts. The image in Figure 9 shows that. Ultrasound has a greater capacity to penetrate than light and heat, and when used at an acceptable intensity, it has no harmful effects on people. The only approach that can transmit fast changes in cardiovascular parameters, including the absolute mean and peak blood flow velocity, back in real-time is the ultrasonography doppler technique. Furthermore, measuring velocity changes is more sensitive than measuring flow to small-vessel lumen decreases. It has been demonstrated that soft, wearable flexible electronic devices can continuallymonitor a variety of vital indicators (F. Wang et al., 2021).

To minimize potential patient harm, a study by Wang uses flexible electronics and the effective properties of the ultrasound method. Here, describes a flexible continuous wave (CW) Doppler ultrasound system for non-averaged real-time continuous monitoring of absolute blood flow velocity. An oblique ultrasound beam is emitted obliquely to the surface of the skin by a piezoelectric transducer to create the Doppler effect. The flexible and thin shape of the device ensures flexible light contact

with the curved surface of the skin. The construction of the array and the use of the double-beam Doppler ultrasound (DBUD) method avoids the influence of the doppler angle on velocity measurements, allowing the determination of absolute velocity and eliminating the need for calibration. The device's extraordinary ability to track blood flow velocity is first demonstrated using an ultrasound phantom and later in a human artery (F. Wang et al., 2021).

1.7.3 Impedance Plethysmography

A method that can measure plethysmography and identify the arterial pulse waveform is called bioelectrical impedance. As seen in Figure 10, this technique is collectively known as bioelectrical impedance plethysmography, often known as IPG or just impedance plethysmography. By infusing a minute amount of AC into the body and then detecting the potential caused by blood flow, it gauges changes in blood volume. This method has the benefit of being able to measure a bigger volume of tissue than a single artery or superficial body portion. It only takes two electrodes to drive current, and an additional pair may be used to measure the voltage drop in any area of the body. It is possible to determine the impedance of the body part housed by these electrodes by measuring current and voltage (Bejarano Monroy, 2019; Ansari, 2013).

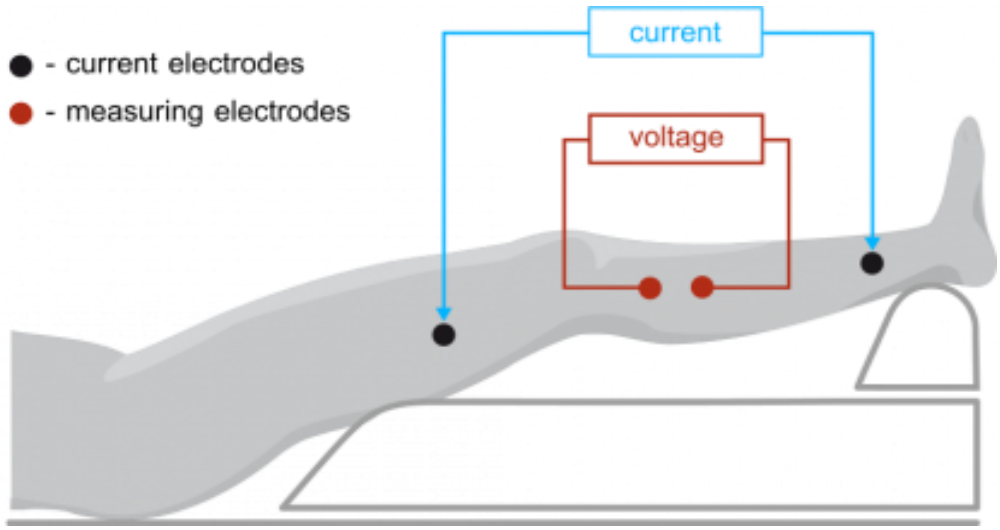

Figure 10. Impedance Plethysmography Technique (IPG)
Source: (Impedance Plethysmography (IPG) - Medis, n.d.)

The information on circulatory issues provided by bioelectrical impedance plethysmography is highly comprehensive and instructive. This technology has led to the development of several techniques for plethysmography, blood flow, and cardiac output estimation. Some of these techniques can involve the examination of the arterial pulse waveform or venous occlusion plethysmography. Below is a quick glance at the advantages and disadvantages table (Table 1) (Ansari, 2013) summarizing which technique leads to more benefits (Bejarano Monroy, 2019; Ansari,2013).

Table 1. Advantages and disadvantages of technologies that can measure blood flow or bloodpressure.

Technique	Measure	Advantage	Disadvantage
Photoplethysmography (PPG)	• Blood Volume • NIRS (Blood Flow estimation)	• Non-Invasive • Easy to use • High accuracy	• Small Volume of tissue measurement • Localized measurement
Doppler Ultrasound	• Instant blood flow estimation • Blood Velocity	•Non-Invasive •Portable •Low energy consumption	• Skilled Operation • Single vessel measurement • Low-depth penetration
Impedance Plethysmography (IPG)	•Blood Volume •Blood Flow Estimation	• Non-Invasive •Portable •Low energy consumption • Easy to Use • Measure a large number of tissues	• Signal close to the noise floor

Source: (Ansari, 2013)

1.8 Contribution and Impedance Plethysmography With Multiple Electrodes

Understanding the value of how impedance works upon impedance plethysmography concepts, we investigated how multiple electrodes can be utilized to result in information-rich signals. We have tried researching the impedance using ECG electrodes to find the variations in artery diameter as a result of pulsatile blood flow. In this report, we looked upon the impedance of the finger. To the best of our knowledge, multiple electrode IPG has not been extensively exploited in the literature so far.

2. LITERATURE REVIEW

2.1 Photoplethysmography

Plethysmography is used to measure blood volume changes in various bodily areas. It may be necessary to undergo an analysis to check for blood clots in the arms and legs. It can also keep track of the penile pulse's intensity (Levy et al., 2018) Photoplethysmography (PPG) is a technique introduced in the 1930s to measure how much light is passing through and reflected by functioning tissue arteries and veins. To determine how much light is absorbed and reflected using the light method, identify how much blood is present. In the research paper of (Lee et al., 2011) about the relations between ac-dc components and optical path length in photoplethysmography, it is mentioned that the PPG signal monitors changes in blood volume rather than blood vessel pressure. In various terms, the PPG signal indicates the blood volume fluctuation in the sensor coverage region. PPG measures changes in blood volume using the photoelectric approach, both transmissive and reflecting. The sensor coverage area includes veins, arteries, and many capillaries. The consequence is that the PPG signal is a complex and unique mixture of blood flow in the veins and arteries of the cardiovascular system. A PPG signal contains both pulsatile and non-pulsatile blood volumes (Elgendi et al., 2019).

2.1.1 Further Research

Different types of biosensors are based on photoplethysmography techniques which are classified in the literature based on their biological content; some are described below.

A novel approach for the parallel collection of projecting photoplethysmography (PPG) signals in a broad spectral range (UV to near-IR) has been devised, and the potential for assessing blood microcirculation at different depths from the skin surface is described. PPG signals were detected concurrently at (CW) Flexible Continuous Wave laser wavelength sets of 405, 532, 645, 807, and 1064 nm. Various signal baseline responses to breath holding have been found, as well as varied forms of PPG pulses originating from the same heartbeat but captured at different wavelengths, showing a deep variation of skin blood pulsation dynamics (Spigulis et al., 2007).

Yibin Li talks about peripheral pulse transit time (PPTT), which is suggested as a method for approximating non-invasive continuous blood pressure (NCBP). Overall, the viscosity of the artery wall and the reflection of the pulse wave significantly influences the blood pressure reading that is obtained. To adjust for these effects, the peak delay (PD) between two separate pulse waves and the heart rate (HR) are used to recompense these influences. It discusses how to estimate NCBP with the assistance of PPTT. According to the findings of an investigation involving 16 participants, the PPTT and SBP/DBP were correlated 0.728/0.520. In addition to this, the standard deviation of the difference between the estimate of the SBP and the DBP and the measurement value of the sphygmomanometer is 6.71/4.54mmHg, which leads to portable and wearable NCBP (Li et al.,2016).

Examine several observations which are acquired using reflection mode PPG that are difficult to explain using the generally accepted concept of PPG signal generation. The physiologic model of light interaction with living tissue recently suggested by group demonstrates that it adequately explains all findings. According to this hypothesis, pulsatile transmural pressure of the arteries compressed or decompresses the density of capillaries in the dermis, changing blood volume in the capillary bed, which regulates the strength of remitted green light (Kamshilin & Margaryants, 2017).

Photoplethysmographic data are useful for examining heart rate variability in real-world applications. Few studies have examined how to correct for the low timing resolving of low- sampling-rate signals for accurate heart rate variability analysis, even though lowering the sampling rate of signals is an important consideration for contemporary wearable devices that enable continuous monitoring around the clock. In this study, Jae contrasted the standard cubic spline interpolation method with the parabola approximation strategy for the period, frequency, and nonlinear domain variables of heart rate variance. For each parameter, the intra-class correlation, measurement error standard deviation, Bland-Altman 95% limits of agreement, and root mean square relative error (RMSE) were presented. Additionally, the time needed to determine each interpolation method was investigated. The findings demonstrated the effectiveness of parabola approximation as an algorithm-based strategy for compensating for the low temporal precision of pulse beat intervals. The method also performed well when compared to the conventional cubic spline interpolation technique. The parabola approximation technique is still an effective interpolation method for analyzing trends in HRV (Heart rate variability) measurements, even though the absolute values of the heart rate variability variables calculated to use a signal sampled at 20 Hz were not exactly matched with those calculated using a reference signal sampled at 250 Hz. (Baek et al., 2017).

Using light-based technology, PPG sensors measure the rate of blood flow as it is affected by the heart's pumping action. In order to forecast human behaviors, the author offers a unique approach for extracting significant elements from PPG data. They take advantage of the fact that PPG signals are susceptible to noise from motion artifacts and extract, rather than discard, motion artifact signals together with cardiac and respiratory signals to forecast the kinds of activities users would engage in. Convolutional and recurrent neural networks are used to predict a variety of commonplace behaviors from raw PPG data. The outcomes show the viability of this technique in predicting five types of activities (standing, walking, jogging, leaping, and sitting), as well as fresh insights into how to employ PPG sensors for human activity detection. The data was generated by the wrist-worn smartwatches of 12 individuals (Boukhechba et al., 2019).

Early detection and confirmation of atrial fibrillation (AF) are critical for avoiding stroke and other serious health implications. The sporadic and asymptomatic character of AF makes diagnosis difficult. Wrist-worn devices that employ photoplethysmography monitoring have lately been presented as a feasible solution due

to their ability to monitor heart rate and rhythm for long periods at low levels. This study describes the current state of the art in AF detection using wrist-worn sensors, explores the technology's potential and current knowledge gaps, and recommends future research routes. The fore leading technologies for AF detection are extremely accurate. Due to a lack of suitable accessible datasets, objective comparison of outcomes and techniques among studies is currently challenging (Eerikäinen et al., 2020).

Designed a model of the photoplethysmography signal obtained from the radial artery at the floating surface of the forearm. The author performed this by using the connection between both the Monte Carlo light transport model and the finite element vessel biomechanics technique. The model has qualities that are similar to those found in PPG signals obtained using a commercial device. They monitor how well the body mass index is affected by the PPG signal. Moreover, an AC-to-DC signal ratio deterioration of the PPG signal of up to 40% was noted (Boonya-ananta etal., 2021).

A study compares PPG-based BP estimation utilizing optical sensors on the finger and wrist. PPGs and reference continuous BP values collected from 22 healthy subjects undergoing two cold pressor tests were used to train and evaluate subject-specific linear regression models with pulse transit time, PPG intensity ratio, and heart rate as features for BP estimation. The mean standard deviation of differences and mean absolute difference between reference and calculated systolic BP values for finger PPG signals were 0.47 ±10.44 mmHg and 7.78 mmHg, respectively, and 1.05±12.86 mmHg and 9.69 mmHg, respectively. With F1 values of 0.81 and 0.76 for finger PPG, and 0.75 and 0.61 for wrist PPG, increases and reductions in systolic BP of at least 10 mmHg were recorded. With finger PPG signals, models performed better (Paliakaite et al., 2021).

WrisTee is a wearable gadget that tracks vital signs on the wrist for remote health monitoring. WrisTee uses three optical sensors and four light sources to measure 12 PPG signals at three different places along the radial artery. PPG signals with opposing polarity were identified and named in-phase and invert-phase signals. Based on the Beer-Lambert law (A= εbc), they gave a unified viewpoint on their differences and demonstrated that both signals may be employed for cardiac monitoring utilizing data from a specific patient. The R-PTT standard deviation utilizing reflective pulse-transition time. They proposed a technique for selecting the optimal wavelength to maximize signal quality while minimizing storage, electrical sources, and computing costs. The author suggested a method for determining a suitable wavelength to obtain the highest signal quality while reducing storage needs, power resources, and computational expenses. They researched 10 volunteers to test the feasibility of the proposed technique. WrisTee can find the best locations and wavelengths for monitoring vital signs, and a convolutional neural network is an excellent choice for phase classification, according to our research. Furthermore, using in-phase and invert-phase PPGs for health monitoring is a novel method for bio-signal medical research (Long & Chung, 2022).

A substantial amount of research on remote vital sign monitoring of the human body has been undertaken in recent years. Remote photoplethysmography (rPPG) is a camera-based, unobtrusive technique that permits continuous monitoring of changes in vital signs and thereby aids in the early and successful diagnosis and treatment of

illnesses. Because of recent breakthroughs in computer vision and its numerous applications, rPPG is in great demand. This study provides an overview of several remote photoplethysmography technologies and analyzes all aspects of heart rate analysis. This study investigates the difficulties of the video-based rPPG approach and expands it to current advances in the literature. They explore the gap in the literature and make recommendations for further research (Premkumar & Hemanth, 2022).

When measuring blood pressure, the distal waveform lags behind the proximal waveform, indicating there is a phase difference between the IPG and PPG. The most common places to collect distal waveforms are on the fingers, chest, legs, and wrists, this also includes PPG techniques where measurement instruments are fastened to these areas of the human body. Wearable sensors can result in a number of issues when used to measure blood pressure while wearing them during sleeping on a regular basis for an extended length of time. On the other hand, PPG might not be appropriate for dementia patients because the devices used may make the patient uncomfortable and prompt them to take them off. Data might become corrupted when it is obtained from cold or warm places that include sunlight. PPG devices require high power to operate, are vulnerable to ambient exposure and movement of body parts. Signal quality varies between skin tone, obesity, and diabetes. However, with IPG technique, it is possible to analyze and evaluate many different tissues in a human body indirectly by measuring their impedance, which offers information about the body's tissue properties. Access to additional physiological metrics like bio-impedance and electrodermal activity is also possible. The main reasons to employ these techniques are their compatibility with compact form factor devices, relative low power requirements, mechanical robustness, and good customer acceptance ratings with ease of access to users. IPG can also increase cleanliness, decreases the likelihood of running out of disposables, and lowers the risk of infection. IPG is much easier to use then compare to PPG and also has more benefits (De Pinho Ferreira et al., 2021; Le et al., 2020; Arai et al., 2021).

2.2 Impedance Plethysmography

The history of impedance plethysmography (IPG) begins in the 1932s when Atzler and Lehmann noted changes in the capacitance between two parallel plates held across the human chest. The heart's activity and these alterations were shown to be synchronized. Jan Nyboer and his colleagues initially presented the method in its current form in 1940. (J. P. Babu et al., 1990). In the IPG procedure, any area of the body's electrical impedance is measured using either the constant current method or the bridge method, and changes in the impedance are noted as a function of time. A body segment's electrical impedance is negatively correlated with the amount of blood present since blood is an excellent electrical conductor. Electrical impedance decreases according to the rise in pulsatile blood volume in the body segment brought on by systemic blood circulation. This provides sufficient information about blood circulation from variations in electrical impedance. The electrical impedance lowers according to the increasing pulsatile blood volume in the body segment brought on by systemic blood circulation. The variation in electrical impedance thus provides sufficient information regarding blood circulation (J. P. Babu et al., 1990).

2.2.1 Further Latest Research

Different types of biosensors are based on impedance plethysmography techniques which are classified in the literature based on their biological content; some are described below.

Calin Corciova et al, published four papers that describe IPG in different ways. The first way was research about developing a prototype for a piece of medical equipment that can determine the rate of blood flow and do various calculations based on the plethysmographic wave at a low cost. On a simple circuit board with connections for electricity and bioimpedance electrodes, they constructed an equilibrated bridge that was built manually. To drive and receive data from the circuit, a programmed function generator and an oscilloscope were both linked to a computer and given the corresponding tasks. The AC (alternate current) that is being supplied has a frequency that ranges from 20 kHz to 250 kHz. It is the patient's skin impedance that will rise at higher frequencies, only a minimal quantity of energy will be provided to them. This will ensure that the system is not compromised in any way. The functionality of the circuit was confirmed by measuring the impedance across a test circuit and comparing the values that were measured to the values that were predicted. This was done at a variety of frequencies. When the program obtains data, it immediately puts that data onto a data sheet so that it may be analyzed (Corciova et al., 2011). Secondly, C. Corciova further explored that the device creates a sinusoidal pulse at an adjustable frequency (between 10 and 200 kHz) and an adjustable intensity. At its output, the gadget transmits an analog signal that is representative of the changing impedance of the portion that is being examined. Both the injection of the sinusoidal pulse and the collection of the bioimpedance signal were carried out with the assistance of disposable electrodes. The introduction of a data collection device manufactured by National Instruments NI USB 6009 makes the process of acquiring the bioimpedance signal on a personal computer much simpler. MATLAB was used for managing the bioimpedance signal processing, as well as the user interface and the display (Corciovă et al., 2011). In the third research, display results and words with an understandable interface C. Corciova's system can obtain real-time monitoring as a result of its combination of the sophisticated analog amplifier and the calculating power of digital signal processing. The bioimpedance measurement device employs the utilization of a generator which is controlled by a microcontroller. LabView was used to control all aspects of the impedance signal processing, including the user interface and the kind of display. This technique makes it possible to tune the output signal flexibly, with the frequency and duty cycle being readily modifiable. Experiments are carried out to discover the optimal interrelationship that should exist between the output characteristics of the current injector, the power supply, and the electrode spacing (C. Corciova, R. Ciorap, 2012). In the fourth research, the goal of the project is to create a medical gadget that detects blood circulation and calculates hemodynamic parameters based on the plethysmographic signal in the peripheral region. A computer is linked to a function generator. This regulates the injecting current and gets information from the circuit. The AC (alternate current) that goes through the subject is limited by a series resistor. The supplied current has a frequency range of 10 kHz to 250 kHz. The skin resistance increases at different frequencies, and only a tiny quantity of energy is transmitted to the patient, assuring the system's reliability. The device was confirmed by evaluating its output current at

various frequencies and comparing measured and predicted impedance values along a test circuit. Data is gathered by the program and inserted into soft modules for analysis (Corciovaet al., 2011).

In the study of Bera, approaches for measuring bioelectrical impedance can be used to characterize biological tissue non-invasively. These tissue parameters' impedance responses change depending on the frequency of the applied signal. In order to better understand the morphology, physiology, and pathophysiology of living tissues, impedance measurement carried out across a broad frequency spectrum gives new information on the tissue interiors. This work further discusses the BIA, EIS, IPG, ICG, and EIT techniques and their applications in a number of industries. It also provides a technical perspective on the various impedance approaches (Bera, 2014).

The ankle-brachial index (ABI) is regarded as the gold standard in the identification of peripheral arterial disease (PAD), and alternative noninvasive approaches have gotten far too little consideration. As a result, the study's goal was to assess the diagnostic performance of impedanceplethysmography in detecting PAD and evaluate it to other approaches. This research included 66individuals with an average age of 76.1 9.6 years who have been tested for different cardiovascular illnesses at Kaunas Clinical Hospital between 2011 and 2012. All of the patients were under observation for PAD. A new generation Niccomo TM gadget was used for impedance plethysmography. The clinical diagnosis of four impedance plethysmography parameters was determined using receiver operating characteristic evaluation: crest time (CT), crest width (CW), pulse amplitude (Pampl), and alternating blood flow (ABF). Impedance plethysmography, particularly it is component CT, is a non-invasive option for the diagnosis of PAD and might be utilized for screening individuals with PAD (Mašanauskiene et al., 2014).

According to the Isabel Morales research, create a multi-dimensional lesion warning device, it is necessary to take into consideration several different elements, including temperature, humidity, the condition of the tissue, pressure, and friction. They are investigating the use of the sensing resistor (FSR) to detect not only plantar pressure but also plantar bioimpedance, thereby reducing the total number of sensors that are required. Due to which FSRs have conductive electrodes that are covered by a polymer film, the contact that is made with the subject may be thought of as a capacitive electrode. To measure the voltage that results from injecting current using two homologous FSR contacts while also detecting the voltage coming from the other two contacts, a specialized impedance plethysmography detection circuit is necessary. For the very first time, four sole pressure sensors are employed not only as pressure sensors but also as bioimpedance electrodes to detect heart activity using ordinary components at frequencies up to 50 kHz (Morales & Gonz, 2015).

The author Hersek presents a reliable vector bioimpedance measurement system of knee joint health in a vertical direction. This system is capable of getting high-resolution static and dynamic bio resistance and bio reactance signals from the knee joint. Within a bandwidth of 0.1 to 20 Hz, the front-end has a space requirement of and power consumption of 0.25 W when it is supplied with ± 5 V. It achieves a dynamic range of 345 Ω and a noise floor of 0.018 mΩ (resistive) and 0.055 mΩ (reactive),

individually. A microcontroller helps with real-time calibration which also makes it possible to store data on a micro secure digital card and reduces the amount of error caused by the environmental variability that can be encountered outside of the laboratory settings. After the signals have been gathered, they go through physiology to create customized algorithms that can extract musculoskeletal and cardiovascular aspects from the knee joint. The researcher worked on the feasibility of the findings by identifying statistically significant variations between the damaged and contralateral static knee impedance values for two patients. They illustrate the sensitivity of the dynamic impedance measurements in a second feasibility study by using a cold-pressor test. This test shows that higher downstream peripheral vascular resistance is related to a 20% drop in pulsatile resistance. The approach presented will serve as the foundation for future initiatives aimed at continuously measuring the state of joint health during typical day-to-day activities (Hersek et al., 2016).

Furthermore research, a straightforward bioimpedance plethysmography technique was used to determine the pulse wave velocity (PWV) of a patient's blood as it retraveled the radial artery located in the wrist to the middle finger. After that, an electrocardiogram was coupled with a bioimpedance technique to determine the PWV using the ECG and the pulse waves applied to the middle finger. According to the findings of the statistical analysis, a momentary hindrance in the flow of blood did not have any effect on the PWV of typically healthy adults. In addition to this, multiple regression analysis was used to formulate an equation for the estimation of two distinct forms of PWV as well as the importance of both types of PWV to other physiological parameters. According to the results of multiple regression analysis, the abdominal circumference and height are both independent predictors of the PWV measured from the radial artery in the wrist to the middle finger (wfPWV) ($r = 0.893$) (Huang et al., 2017).

Huynh and Chung approach worked on a separate system that consists of two devices that are positioned at two distinct locations. This research examined radial electrical bioimpedance (REB) as a possible indication for blood pressure measurement to identify a technique that would be more sensitive to utilize in a device that measures blood pressure. The experiment was carried out on 8 healthy volunteers, each of whom had an ambulatory blood pressure monitor attached to their upper arms for comparison purposes. In the study's findings, the correlation of estimated systolic (SBP) and diastolic (DBP) blood pressure versus the reference was found to be 0.84 ± 0.05 and 0.83 ± 0.05, respectively. These correlations proved the potential of the approach that was developed. REB properly records DBP with a root mean square error of 7.5 ± 1.35mmHg. REB also did a good job of following the DBP (Huynh & Chung, 2017).

Blood flow was performed using a fuzzy logic toolbox with many different activities, including dehydration, exercise, cool skin, warm skin, and breath-holding activity. ECG is performed immediately after measuring blood flow using the impedance plethysmography technique. The correlation coefficient is determined linearly by 18 subjects by comparing the changes in peak amplitude of the plethysmographic waveform of forearm impedance with the changes in stroke volume before and after the 25 seconds of breath-holding activity. Last but not least, the plethysmographic waveform of forearm impedance can be used to analyze the changes

in a heartbeat that are correlated with the changes in heart stroke volume. The process may be observed in its entirety, including its cycle sequence, to determine how well the heart is pumpingblood (Ramkumar & Babu, 2017).

Research tells how it moved ahead in managing current injection and measuring amplification so that the circuit IC AD5933 may achieve its optimum level of performance (Johannes Schneider, Marc Schroth, Maik Holzhey, Blöcher, Timon, 2019). The author claims that by monitoring the impedance of blood vessels at the wrist, impedance plethysmography (IPG) offers a potential low-power alternative for detecting pulse waves and breathing. However, because of the low signal-to-noise ratio (SNR) and unpredictable measurement circumstances, the measuring principle places tremendous requirements on the analog front end. A strategy for using impedance plethysmography is described in this research. The suggested circuit depends on the impedance measurement IC AD5933, as well as adaptive feedback control to regulate current injection and monitoring amplification to find the best operating point. Experiments show that the device has the potential to be a viable solution for continuous vital sign monitoring on the wrist (Johannes Schneider, Marc Schroth, Maik Holzhey, Blöcher, Timon, 2019).

An organized model is now being built on an individual basis to calculate the amount of blood flow by using the impedance plethysmographic method. To verify the accuracy of this measurement, an echocardiogram was performed concurrently with the measurement and used todetermine the stroke volume. The subjects with low pressure, the subjects with high pressure, andthe normal individuals all go through the process of having their data analyzed for validation. With the aid of the IPG device, the greatest peak voltage amplitude is measured, and the blood flow volume is calculated for the computation on a per-minute basis. The difference between theend-diastolic volume and the end-systolic volume is what's used to regulate the stroke volume while at the same time as it's being used to control other aspects of the volume of the stroke (RamKumar & Ganesh Babu, 2019).

It is an ultimate technique selected that makes use of a current with a frequency of 50 kHz that is injected into the thorax of the subject using a couple of textile electrodes, as well as envelope detection of the trans-thoracic voltage that is obtained from a couple of different embedded electrodes. Both the baseband electrocardiogram (ECG) signal and the trans-thoracic impedance signal, which encodes respiratory actions, are included in the signal that is produced as a finding result of this process. By using the appropriate filtering, it is simple to separate the two signals, and then it is possible to get the cardiorespiratory rates It is a completely wearable and wirelessly sensitized belt is presented (Piuzzi et al., 2020).

The purpose of the study is to determine whether or not it is possible to use multi-frequency bioimpedance analysis for measuring hemodynamic properties. To do this, one of its applications, known as electrical impedance spectroscopy (EIS), will be investigated by us to determine how variations in radial artery diameter are caused by blood flow. In continuation of the research that have done in the past, the present study makes use of a commercial instrumentknown as the Quadra® Impedance Spectroscopy device to take impedance readings of the forearms of three different subjects under

normal conditions while simultaneously occluding the artery with a cuff. This was done concurrently with measurements taken using an ultrasound instrument, which served as a reference. After measuring the impedance spectra over some time, waveforms were obtained that reflected changes caused by blood flow. The occluded impedance response was used to take into consideration the contributions from the adipose and muscle domains, which led to arterial resistance. Calculating the diameter of the artery based on its impedance required the use of a modified relationship, which, when compared to ultrasound data, revealed a striking resemblance. The comparison with the ultrasonic measurements showed that there were discrepancies in phase and amplitude. This was mostly due to the approximation of the connection between impedance and diameter as well as the disregarding of the impedance phase analysis. This study demonstrates that EIS has the potential, with further development, to become a method for assessing the blood flow-induced variation in arteries. Additional research and development might be beneficial in bringing this technology into mainstream clinical practice for hemodynamic monitoring (Gautam Anand 1, 2020).

Non-invasive evaluation of endothelial (the main type of cell found in the inside lining of the blood vessel) function is based on peripheral vascular circulation in response to generated reactive hyperemia of the radial artery. This research looks into the usefulness of impedance plethysmography as an alternative to traditional modalities for estimating peripheral vascular flow changes associated with the reactive hyperemia process. The findings show that bio-impedance varies consistently during the reactive hyperemia process at higher measurement frequencies and that these fluctuations are consistent with a typical tissue impedance model. Moreover, estimated bioimpedance characteristics have demonstrated the capacity to differentiate between diabetic and healthy groups, which is beneficial in evaluating endothelial dysfunction (Samarawickrama et al.,2020).

In order to achieve the high-resolution IPG-based carotid pulse detection required for cardiovascular applications, this study proposes an ideal measurement parameter in response to visible carotid artery pulsation. They conducted extensive study to determine the best values for the many factors that influence the IPG measurement resolution. The IPG equipment was set up in a practical situation and fixed on the subject's neck immediately above the carotid artery in order to examine the measurement parameters in this experiment. Using the ideal measurement settings, the test findings within six participants produced an arterial impedance variation of 2137 m. These requirements included a position on the left side of the neck, an excitation frequency of 50 kHz, a smaller area of 2 cm2, and electrode spacings of 4 cm and 1.7 cm for excitation and sensing functions. The significance of this study lies in the discovery of an enhanced carotid pulse sensing method based on IPG that considerably improves the accuracy of readings used in cardiovascular monitoring (T. W. Wang et al., 2021).

According to the Babu, impedance plethysmography, a proposed straightforward method, is used to quantify cardiac output. The main goal of this planned study is to measure cardiac output non-invasively using IPG in a range of healthy male individuals in two distinct age groups and to compare the results with a prior study that used a variety of electrode insertion techniques. In addition, a comparison of the cardiac

parameters between the two age groups that have been described has been listed. The preceding phase of the research was carried out on nine healthy male volunteers who were divided into two age groups: those between the ages of 15 and 24, and those between the ages of 25 and 34. The resulting cardiac output is observed to be 5.07 ± 0.8 & 4.9 ± 0.67, and the resulting Cardiac Index (CI) is observed to be 2.84 ± 0.44 & 2.74 ± 0.35 for the first and second chosen respective classes of age groups. The average value of Stroke Volume (SV) Mean value Standard Deviation is observed to be 52.3 ± 7.8 & 56.6 ± 8.4 (C. G. Babu et al.,2021).

Table 2. Display of the Mean and Related SD Values

Previous Study Data			Proposed Study Data					
Age: 21 to 35 years			Age: 15 to 24 years			Age: 25 to 34 years		
n=38			n=27			n=27		
CO	CI	SV	CO	CI	SV	CO	CI	SV
5.14±0.61	3.05±0.24	65.03±8.46	5.09±0.89	2.89±0.54	52.3±7.8	4.9±0.65	2.67±0.23	56.6±8.4

Source: (C. G. Babu et al., 2021)

The IPG data are also being retrieved, as is the measurement of peak amplitude, which ranges between a mean value of 2.10 ± 0.54 volts and a mean value of 2.50 ± 0.45 volts. volts accordingly for the respective cluster of age groups. It has come to attention that the p-value in each of these instances is lower than 0.004 and that the correlation coefficient between IPG and SV data is roughly in the region of 0.35. With the help of the available selected data, it has been deduced that the correlation of cardiac output through the stroke volume is estimated by the IPG waveform and that this estimation provides an adequate correlated value after being tested on a variety of male subjects while they were in a healthy condition (C. G. Babu et al., 2021).

According to Isabel Morales research, the foot impedance plethysmography was carried out with two distinct kinds of electrodes, namely dry and capacitive, in addition to sole force sensors. A tetrapolar configuration has been employed for impedance plethysmography with threedistinct plantar settings. The Figure below shows the details of the setting. These plantar setups include four skin contact electrodes, four capacitive contact electrodes, and two force-sensing resistors (FSRs). Because the top substrate of FSRs comprises interdigitating conductive electrodes as well as a semiconductive polymer, this study has taken into consideration the possibility that FSRs may be used as capacitive electrodes. All of the measurements were taken using an excitation current of 1 milliampere (mA)/10kHz and they attempted to find impedance plethysmography signals by placing them beneath the feet of a person who was standing. Contact electrodes can provide a reliable cardiac pulse signal, in contrast to capacitive contact via the socks, which is subject to interference from the mains. Because of the force-sensing resistors' force-dependent resistance, which was coupled in parallel with the capacitive coupling, the heart pulse could not be detected by them. However, these findings provided that higher frequencies and bigger sensor areas are used to assist in the detection of changed skin states in diabetic foot patients (Morales, González-Landaeta,

et al., 2021).

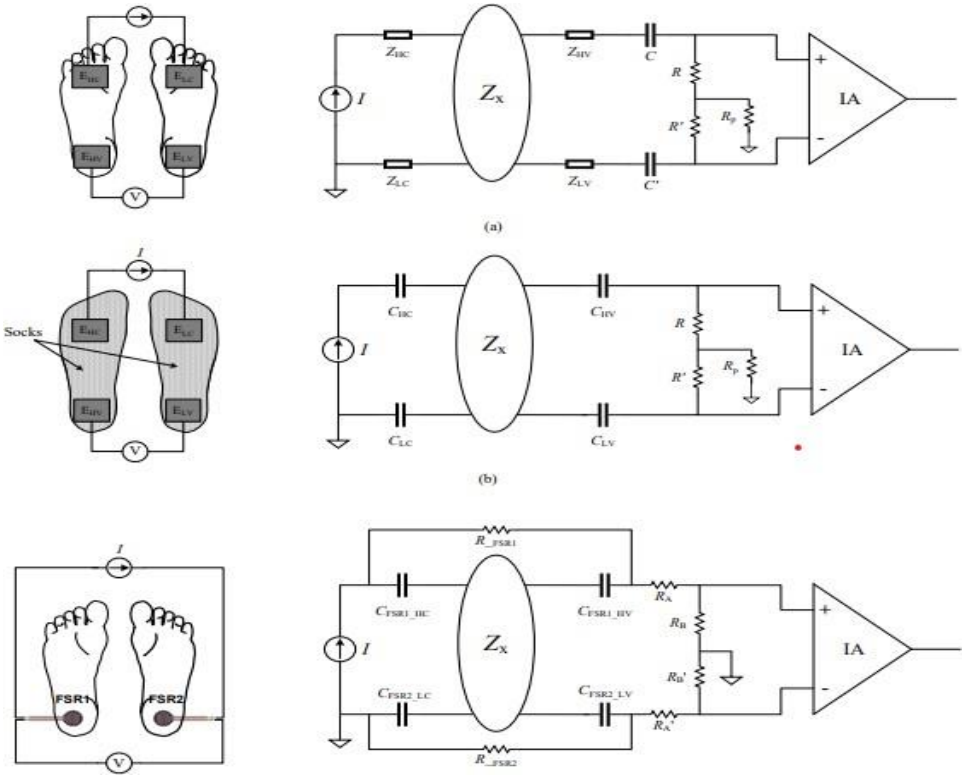

Figure 11. Plantar tetrapolar setups and their corresponding circuits. a) electrodes for contactwith skin b) capacitive electrodes across socks c) FSR skin contact sensors
Source: (Morales, González-Landaeta, et al., 2021)

Diabetes and Foot Ulcers are dangerous complications of Diabetic Foot. Temperature, pressure, humidity, and friction are typically considered when developing amultidimensional ulcer opening warning device. To identify plantar pressure as well as plantar bioimpedance, they use basic adjustable Force Sensing Resistors FSR 402. This FSR consists of conductive electrodes coated by polymer films, the interface with the subject can be thought of as a capacitive electrode. It is necessary to use a special bioimpedance detection circuit to inject current through two homologous FSR 402 interactions and measure the resulting voltage throughthe other two available contacts. This circuit can detect cardiac activity from the bottom of the foot. Pressure sensors are being used as bioimpedance electrodes for the very first time (Morales, Gonzalez-Landaeta, et al., 2021).

In the literature there are many articles on various elements of blood pressure and flow, after the use of Fourier analysis in the study of hemodynamics. Additionally, there are several significant articles on impedance and its clinical use in the investigation of the circulation. The most novel aspect of our study as compared to the state of the art where the electrodes are placed on the same positions often the wrist, legs, or chest with frequencies as low as 10 kHz, we apply multiple electrodes to the

index finger at varied positions with 100 Hz frequency. With our proposed technique we can record the finger's blood flow in both active and passive states, while it is moving or at rest. When the blood is not circulating (due to some reason like heart issue, artery blockage, and diabetes etc.) in the artery, the proposed scheme can give us a signal that the blood is not circulating.

In our proposed design, the area through which we measure the blood flow is entirely different which is the forefinger area, in order to make the device easily wearable and portable. More specifically, different authors use thorax surface (Piuzzi et al., 2020), neck (Corciova et al., 2011; T. W. Wang et al., 2021), lower limb (Morales, Gonzalez-Landaeta, et al., 2021; Mašanauskiene et al., 2014; Morales & Gonz, 2015), knee (Hersek et al., 2016) and upper limb (Corciovă et al., 2011; Bera, 2014; Huang et al., 2017; Huynh & Chung, 2017; Ramkumar & Babu, 2017; Ram Kumar & Ganesh Babu, 2019; Gautam Anand 1, 2020; Samarawickrama et al., 2020; C. G. Babu et al., 2021) for measuring the blood flow. Furthermore, they measure the impedance through either one pair of electrodes or two pair of electrodes. However, we utilize multiple pair of electrodes while changing their positions. This has been discussed in detailed in the methodology section.

3. IMPLEMENTATION MEIP

In the chapter of implementation, the framework of the implementation of MEIP is discussed which we have performed by constructing a 2D model of a finger encompassed by silver electrodes in COMSOL MULTIPHYSICS 5.6 simulation environment to measure the impedance at different positions ofthe finger. The study was performed under normal resting conditions where an experimental procedure was set up to measure the impedance response from the finger. Electrocardiograph (ECG) electrodes are utilized in the proposed design for measuring the impedance in response to provided current.

3.1 ECG Electrodes

An electrocardiogram is one of the simplest and quickest ways to evaluate the heart (ECG). Electrodes are microscopic plastic patches that stick to the skin and are placed in specific spots on the arms, legs, and chest. The electrodes are connected to the ECG gadget using lead wires. The electrical activity of the heart is then captured, examined, and printed. Electrical energy is not sent to the body ("Electrocardiogram | Johns Hopkins Medicine," 2021). In order to maintain the blood flowing the way it should, natural electrical impulses coordinate the contractions of the various heart muscle groups. An ECG records these electrical impulses to give details about the heart's rhythm, pace, and strength and timing of the electrical impulses as they travel through the various heart chambers. Any number of heart-related disorders can show changes on an ECG ("Electrocardiogram | Johns Hopkins Medicine," 2021).

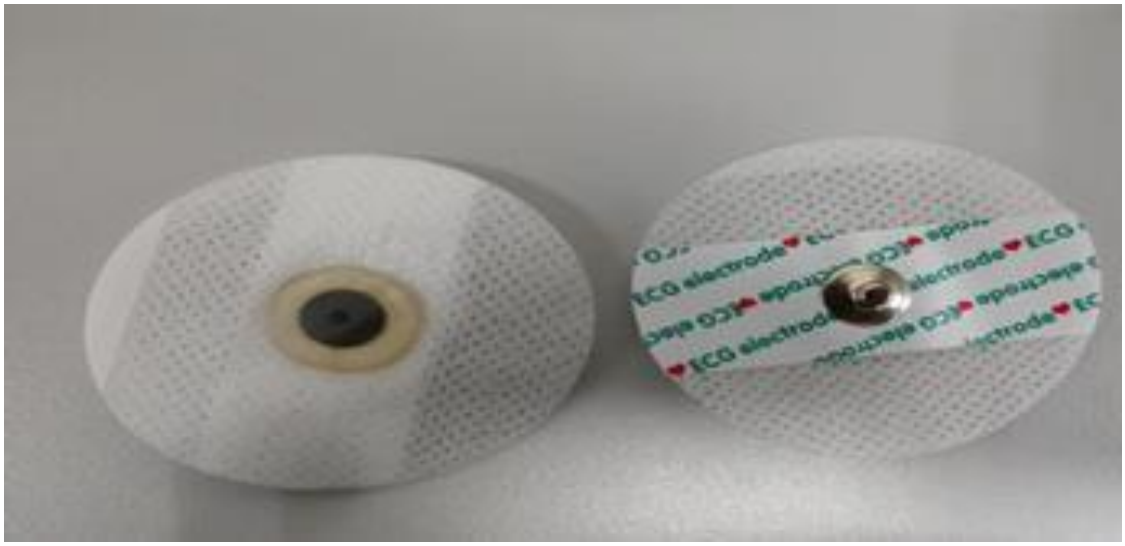

Figure 12: ECG Electrodes

3.2 COMSOL Simulations

The simulation platform COMSOL was created with practical applications in mind. The goal of simulations is to accurately reproduce phenomena seen. whether they are used in a scientific or technical context. Multiphysics, which is a collection of scientific models that take your interests into account, is necessary to do this. Acoustics, electromagnetics, chemical reactions, mechanics, fluid flow, and heat transfer are a few of them. Since each of these effects exists in the real world, the simulation environment must too. This is what COMSOL tries to do and accomplish it in a user-friendly interface intended to boost scientists' and engineers' efficiency in their everyday work (A. Griesmer, 2013).

Sometimes it is more instructive to see what real-world employees of firms have accomplished than to examine hypothetical simulation instances. This may be especially relevantto people working in the power sector since mistakes in design and other errors can have a negative influence on both customer satisfaction and the bottom line (F. Griesmer, 2019). Engineers are creating better things more quickly and for less money. Researchers are looking at recent findings. Innovative medical therapies are being investigated by doctors. There are several ways that educators are interacting with students and the list goes on (F. Griesmer, 2019). One ofthe primary reasons to choose COMSOL is because it has so many complex modules. A few of them are as follows (Shrivastava, 2019) Battery Design Module.

- Chemical Reaction Engineering
- Composite Materials
- Material Library
- MEMS
- Liquid & Gas Properties Module
- Heat Transfer Module
- AC/DC Module

3.3 Structure of COMSOL Multiphysics

The COMSOL Desktop® user interface of the COMSOL Multiphysics® program offers a modeling environment for developing, testing, and displaying Multiphysics models and applications. There are several tools, menus, and windows included in this, including the Model Builder window and nodes, the ribbon, the Settings window, the Information window, the Graphics window, and other elements.

3.3.1 Model Structure

The Model Builder window, which functions as a model tree with all the actions and features for creating and solving models and showing the results, is used to control the modelingprocess. By including a branch, like the geometry branch, these are added to your modeling process. Additional nodes (or subbranches) that are connected to a branch's parent node can exist; everything depends on the order of the operations. The Settings window and characteristics of a node are unique to that node. Aside from containing settings and properties, branches and subbranches can also do so. For

illustrations, look at Branches and Subbranches in the Tree Structure and Settings and Properties Windows for Feature Nodes. The Model Builder offers a wide variety of nodes that may be used to construct models and examine their structural details. There are several types of nodes, including the Component node, which is categorized according to spatial dimension. Due to their dynamic nature, nodes can be easily identified as their status changes. For further information, see at the Model Builder's Component Nodes by Space Dimension, Physics Interface Default Nodes, and Dynamic Nodes (Model & Dialog, n.d.).

3.3.2 Graphics Window

Different toolbar buttons are accessible on the Graphics window depending on the Component's space dimension. The buttons are based on the Component space dimension and correspond to the nodes that show up beneath the physics interface (The Graphics Window, n.d.). These nodes are domain, boundary, edge, and point-level nodes.

3.3.3 Setting Window

Except for a few container nodes like Definitions and Datasets, clicking any node in the Model Builder opens a corresponding Settings window with the same name on all platforms. The Options box provides choices for establishing node-specific actions and properties. If, alter the settings for the physics interfaces and features, it must recompute the solution to consider the changes. This is because when an action or property is changed in the Settings window, its impact on the model is displayed in the Graphics window either instantly or by selecting the corresponding button, which is available in several of the Settings window toolbars. Use the drop-down choices on the Settings window and in the relevant toolbars to select the model's components to specify in a certain way (Settings and Properties Windows for Feature Nodes, n.d.).

3.4 Multiple-Electrode Impedance Plethysmography (MEIP)

In our proposed technique MEIP, we utilize COMSOL to visualize the structure of a human finger strapped with four individual electrodes, from which three electrodes are assumed to be current input sources, and the fourth electrode is taken as ground connection. The complete simulation of MEIP is operated under the frequency domain. To measure the impedance of the finger through electrodes, we assume the parameters of the finger and electrodes with the materials that constitute them while also considering their graphical dimensions. Each of these values, parameters, geometrical dimensions, and material constitution are discussed below.

3.5 Simulation

3.5.1 Parameters

Specific features of modeled objects are described via parameters. In the MEIP simulation, the values used in the model are listed in Table 3, which displays the parameters and variables of the biosensor model that was retrieved from COMSOL and includes the abbreviations, expressions, values, and description of input.

Table 3. Parameter

Name	Expression	Value	Description
finger	15.5[mm]	0.0155 m	finger thickness
skin	1.5[mm]	0.0015 m	skin radius
Fat	2.5[mm]	0.0025 m	fat radius
bone	7.5[mm]	0.0075 m	bone radius
artery	0.5[mm]i	5E-4 m	artery radius
muscle	4[mm]	0.004 m	muscle thickness
source	10[mA]	0.01 A	supply current
Electrode t	0.8[mm]	8e-4	Electrode thickness
Electrode l	10[mm]	0.01m	Electrode length
artery_d	(2*bone+muscle)/2 [mm]	9.5	artery depth
deltaR	0.15[mm]	1.5E-4 m	extension

3.5.2 Geometry Model:

COMSOL provides several axisymmetric geometrical models including 1D, 2D, and 3D. In this simulation, a 2D blood flow biosensor model is built utilizing the assumed and built-in geometric techniques. The finger-simplified model was created in model geometry. A frameworkmade up of five parts was used to build the finger. Figure 13 illustrates the finger's overall diameter which is 15.5 mm (Martuzzi et al., 2014). A variety of tissue layers make up this model (i.e., skin, fat, artery, muscle, and bone). With a total thickness of 1.5 mm (Jasaitiene et al., 2011), the skin layer is made up of the dermis andepidermis. Under the epidermis, there is a layer of fat with a thickness of 2.5 mm (Dilley et al., 2001), followed by a layer of muscle that is 4 mm (Álvarez et al., 2019) thick and circulated around a layer of bone that is 7.5 mm (Sun et al., 2011) thick. Twoarteries, the radial, and ulnar arteries are present in the finger, and they supply the

tissues with oxygenated blood and nutrients. The two arteries were placed parallel to one another with 9.5 mmspacing beneath the skin, hidden within the fat layer, on two sides of the model to simplifythe anatomical arrangement. As illustrated in Figure 13, the artery is of size 1.075 mm while it is under stress, such as when the heart is pumping blood into it, and 0.5 mm when blood is returningto the heart from the artery.

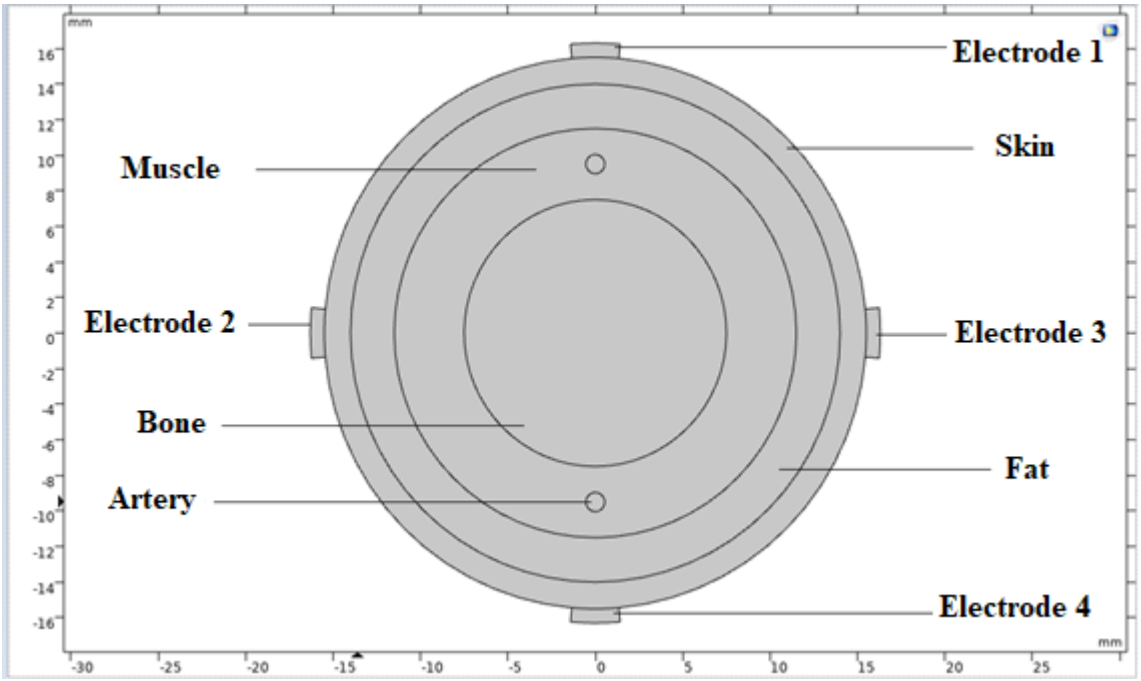

Figure 13. Geometrical model of MEIP

Four electrodes, each measuring 0.8x10 [mm], are being applied to the finger. The electrodes placement is as follows: electrode1 is placed at 0,16.3 [mm], electrode2 is placed at - 16.3,0 [mm], electrode3 is placed directly across from electrode2 at +16.3,0 [mm], and electrode4is placed directly across from electrode1 at 0, -16.3 [mm]. (With similar distances between each electrode, we positioned four multiaxial electrodes above the major artery.)

3.5.3 Material and Properties

3.5.3.1 Tissue Properties

The model replicates the human anatomy by using several tissue layers, such as skin, fat, arteries, muscles, and bones, as illustrated in Table 4. For the different tissue layers, complex permittivity and conductivity values were calculated to get the frequency-dependent dielectric characteristics that are displayed in table 3.2 (Tissue Frequency Chart » IT'IS Foundation, n.d.). In these modeling simulations, numerous frequencies ranging from 0 to 100 GHz have been employed, however, we are only displaying 5 distinct frequencies (10Hz, 100Hz, 1KHz, 10KHz, and 50KHz) that established the dielectric characteristics of tissues, which are displayedin Table 3.2.

Table 4. The dielectric properties of tissues at different frequencies:

MATERIALS	10Hz	100Hz	1KHz	10KHz	50KHz
Skin	0.0002	0.000200001	0.000200065	0.000204082	0.000273088
Fat	0.012206696	0.020810608	0.022404607	0.023830606	0.024246193
Muscle	0.201966739	0.266709174	0.321156604	0.340831688	0.351827808
Bone	0.075563518	0.081031622	0.081529994	0.082623046	0.083421828
Artery	0.7	0.700000006	0.700000484	0.700038264	0.700800987

3.5.3.1.1 Electrical conductivity (S/m)

MATERIALS	10Hz	100Hz	1KHz	10KHz	50KHz
Skin	1135.9904	1135.9398	1135.6193	1133.5616	1126.7574
Fat	7973504.661	457062.2399	24104.2143	1085.2981	172.4172
Muscle	25700364.51	9329046.966	434932.3153	25908.7129	10093.7268
Bone	10020467.96	217032.9911	12320.0379	1657.7721	613.1811
Artery	5259.9782	5259.8264	5258.6084	5248.1698	5197.6999

(b)Electrical permittivity

Source: (Tissue Frequency Chart » IT'IS Foundation, n.d.)

3.5.3.2 Electrode Design:

It is crucial to verify this theoretical study of a finger-electrode interface by simulating a simplified finger model and looking into the electrical properties of the suggested simulation as the influence of Silver (Ag) materials on skin-electrode contact impedance. Four ECG electrodes were applied to the surface of a simplified finger model, and COMSOL, a finite element program was used to investigate the electrical field fluctuations on the finger model according to the size and inner distances of the electrodes. This method establishes the requirements for particular types of electrode bands that have been braided from silver. The following are the characteristics of silver that are already listed in the COMSOL library in Table 5.

Table 5. Properties of Silver Electrode

Property	Value	Unit
Electrical conductivity	61.6e6	[S/m]
Coefficient of thermal Expansion	18.9e-6	[1/K]
Heat capacity at constant Pressure	235	[J/(kg*K)]
Density	10500	[kg/m^3]
Thermal conductivity	429	[W/(m*K)]
Relative permittivity	1	1
Young's modulus	83e9	[Pa]
Poisson's ratio	0.37	1

3.5.4 Theory

The parameters mentioned above are used as input values for the COMSOL analysis. The simulation provides the following equations which given the direction in which the simulation proceeds.

$$\nabla \cdot D = P_f \tag{3.1}$$

The equations are categorized into multiple domains such as the frequency domain, and the electric current. The stationary equation of continuity must be considered when working with stationary electric currents in conductive material. The point version of Gauss's law states the following in a stationary coordinate system. P_f is the free electric charge density and $\nabla \cdot D$ is the divergence of the electric displacement field as shown in equation 3.1.

$$D = \epsilon_0 \epsilon_r E \tag{3.2}$$

where the attributes of the substance ϵr. The material's permittivity and permeability are defined, respectively, as $\epsilon = \epsilon_0 \epsilon_r$. From this point forward, unless it is necessary for clarity, we shall allow ourselves to omit the subscript f from the free charge density and current density, where ε is referred to as the dielectric's permittivity. Alternately, this might be stated as equation 3.2, ϵ_0 is the permittivity of free space, ϵr is the relative permittivity, and E stands for the total energy of the electric field and D electric displacement.

$$V = IR \tag{3.3}$$

Let's look at a conducting substance like copper, which contains a lot of charge

carriers. When such materials are exposed to an electric field, a current flow, the strength of which is inversely correlated with the applied field is shown in equation 3.3. where V is known as voltage, current is denoted by I, and resistance by R.

$$J = \sigma E \tag{3.4}$$

where σ is yet another material attribute and specifies the conductivity of the conducting substance. Any practical dielectric will have a tiny but nonzero conductivity, it should be emphasized. A popular simplification for excellent conductors takes them to be perfect electrical conductors, σ is an inherent characteristic of bodies of materials containing free charge carriers that establishes a linear relationship between the applied electric field E and the electrical current density J conducted in the material given in equation 3.4.

$$\nabla . J = Q_j \tag{3.5}$$

Where, the model, which considers electric current in conductive medium, resolves the continuity equation Q_j using a current source from equation 3.5.

$$\rho^{(t)} = \rho_0 e^{-t/e} \tag{3.6}$$

$$J = \sigma E + jmD + Je \tag{3.7}$$

Where, J is the current density. It answers for equation 3.7 in the time-dependent research. Considering electric displacement, the medium's conductivity is $\boldsymbol{\sigma}$, while the external current density is Je.

$$E = -\nabla . v \tag{3.8}$$

One of the first uses of these equations was the Laplace equation, which is utilized in physics. The initial use of the Laplace equation formula was in electrostatics, where the electric potential V and electric field are connected by the equation 3.8 Gauss's law directly leads to the relationship between the electrostatic potential and the electric field.

3.5.5 Mesh

This proposed MEIP model used physics-controlled mesh by design, which is based on the unstirred tetrahedral mesh. This mesh is automatically generated and adjusted to the device's physics setting, with the unit size defaulted to a standard. The mashing process is invisible, consisting of a scale and a free tetrahedral node. This simulation is using some manual mash sizes (element size parameter), shown below in table 6, and Figure 14 shows the model mash.

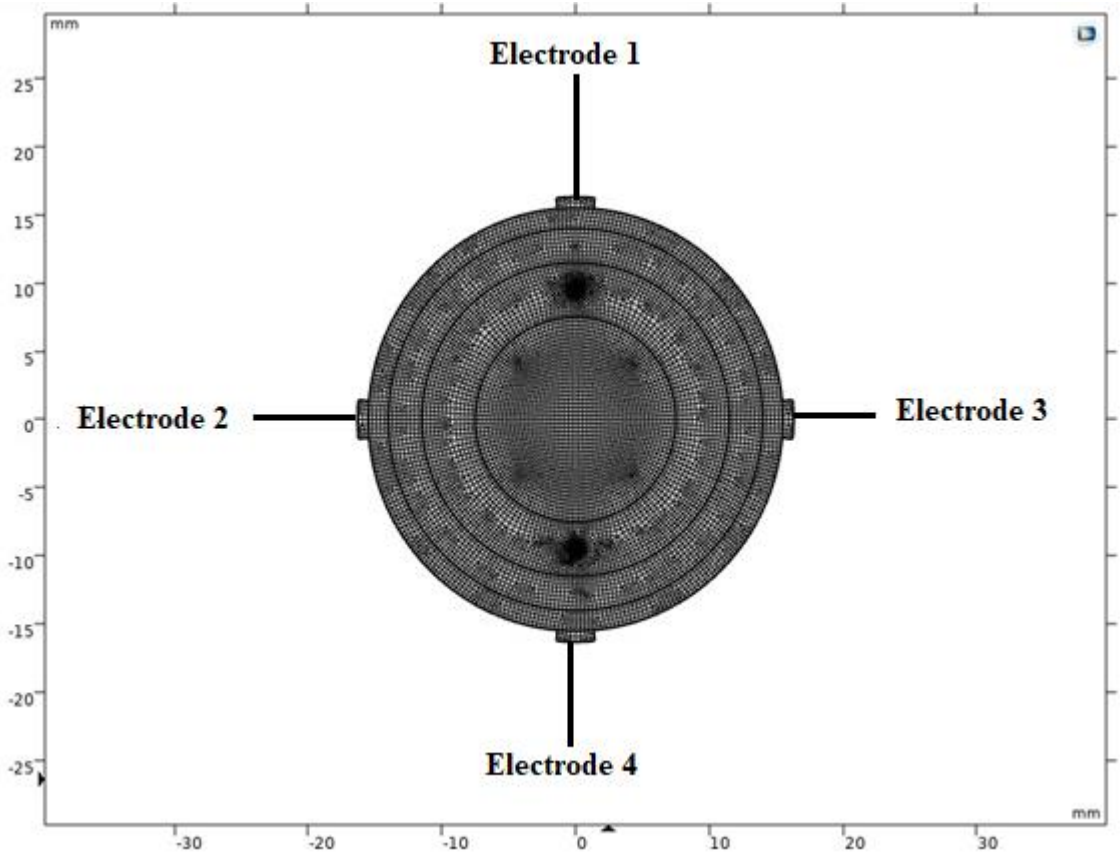

Figure 14. Mesh

Table 6. Mesh size values

Maximum element size	0.326 (mm)
Minimum element size	6.52E-4 (mm)
The maximum element growth rate	1.1
Curvature factor	0.2
Resolution of narrow regions	1

3.5.6 Study

The equations and physics interfaces included in the computation and mesh selection are controlled by study steps. This simulation uses a frequency-dependent model study that computesthe model response. Table 7 shows the frequency-dependent study.

Table 7. Frequency domain

Frequency	**Hz**
Start	1
Steps per decades	2
Stop	10e10

3.6 Physical implementation setup

In the physical experiment, we just take the reading from different frequencies (100Hz, 10KHz) with different positions of electrodes top-side and then side-bottom. In the physical experiment, we use 3 electrodes, the position of the electrodes is side, bottom, and top.

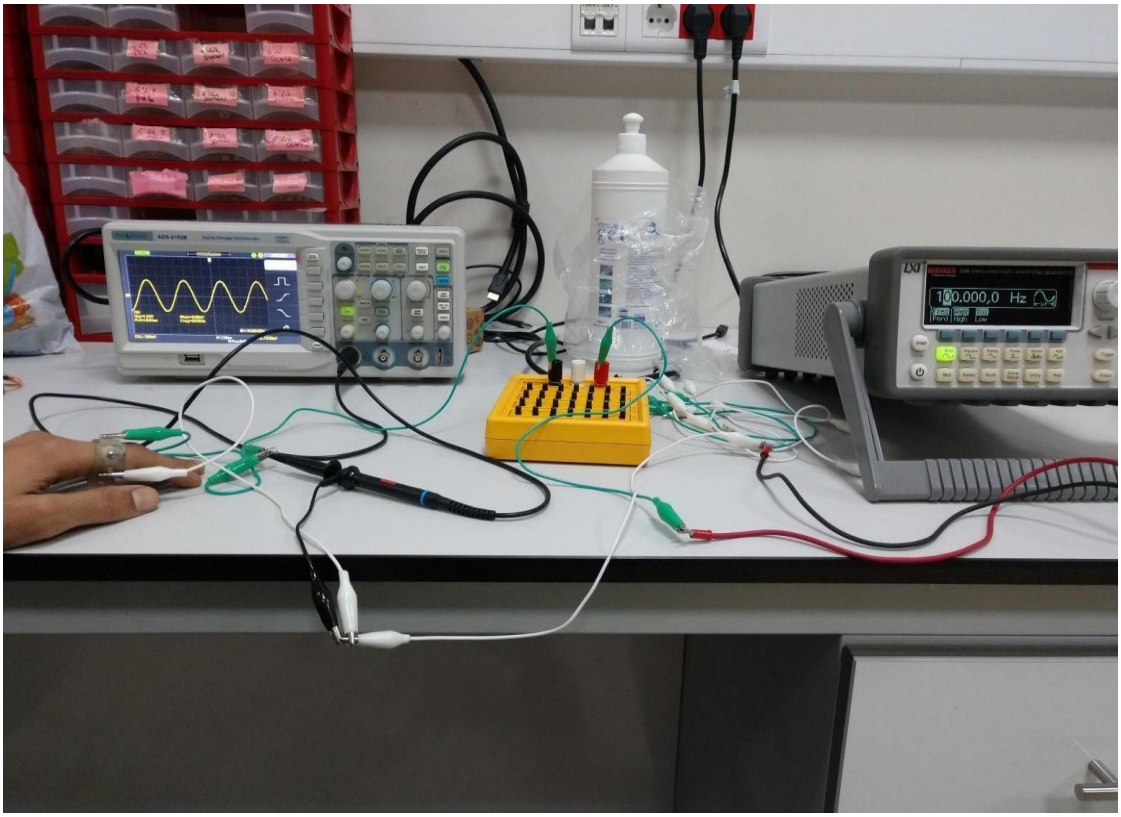

Figure 15. Measurement setup

As can be seen in the image Figure 15, in the experiment, 2 oscilloscopes are used where one is placed at the input and the other is placed at the output to ensure that the signal being transmitted is not affected by external factors and is indeed the correct signal. Furthermore, the use of 2 oscilloscopes serves as a feedback mechanism that confirms that the input signal has the desired frequency and amplitude. The second oscilloscope (connected at the output) also serves to capture the resultant data.

The frequencies used are 100Hz and 10kHz with a combination of a 1Mohm resistance. The frequency of 100Hz is used based on the simulation which suggests that at this frequency theoutput ac impedance variation will be maximum. The frequency of 10kHz is used as the literature review has revealed that as high as 95% of papers have documented the use of 10kHz frequency. The selection of these 2 frequencies allows us to compare the results obtained by the simulation conducted on COMSOL and the results existing in the literature.

3.6.1 Positioning of Electrodes Side-Bottom

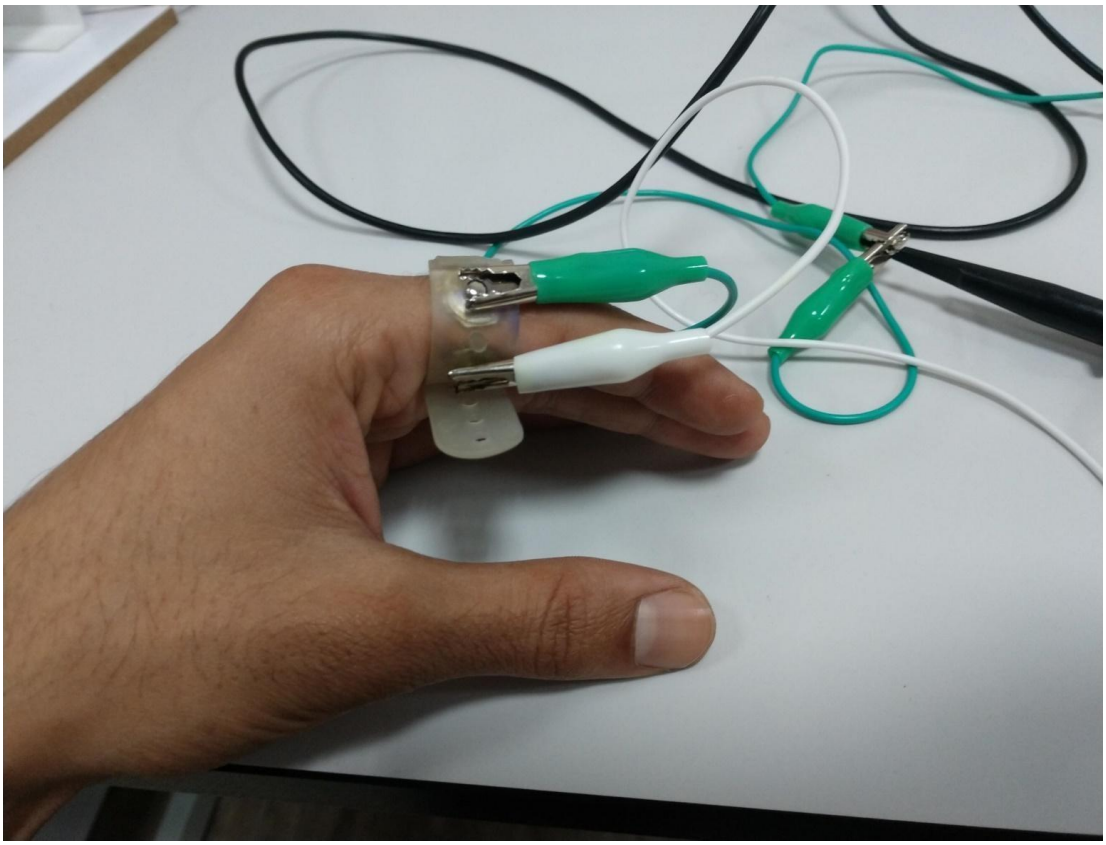

Figure 16. Position of electrodes side-bottom

As seen in the image Figure 16, the electrodes are attached in a side and bottom arrangement where one of the electrodes is placed on the side of the finger and the other is placed at the bottom. This allows the results to be calculated with the top-bottom configuration in order to determine the ideal positioning of the electrodes which can provide the most optimum results.

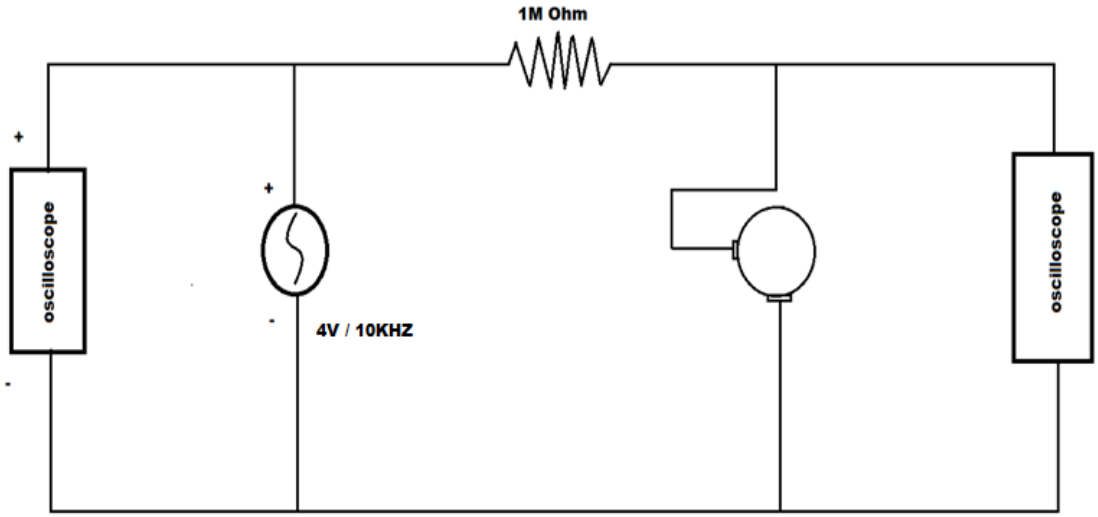

Figure 17. Block diagram of position of electrodes side-bottom

The image in Figure 17 provides a block diagram of the side-bottom arrangement of the electrodes.

3.6.2Positioning of Electrodes Top-Bottom

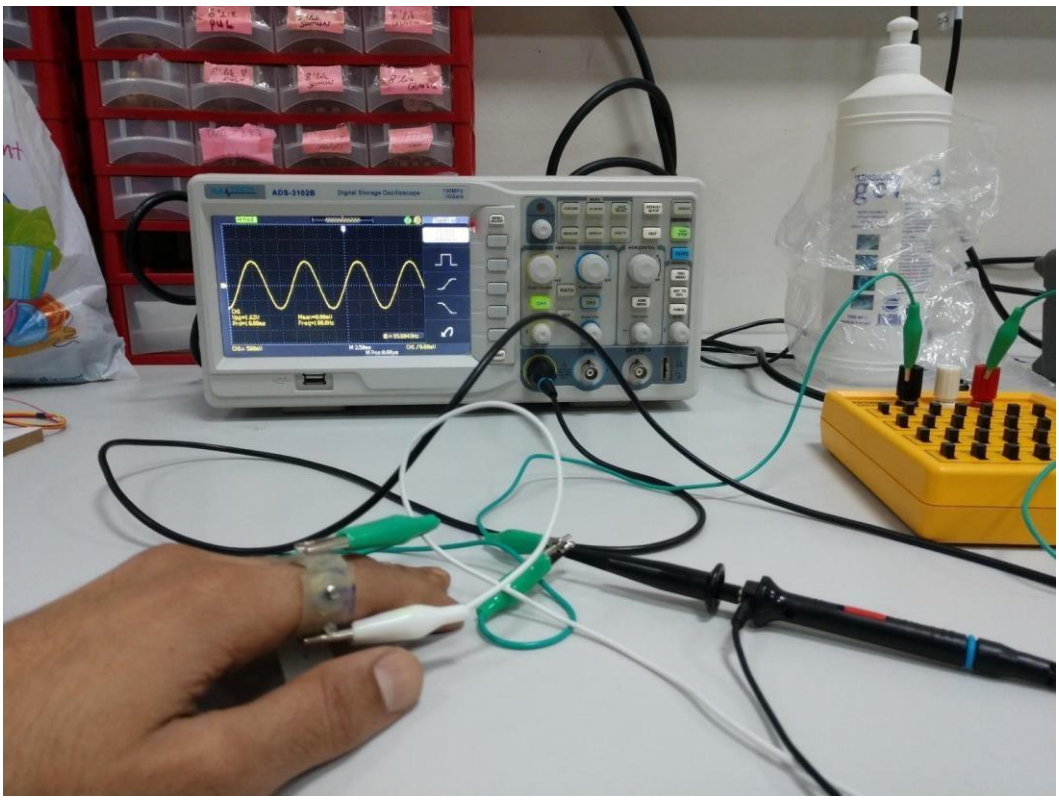

Figure 18. Position of electrodes top-bottom

As seen in the image Figure 18, the electrodes are attached in a top-and-bottom arrangement where one of the electrodes is placed on the top of the finger and the other

is placed at the bottom. This allows the results to be calculated with the side-bottom configuration in order to determine the ideal positioning of the electrodes which can provide the most optimum results.

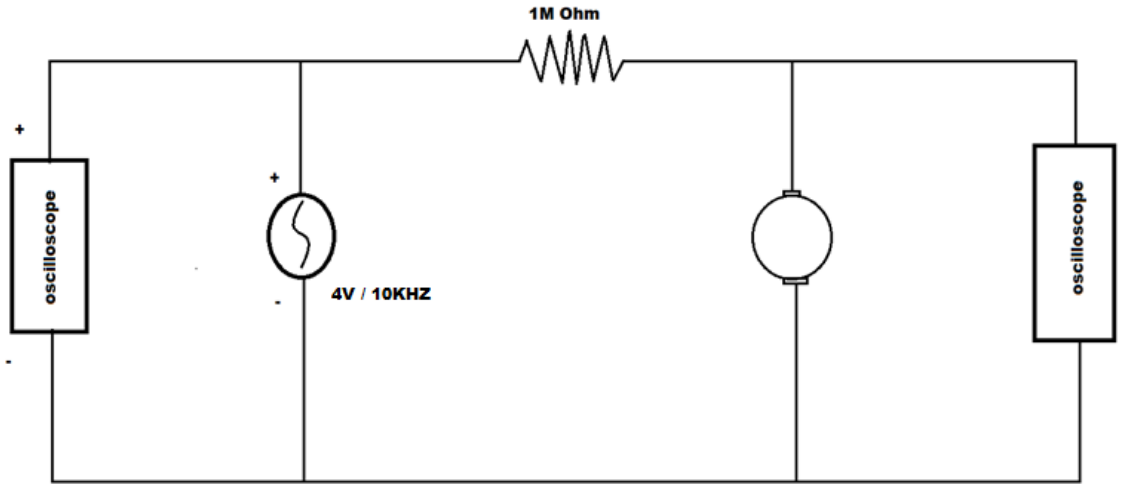

Figure 19. Block diagram of position of electrodes top-bottom

The image in Figure 19 provides a block diagram of the top-bottom arrangement of the electrodes. Furthermore, ECG gel is used at the input stage between the electrodes and the skin in order to ensure that there is no effect on the type of skin (balanced skin, oily/acne-prone skin, dry skin, sensitive skin many more) as well as the presence of hair and hair follicles on the input data. This also ensures that there is no breakage of the signals mid-experiment as the ECG gel is a good conductor of electricity. For the COMSOL simulation, 4 electrodes are used where three are used as a source at 10mA and one is used as output. The applied current at the input is set as 10mA since a higher current value can increase the chances of muscle damage, kidney failure, and even heart attacks.

4. RESULT

4.1 COMSOL Simulation

The COMSOL simulation was performed for three electrodes positioned individually and the data for each was recorded. The data of each electrode is then measured for 2 conditions i.e., when the artery is at rest (no blood is pumped through the artery) and when the artery is functioning (blood is pumping through the artery) where 0% represents the artery at rest and 15% represents the artery when blood is pumped. All the impedance were calculated with respect to electrode 4.

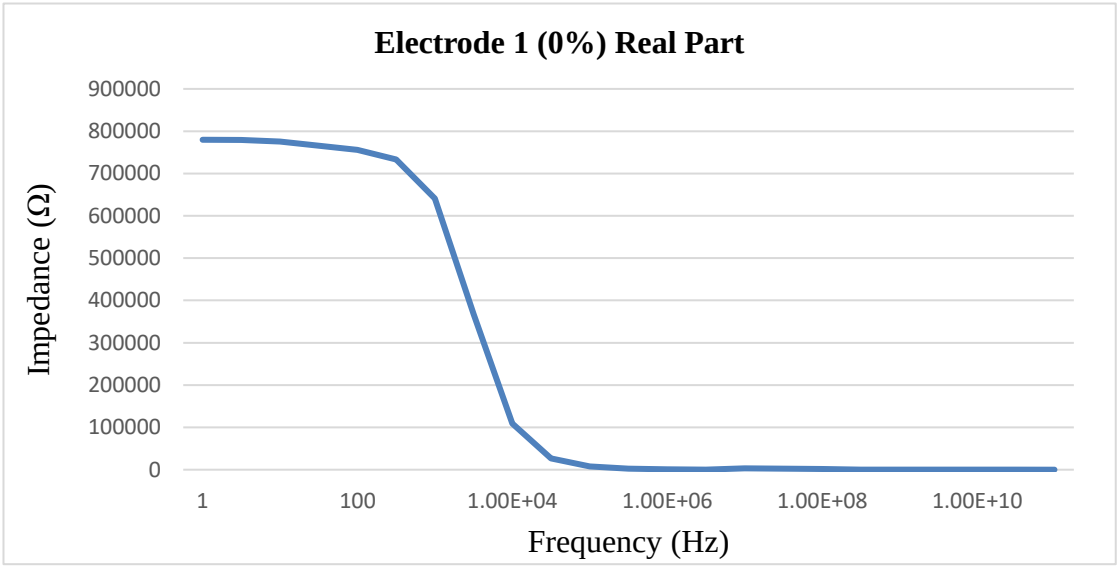

Figure 20. Impedance of real part electrode 1 at rest artery state

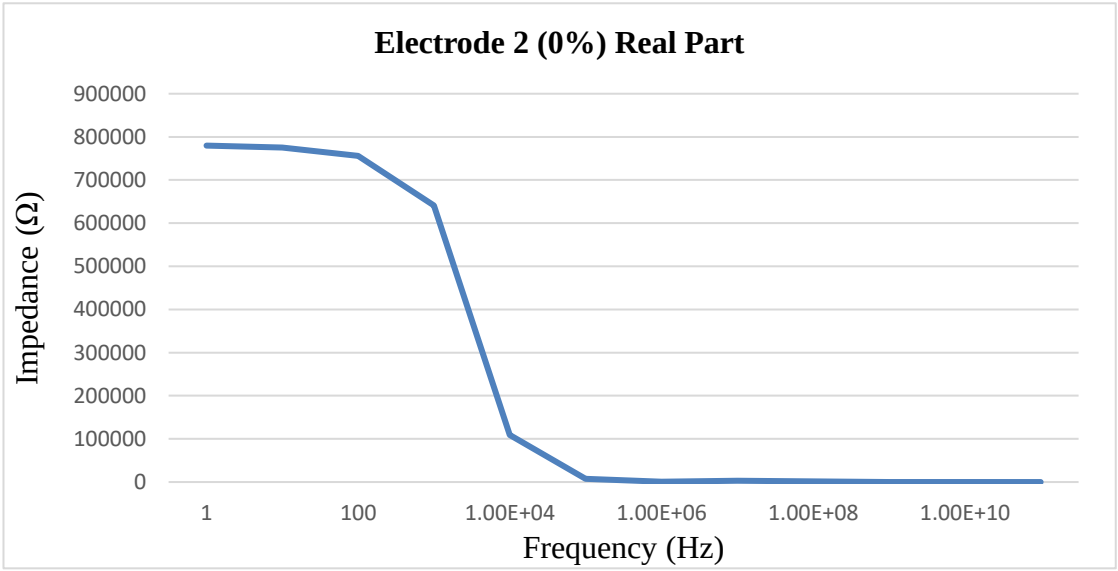

Figure 21. Impedance of real part electrode 2 at rest artery state

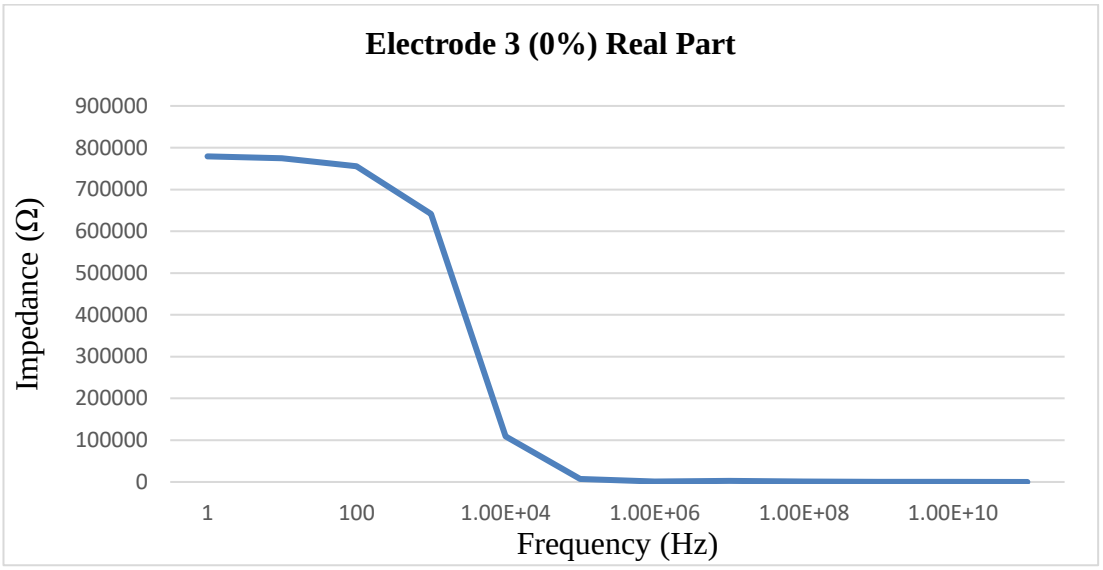

Figure 22. Impedance of real part electrode 3 at rest artery state

Figures 20, 21, and 22 represent the measured real part of impedance obtained when electrodes 1, 2, and 3 are connected respectively and there is no blood flowing in the artery i.e., the artery is at rest. We can see in these Figures that the impedance decreases as we increase the frequency. After 10kHz the impedance approaches to zero and it continuous to remain the same as the frequency further increases.

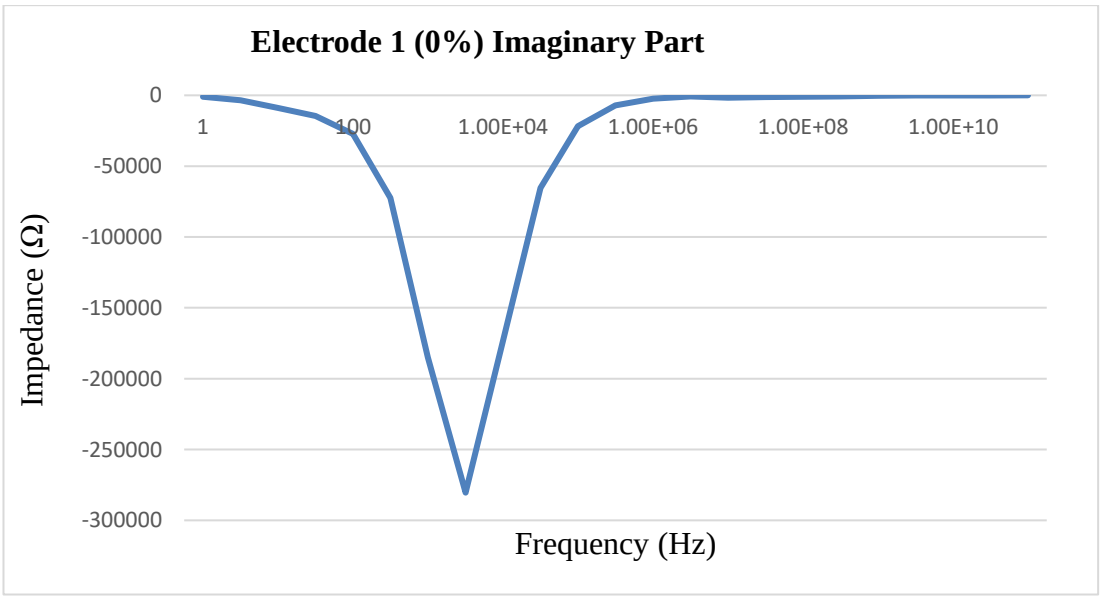

Figure 23. Impedance of imaginary part electrode 1 at rest artery state

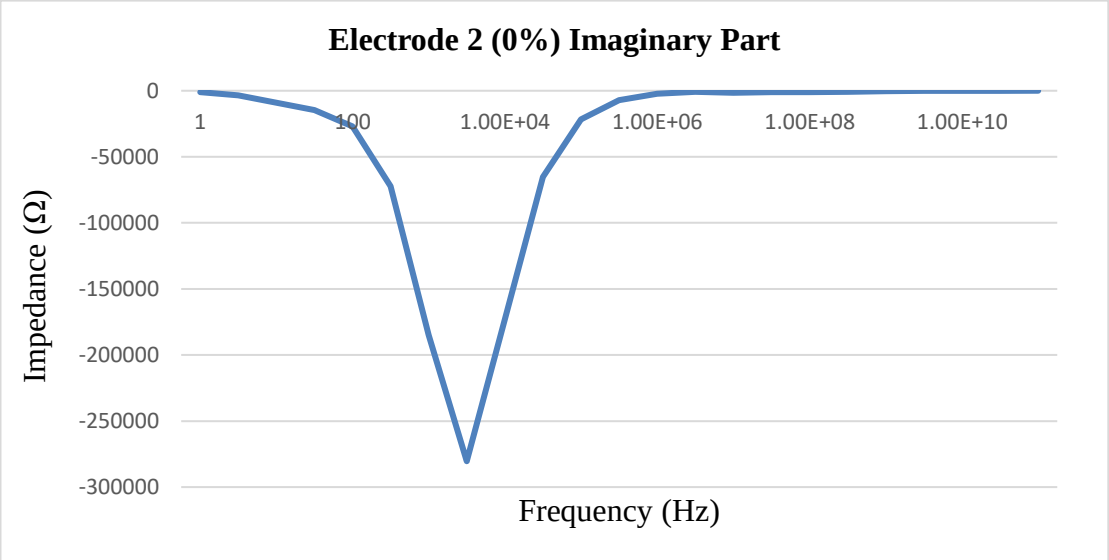

Figure 24. Impedance of imaginary part of electrode 2 at rest artery state

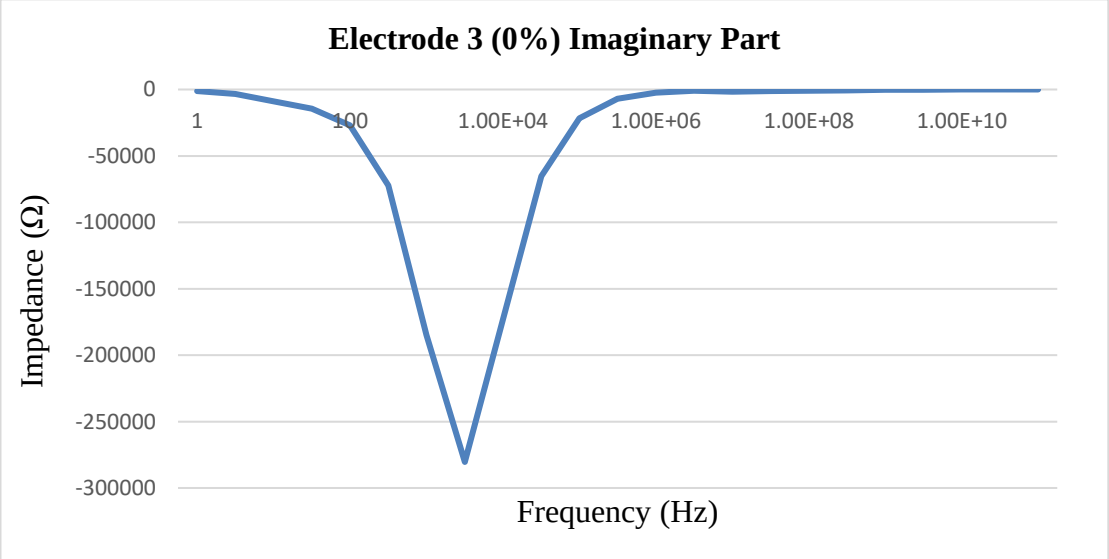

Figure 25. Impedance of imaginary part of electrode 3 at rest artery state

Figures 23, 24, and 25 represent the measured impedance of the imaginary part obtained when electrodes 1, 2 and 3 are connected respectively and there is no blood flowing in the artery as a consequence of the artery being at rest. We can see in these Figures that the impedance decreases as we increase the frequency. It can also be seen that from 1 kHz to 10 kHz the impedance value further decreases exponentially after touching the peak decreased value due to being the impedance of the imaginary part, then it increases further towards zero as the frequency increases to 100 kHz, after that as the frequency increases the impedance remains close to zero.

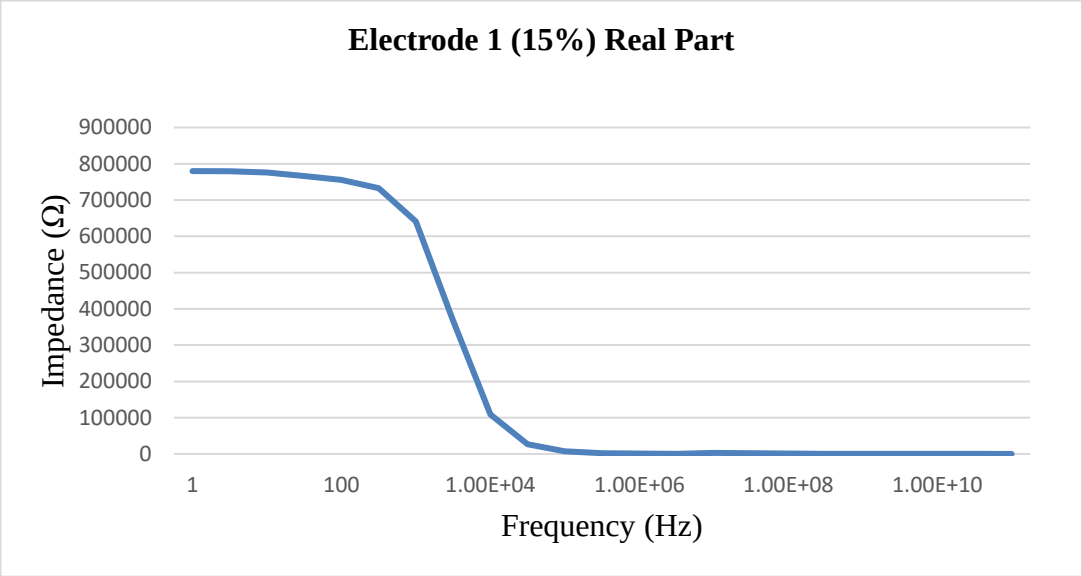

Figure 26. Impedance of real part electrode 1 at pumped artery state

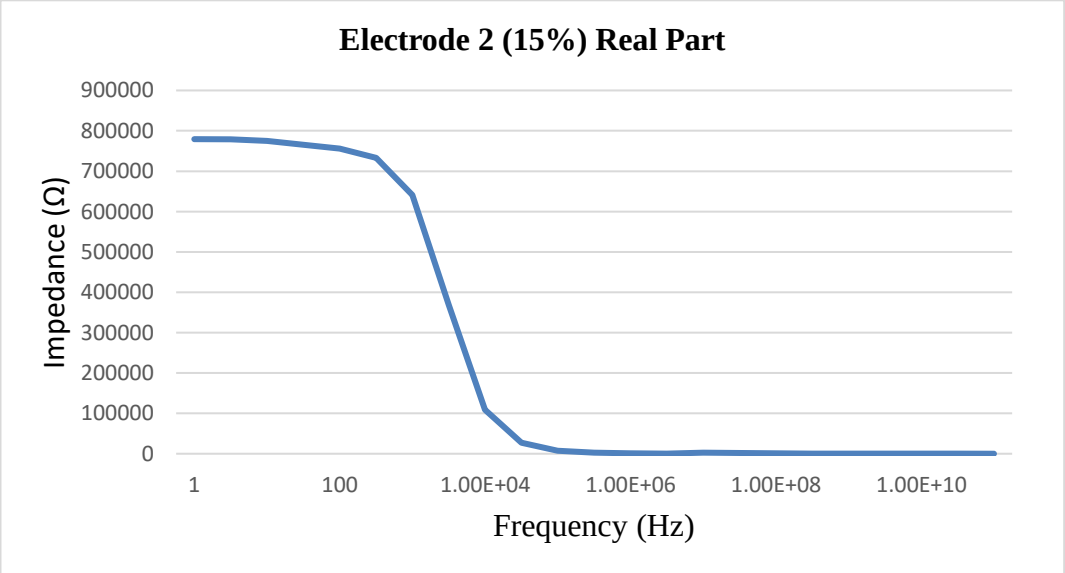

Figure 27. Impedance of real part electrode 2 at pumped artery state

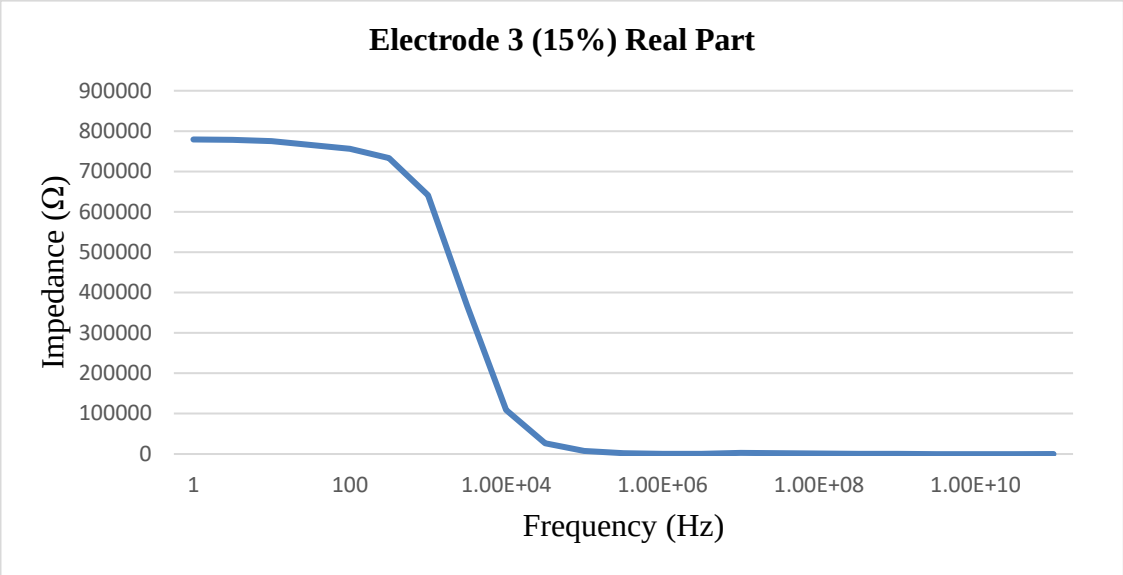

Figure 28. Impedance of real part of electrode 3 at pumped artery state

Figures 26, 27, and 28 represent the measured impedance's real part obtained when electrodes 1, 2, and 3 are connected respectively and there is blood flowing in the artery i.e., the artery is pumped with blood. This graph demonstrates that the impedance decreases as the frequency is continuously increased.

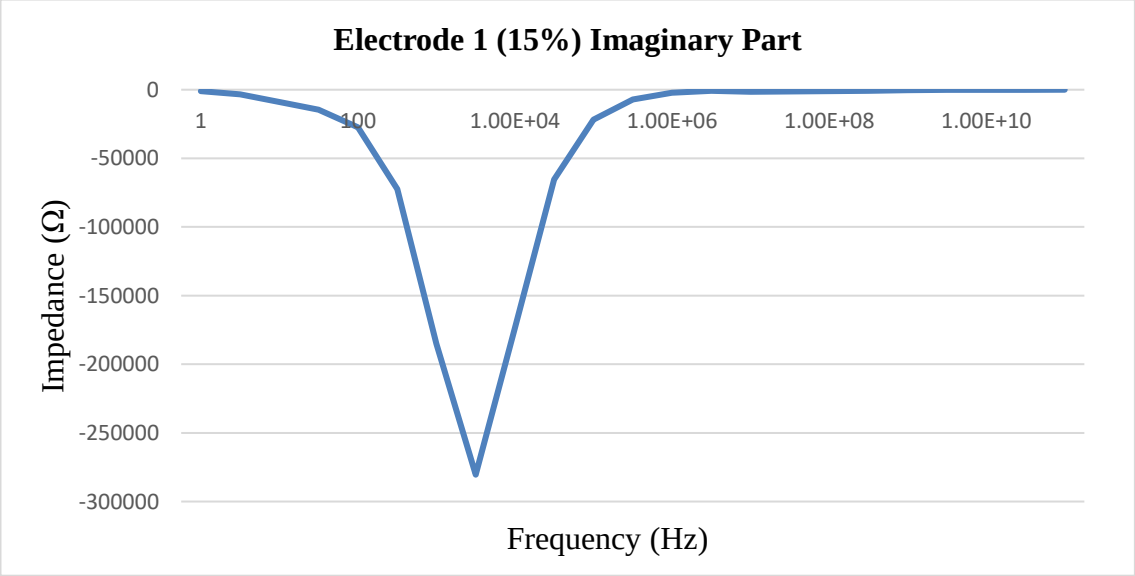

Figure 29. Impedance of imaginary part of electrode 1 at pumped artery state

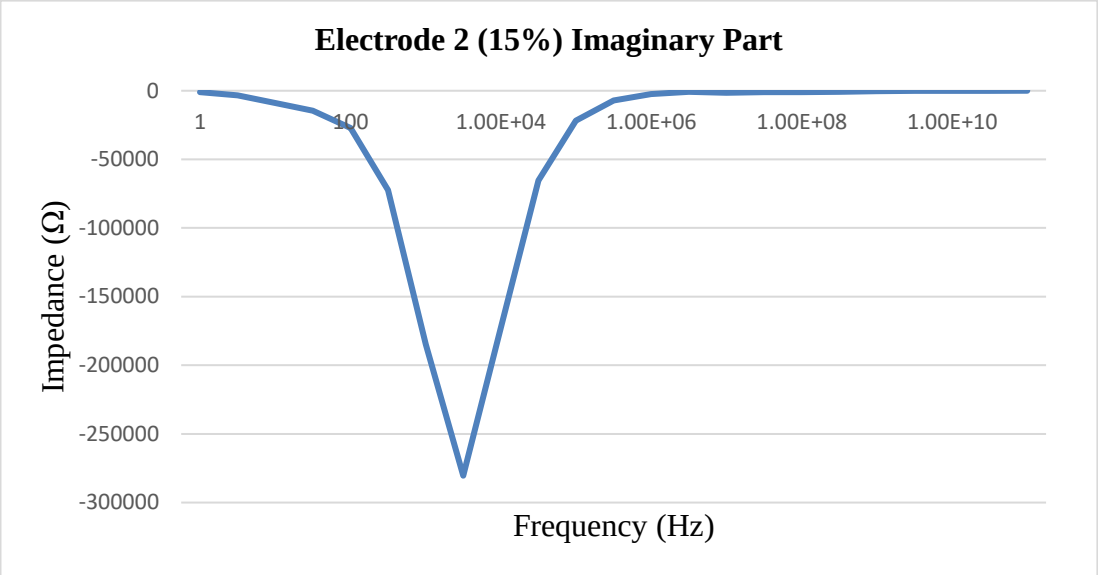

Figure 30. Impedance of imaginary part electrode 2 at pumped artery state

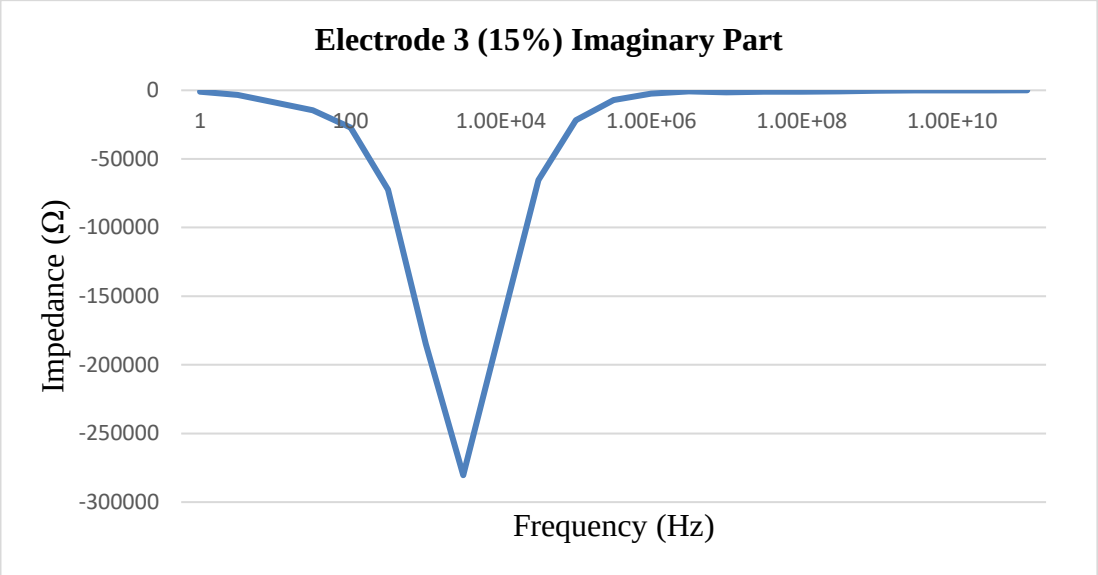

Figure 31. Impedance of imaginary part electrode 3 at pumped artery state

Figures 29, 30, and 31 represent the measured impedance imaginary part obtained when electrodes 1, 2, and 3 are connected respectively and there is blood flowing in the artery i.e., the artery is pumped with blood. In these Figures, we can see that the impedance further decreases as the frequency rises, but at the 10 kHz, it reaches its largest impedance drop value. Once it reaches the peak impedance reduction value, it starts to rise again until it reaches zero.

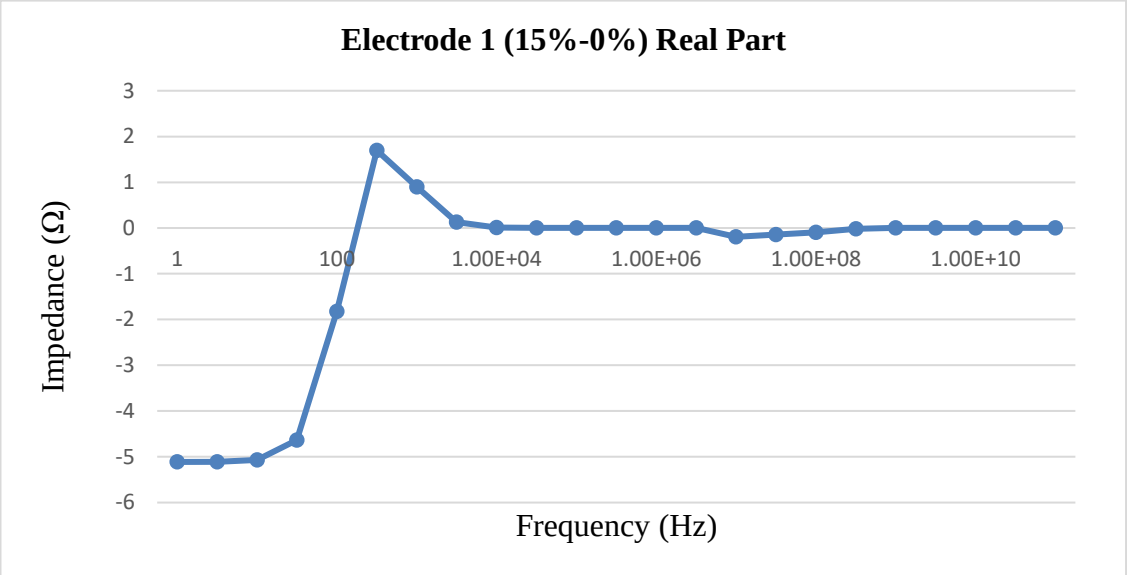

Figure 32. Difference in impedance of real part electrode 1 between pump and rest state

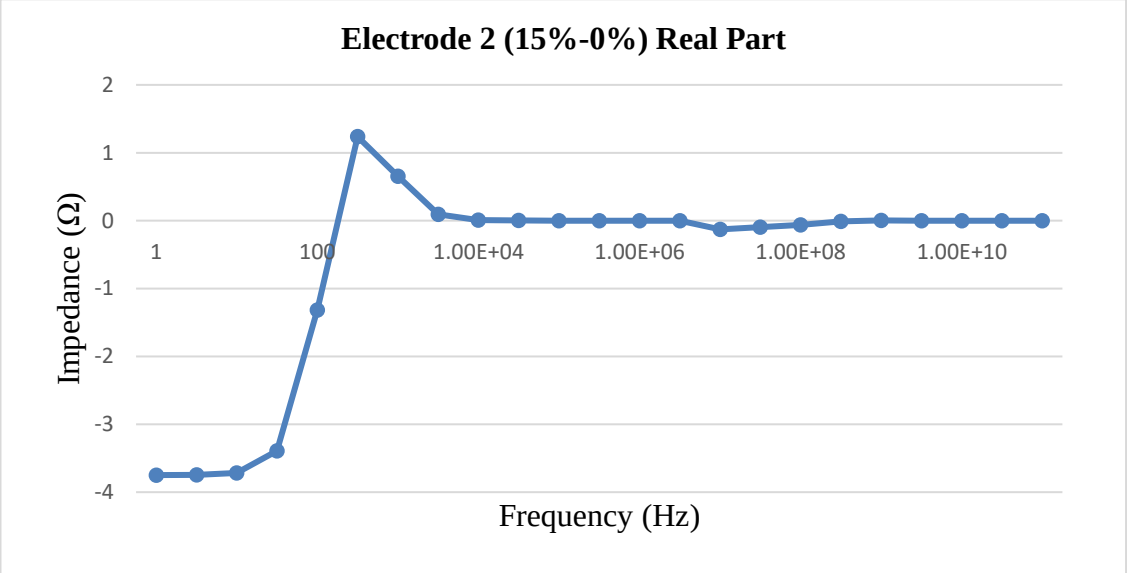

Figure 33. Difference in impedance of real part electrode 2 between pump and rest state

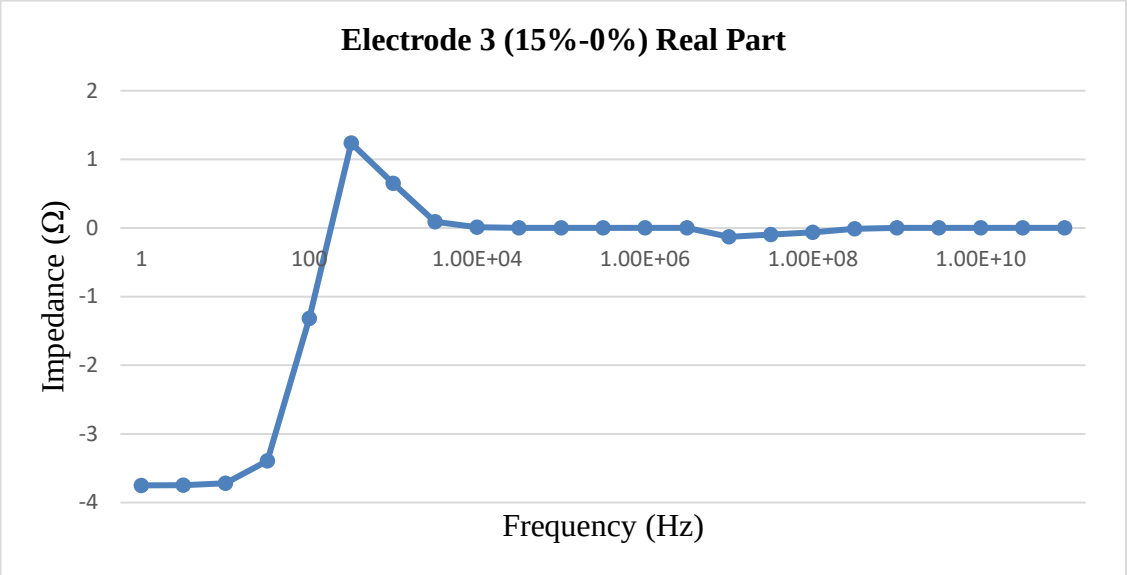

Figure 34. Difference in impedance of real part electrode 3 between pump and rest state

Figures 32, 33, and 34 represent the differences of the impedance real part obtained between the pumping state of the artery and the rest state for electrodes 1, 2 and 3 respectively. Since electrode 2 and electrode 3 have comparable impedances and are depicted in Figures 33 and 34, we focus on electrode 2.

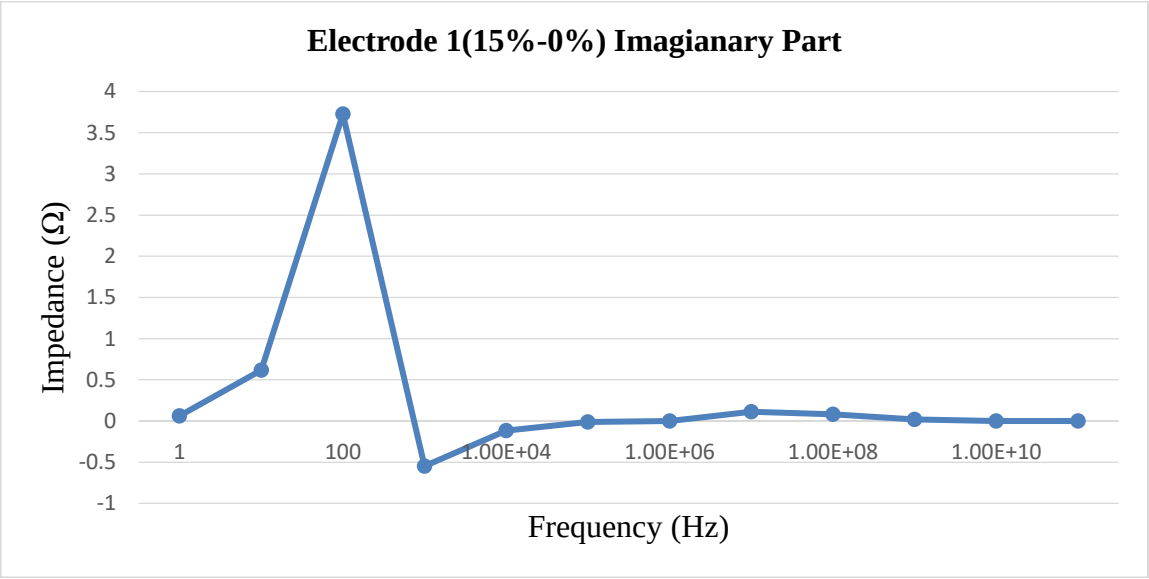

Figure 35. Difference in impedance of imaginary part electrode 1 between pump and rest state.

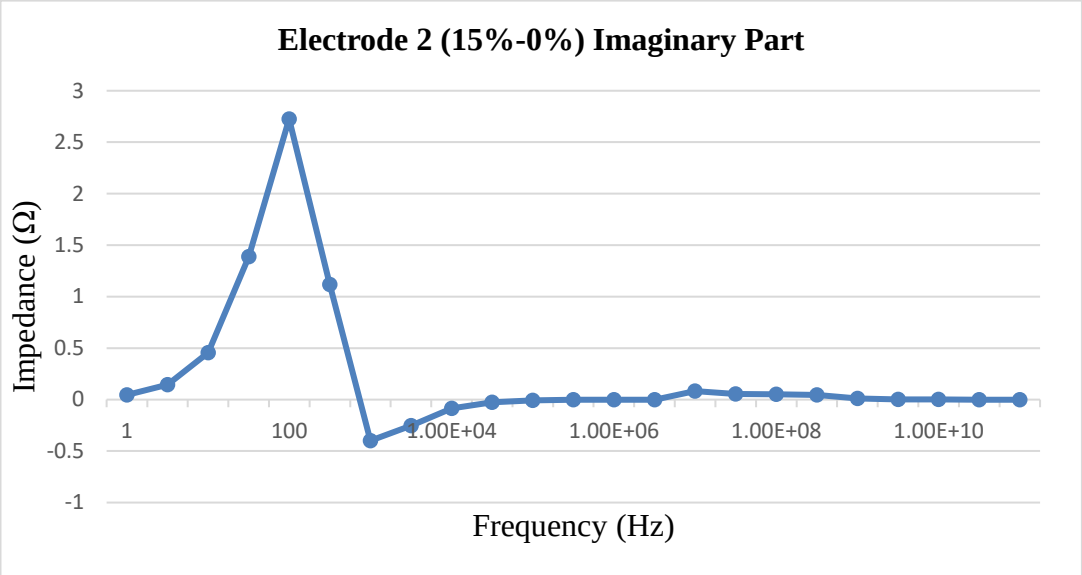

Figure 36. Difference in impedance of imaginary part electrode 2 between pump and rest state.

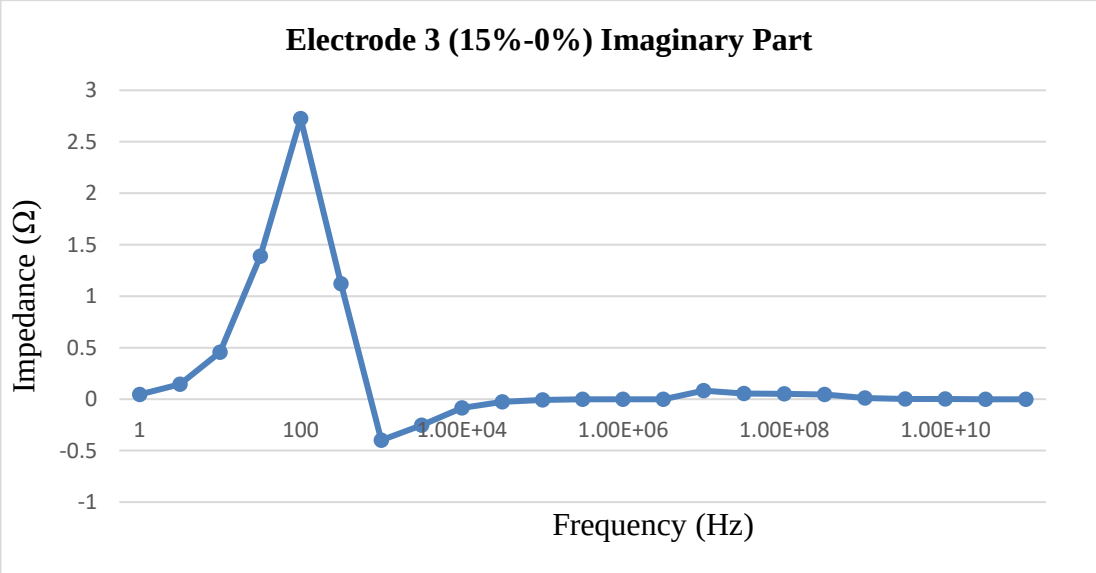

Figure 37. Difference in impedance of imaginary part electrode 3 between pump and rest state

Figures 35, 36, and 37 represent the differences of the impedance imaginary part obtained between the pumping state of the artery and the rest state for electrodes 1, 2, and 3 respectively. Upon closer inspection of the data obtained, it is revealed that the different impedances calculated for electrodes 2 and 3 follow an identical pattern therefore only the data of electrode 2 is chosen to be used for further calculations. Figure 33, 34 distinguishes electrodes 2 and 3 from one another.

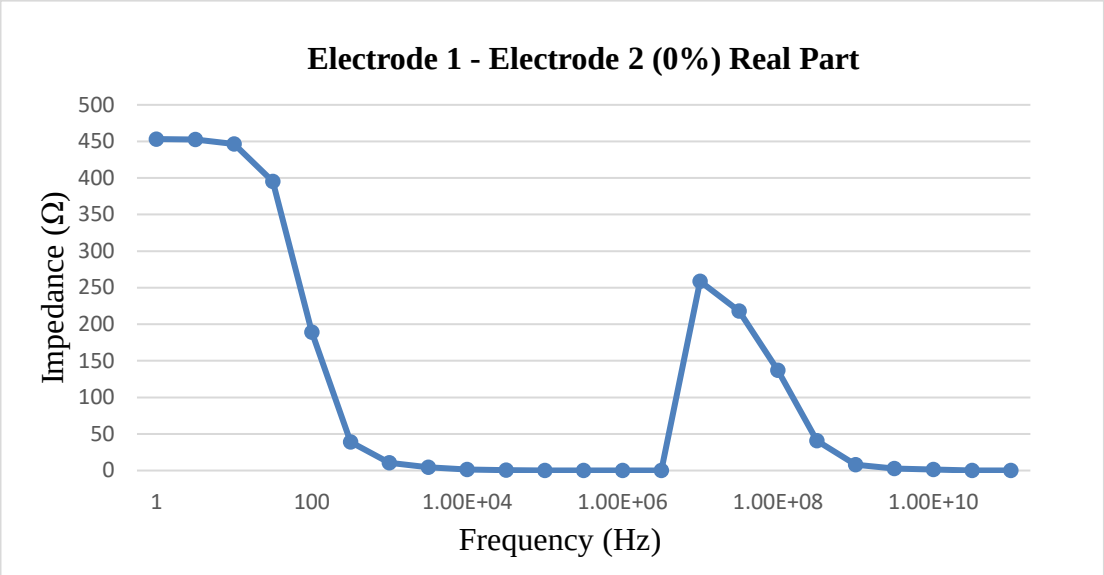

Figure 38. Difference in impedance of real part electrode 1 and real electrode 2 for rest state.

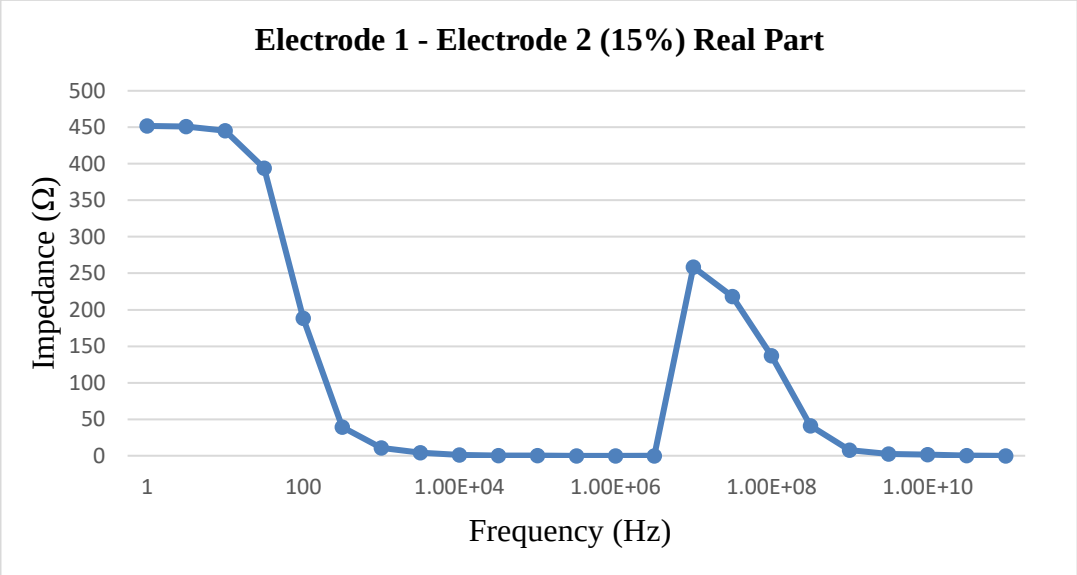

Figure 39. Difference in impedance of real part electrode 1 and electrode 2 for pump state.

Figure 38 represents the difference in impedance of the real part for electrode 1 and electrode 2 for the rest state of the artery. It is obtained by subtracting the data from Figure 24 from the data of Figure 25. Figure 39 represents the difference in impedance of the real part for electrode 1 and electrode 2 for the pumping state of the artery. It is obtained by subtracting the data of Figure 26 from the data of Figure 27. As we can see in both Figures 38 and 39, when the artery is at rest condition in Figure 38 and the artery is pumping in Figure 39, the statistics are very similar. Starting from frequency of 100 Hz, the impedance is zero and it continues to be the same as the frequency increases. In contrast, with a frequency of 1 MHz, the impedance increases from close to 0 to 250 ohm (Ω), but after the frequency increases to 100 MHz, the impedance again

increases, and it continues to be the same as the frequency increases even more.

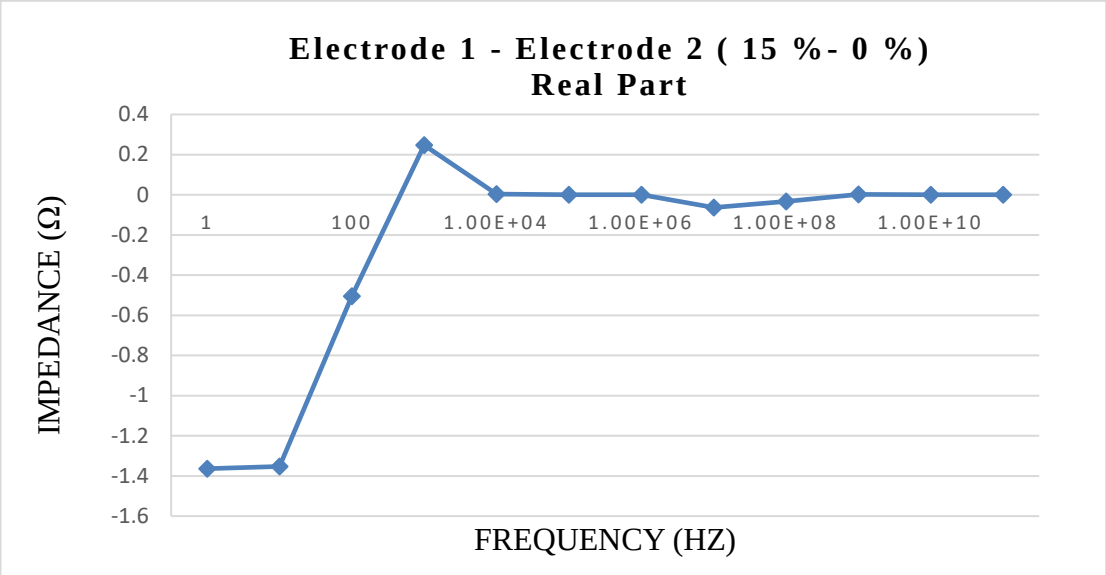

Figure 40. Difference in impedance real part of electrode 1 and electrode 2 for pump and reststate

Figure 40 represents the difference in impedance of electrode 1 and electrode 2 for the pumping and rest state. It is obtained by subtracting the data from Figure 38 from the data of Figure 39. As we raise the frequency, the impedance rises, as seen in the Figure. After 100 Hz, the impedance starts to fall until it approaches to zero, and it stays the same as the frequency rises.

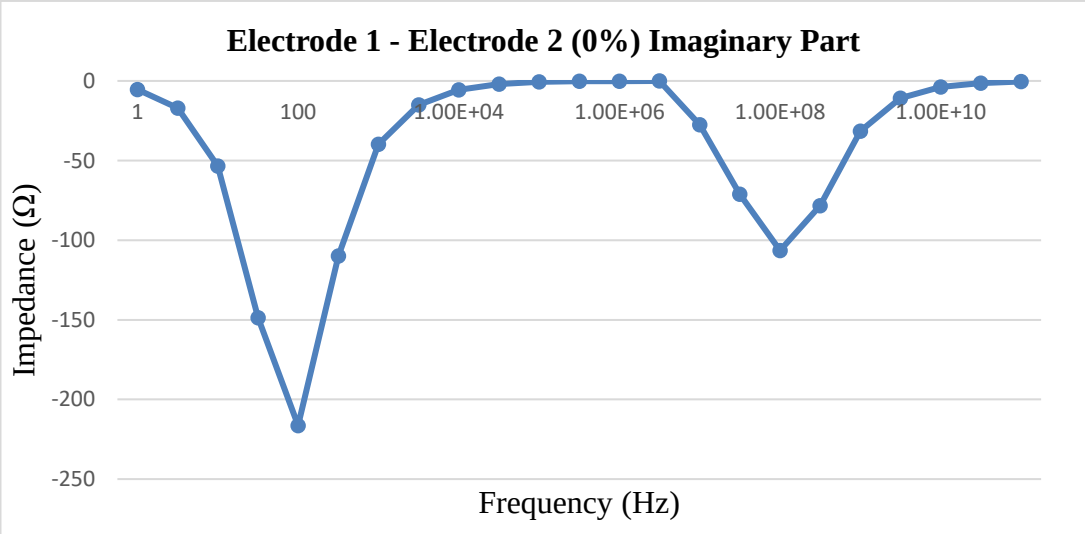

Figure 41. Difference in impedance imaginary part of electrode 1 and electrode 2 for rest state.

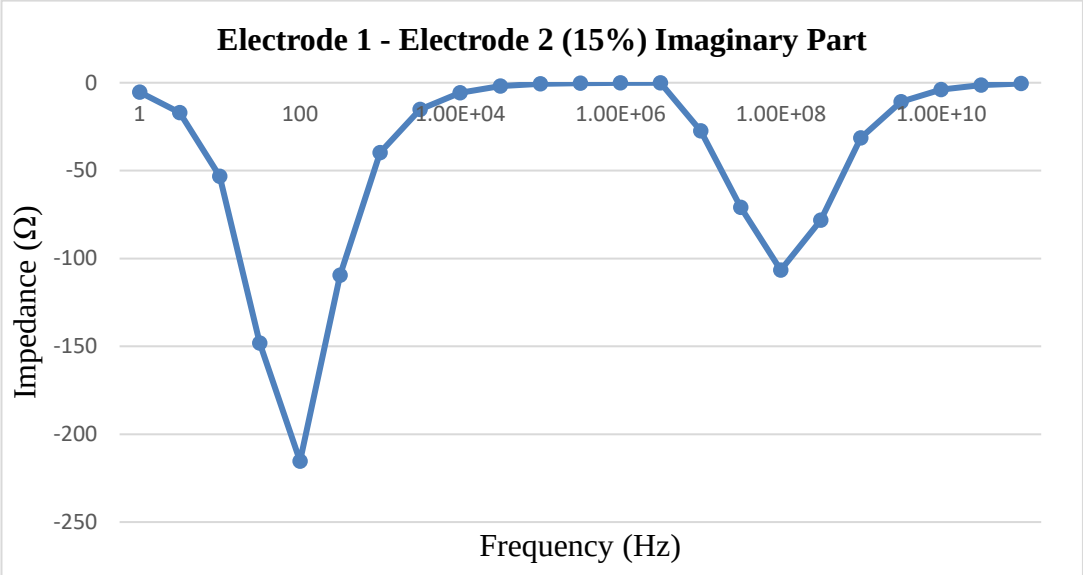

Figure 42. Difference in impedance imaginary part of electrode 1 and electrode 2 for pump state.

Figure 41 represents the difference in impedance of the imaginary part for electrode 1 and electrode 2 for the rest state of the artery. It is obtained by subtracting the data of Figure 27 from the data of Figure 24. Figure 42 represents the difference in impedance of the imaginary part for electrode 1 and electrode 2 for the pumping state of the artery. It is obtained by subtracting the data shown in Figure 29 from the data of Figure 30. Figures 41 and 42 show the status of the artery while it is at rest and when it is pumping, respectively. The results show that the impedance decreases with increasing frequency at 100 Hz, it reaches its maximum impedance drop value. It begins to grow once further until it approaches zero after reaching the maximal impedance reduction value. After 10 kHz, the impedance approaches to zero and doesn't vary as the frequency increases. Contrarily, at a frequency of 1 MHz, the impedance increases, but at a frequency of 10 GHz, it is close to zero and stays that way as the frequency rises further.

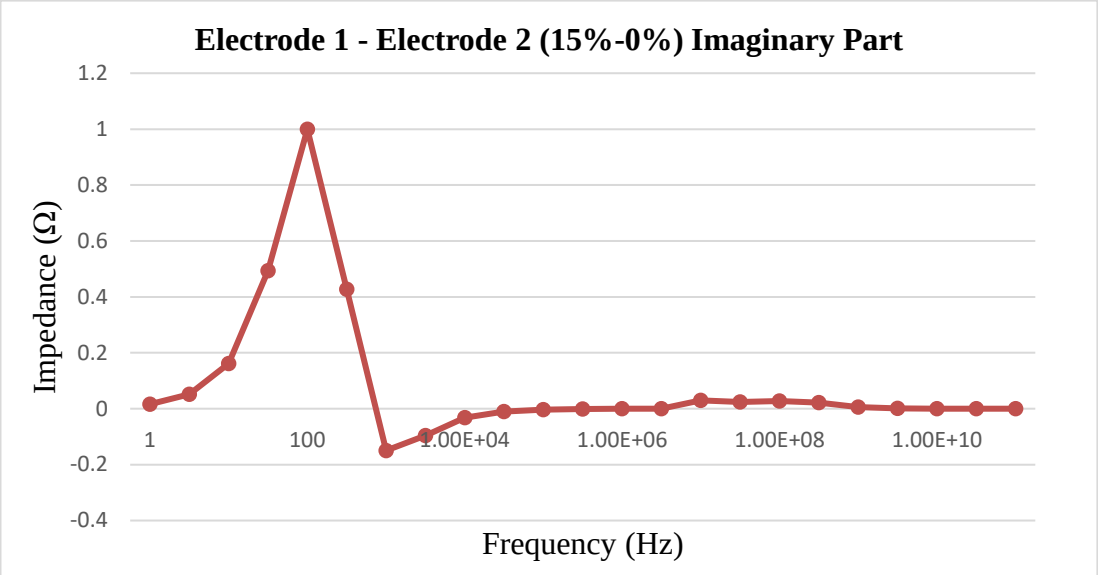

Figure 43. Difference in impedance imaginary part of electrode 1 and electrode 2 for pump andrest state

Figure 43 represents the difference in impedance of the imaginary part of electrode 1 and electrode 2 for the pumping and rest state. It is obtained by subtracting the data given in Figure 41 from the data of Figure 42. We can observe that the impedance rises as the frequency rises until it reaches the impedance highest point at 100 Hz, but after that, the impedance falls. Moreover, the impedance is close to zero at the frequency of 10 kHz, and it stays the same as the frequency rises.

4.2 Physical Implementation Result

In the practical implementation of MEIP, electrode 4 is used in the bottom position which acts as a ground, electrode 1 is placed in the top position while electrode 2 is in the side position. These electrodes are used for collecting data individually and the data for each is recorded. The configurations of these electrodes are taken to be Side-Bottom and Top-Bottom which indicates the connection from electrode 1 to 4 and 2 to 4. The data of each electrode is then measured by 2 frequencies 10kHz and 100Hz.

4.2.1 Using 100Hz Frequency

4.2.1.1 Applied Signal

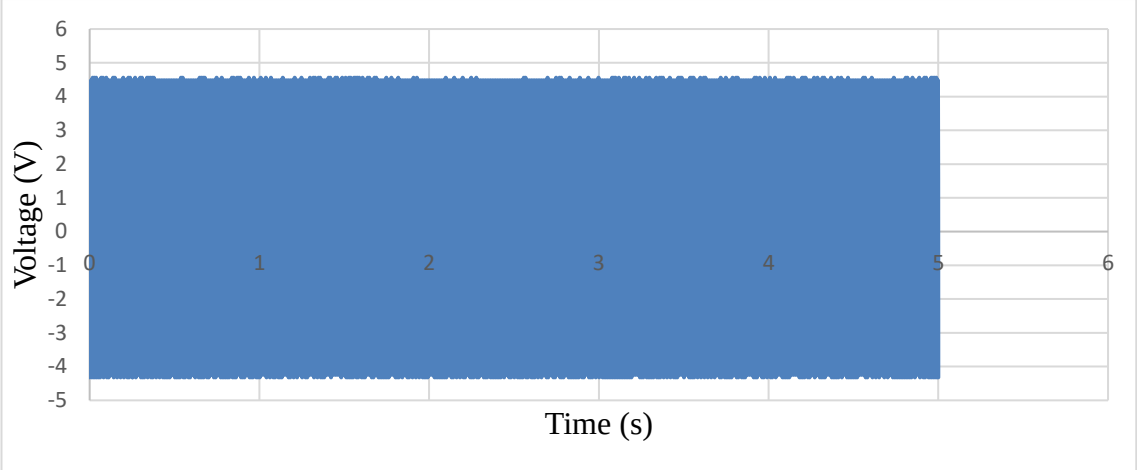

Figure 44. Input wave for 100Hz and 4.0Vpp

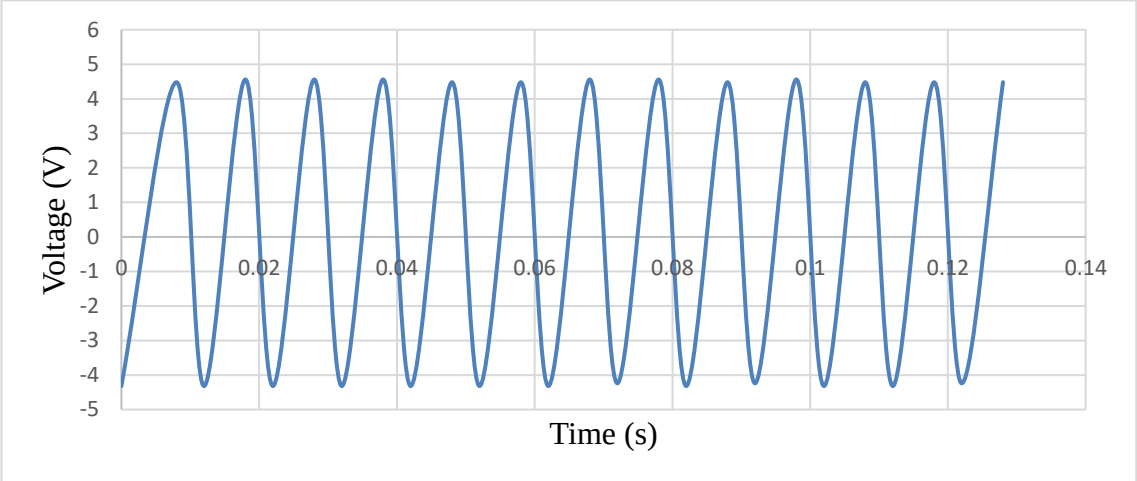

Figure 45. Input wave as above (expanded to show wave structure)

Figure 44 shows the input wave that is supplied to the experiment. As mentioned before, this wave is used as a back checker/feedback mechanism to ensure that the correct data is supplied in the experiment. Figure 45 is the expanded version of Figure 44 which allows us to observe the wave structure of the input wave and as can be seen, the wave is stable and following a regular pattern thus confirming that the data supplied in the experiment is correct.

4.2.1.2 Side Bottom Configuration Signal

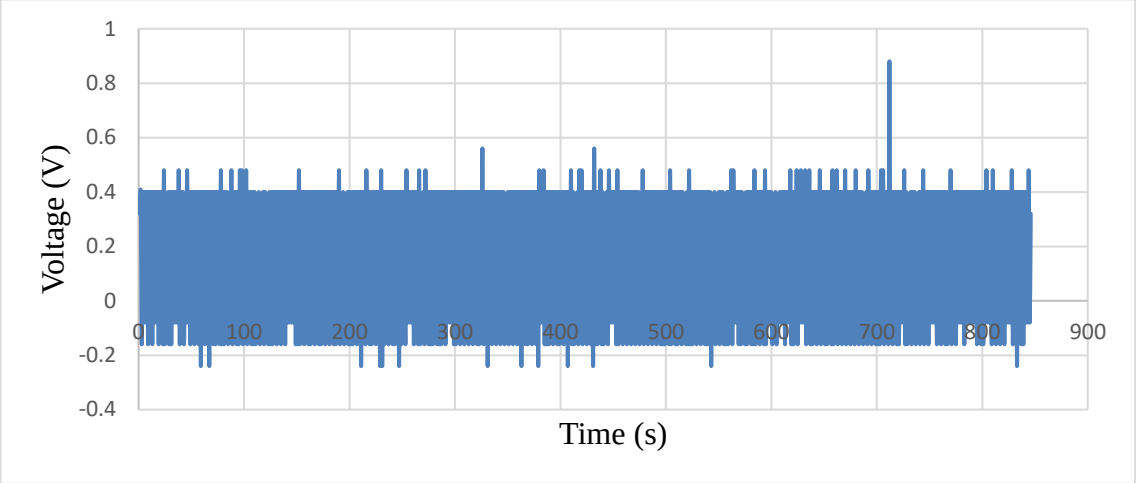

Figure 46. Voltage vs Time for oscilloscope 2 at 100Hz (Side-Bottom configuration)

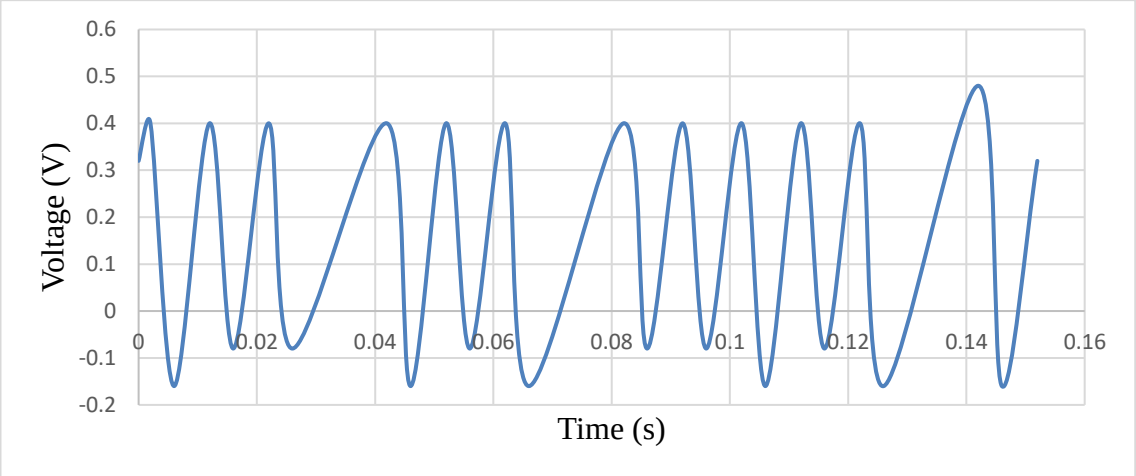

Figure 47. Voltage vs Time for oscilloscope 2 as above (expanded to show wave structure)

Figure 46 is a voltage-time graph for the side bottom configuration which shows the readings on oscilloscope 2. For this experiment, a 4.0 Vpp (peak to peak voltage) is applied and 100Hz frequency. Figure 47 is an expanded view of Figure 46 which shows that there are multiple wavespresent in the data. The voltage obtained is good along with the set frequency thereby indicating that a setup of 100Hz frequency and side-bottom configuration is successful. The time period is taken as 5s.

4.2.1.3 Top Bottom Configuration Signal

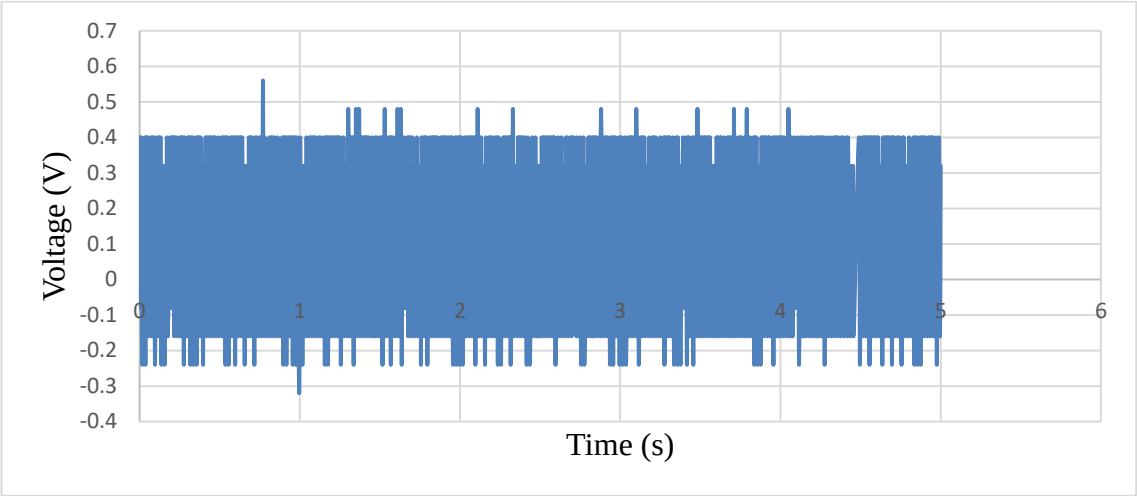

Figure 48. Voltage vs Time for oscilloscope 2 for 100Hz (Top-Bottom configuration)

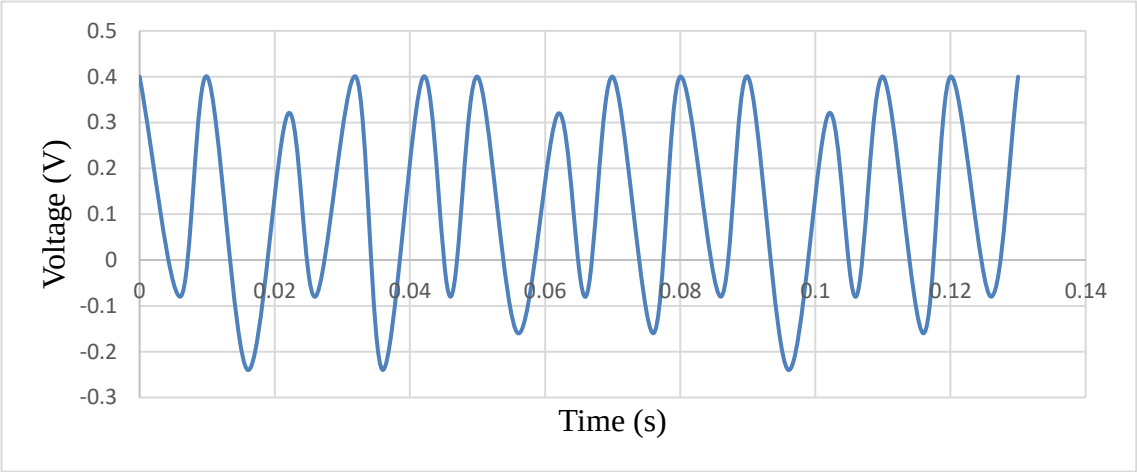

Figure 49. Voltage vs Time for oscilloscope 2 (expanded to show wave structure)

The measurements on oscilloscope 2 are displayed in Figure 48, which are plotted using voltage-time dimensions for the top-bottom setup. A 4.0 Vpp (peak to peak voltage) and a frequency of 100 Hz are used in this experiment. Figure 48 is an enlarged version of Figure 49, which demonstrates the presence of numerous waves in the data. A satisfactory setup for a 100Hz frequency and top-bottom layout is demonstrated by the excellent voltage achieved together with the chosen frequency and the time duration is 5 seconds.

4.2.2 Using 10KHz Frequency

4.2.2.1 Applied Signal

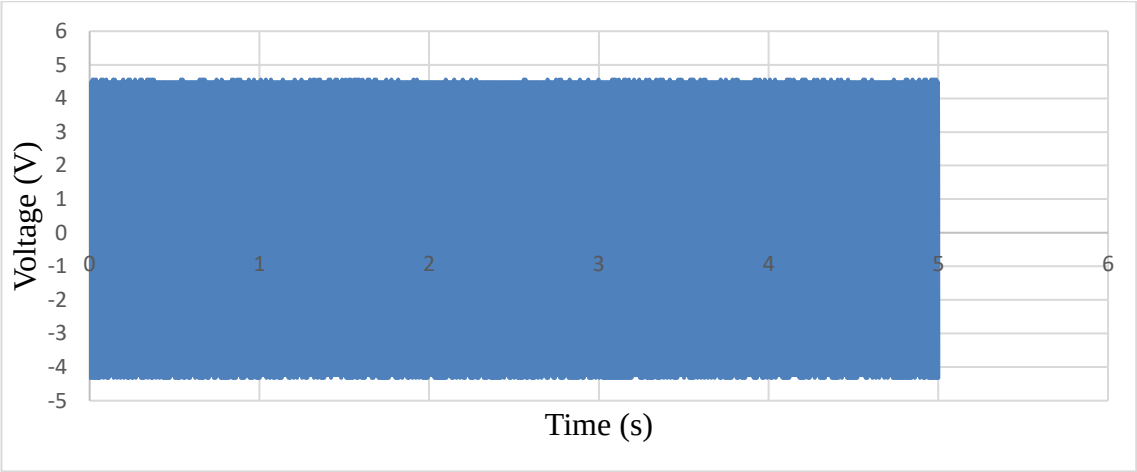

Figure 50. Input wave for 10kHz and 4.0Vpp

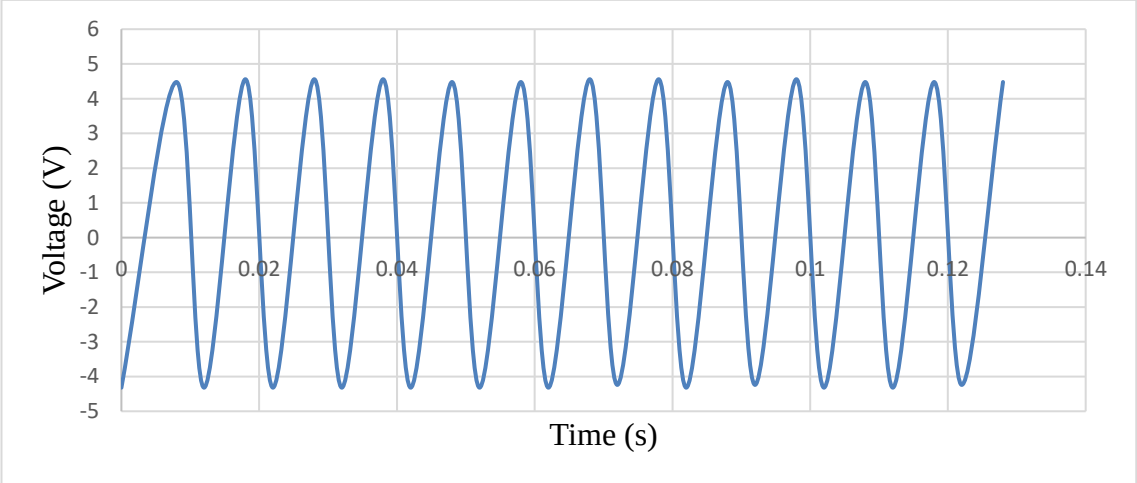

Figure 51. Input wave as above (expanded to show wave structure)

The experiment's input wave is seen in Figure 50. As previously noted, this wave serves as a feedback mechanism and back-checker to make sure the experiment receives the right data. The larger version of Figure 51 and 50, allows us to examine the input wave's structure. As can be observed, the wave is steady and follows a predictable pattern, verifying the accuracy of the experiment's results. In comparison to the state of the art described in the literature, a time period of 5 seconds is taken.

4.2.2.2 Side Bottom Configuration Signal

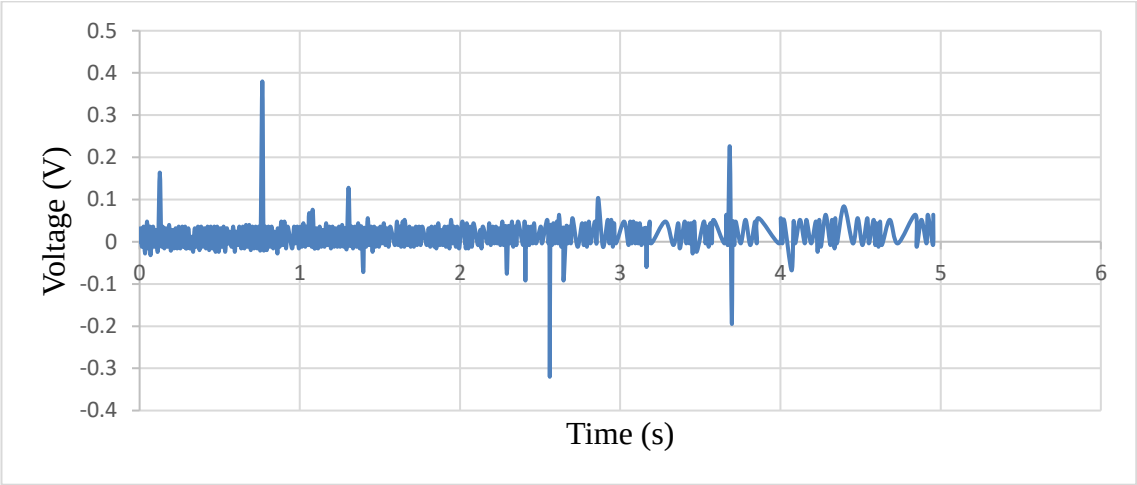

Figure 52. Voltage vs Time for oscilloscope 2 at 10kHz (Side-Bottom configuration)

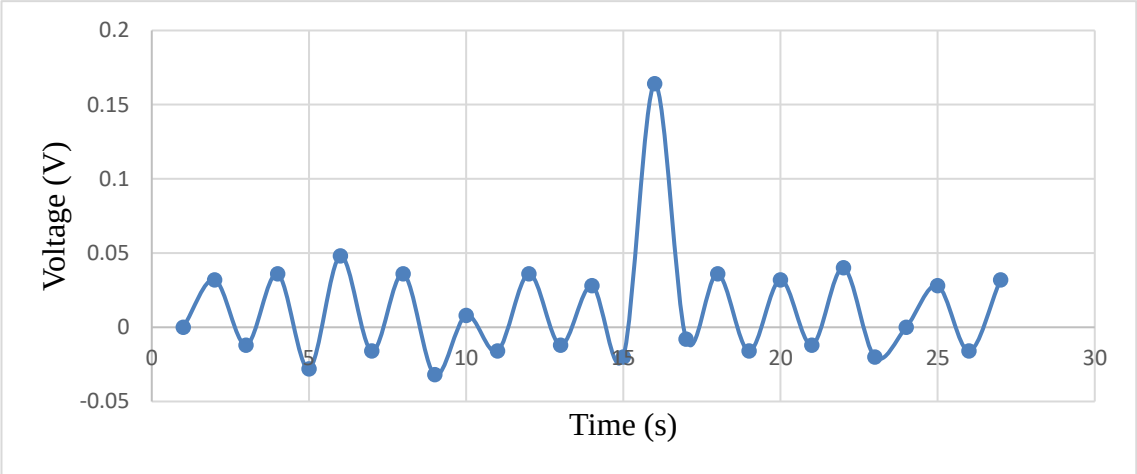

Figure 53. Voltage vs Time for oscilloscope 2 as above (expanded to show wave structure)

Figure 52 is a voltage-time for the side bottom configuration which shows the readings on oscilloscope 2. For this experiment, a 4.0 Vpp (peak to peak voltage) is applied and 10kHz frequency. Figure52 is an expanded view of Figure 53 which shows that there are multiple waves present in the data. The voltage obtained is not as per the required value thereby indicating that a setup of 10kHz frequency and side-bottom configuration is unsuccessful.

4.2.2.3 Top -Bottom Configuration Signal

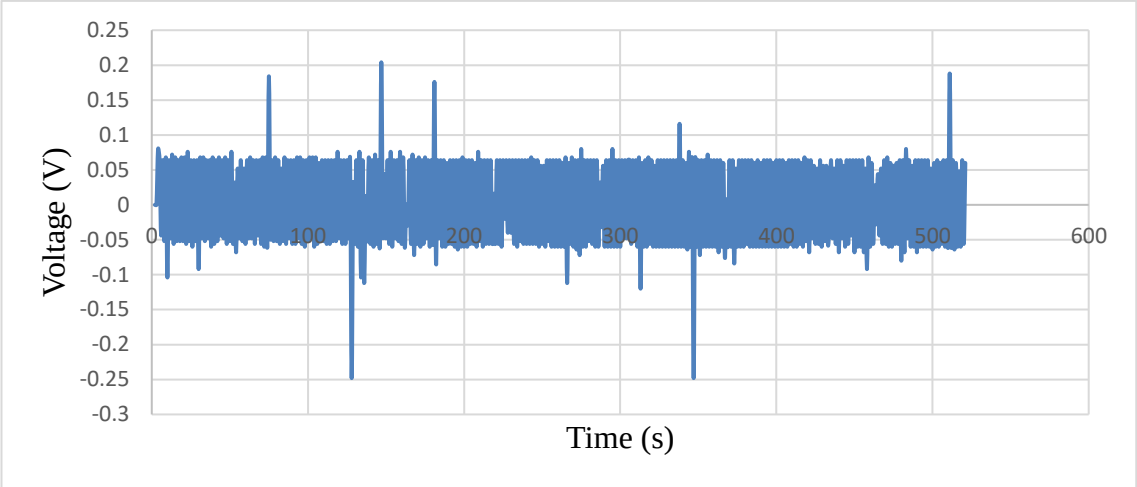

Figure 54. Voltage vs Time for oscilloscope 2 for 10kHz (Top-Bottom configuration)

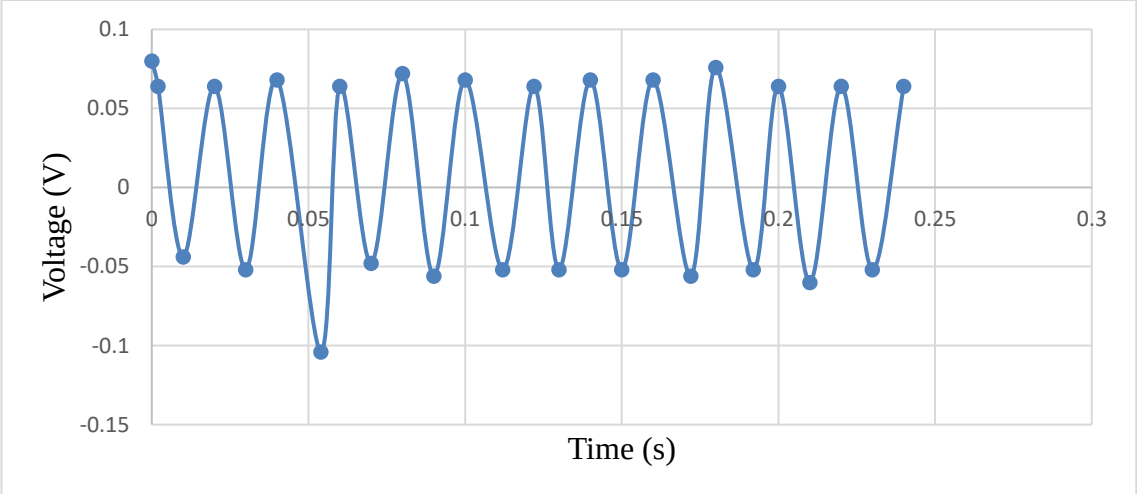

Figure 55. Voltage vs Time for oscilloscope 2 as above (expanded to show wave structure)

Figure 54 is a voltage-time for the top bottom configuration which shows the readings on oscilloscope 2. For this experiment, a 4.0 Vpp (voltage peak to peak) is applied and 10kHz frequency. Figure 54 is an expanded view of Figure 55 which shows that there are multiple waves present in the data.The voltage results presented so far does not clearly show a varying peak amplitude as a result of pulsatile blood flow due change in the impedance. It is believed that this is a direct result of very small changes in the finger impedance that are undetectable with the current setup. Accordingly, the peak voltage amplitude did not noticeably change as a result of voltage division rule. A dedicated impedance analyzer should be used in future tests to better reveal the variations in artery diameter.

5. CONCLUSION AND FUTURE WORK

5.1 Conclusion

In this study, we used the impedance plethysmography technique to find the impedance of a finger. In this technique, the electrical impedance of any part of the body is measured by either the constant current method or bridge method, and variations in the impedance are recorded as a function of time. Since blood is a conductor of electricity, the amount of blood in a given body segment is reflected inversely in the electrical impedance of the body segment. Pulsatile blood volume increase in the body segment caused by systemic blood circulation causes a proportional decrease in the electrical impedance. Variation in the electrical impedance thus yields adequate information about blood circulation. As a result of the increased pulsatile blood volume in the body segment induced by systemic blood circulation, the electrical impedance changes proportionally. The variation in electrical impedance thus provides sufficient information regarding blood circulation.

The study includes COMSOL simulation results compared with experimental results to obtain the optimum parameters for this technique. The COMSOL simulation uses 4 electrodes indifferent positions with a current of 10mA and frequencies up to 100 GHz. It was shown that multiple electrodes can be useful in obtaining impedance change. It is useful because signals cannot be obtained from one pair, or to further support the results. The study was performed under normal resting conditions where an experimental procedure was set up to measure the impedance response from the finger. The framework of the implementation of MEIP is completed in which we have constructed a 2D model of a finger encompassed by silver electrodes in COMSOL simulation environment to measure the impedance at different positions of the finger. The study was performed under normal resting conditions where an experimental procedure was set up to measure the impedance response from the finger. Electrocardiograph (ECG) electrodes are utilized in the proposed design for measuring the impedance in response to provided current.

The finger-simplified model was created in model geometry. A framework made up of five parts was used to build the finger. Figure 3.4 illustrates the finger's overall diameter which is 15.5 mm. A variety of tissue layers make up this model (i.e., skin, fat, artery, muscle, and bone).With a total thickness of 1.5 mm, the skin layer is made up of the dermis and epidermis. Under the epidermis, there is a layer of fat with a thickness of 2.5 mm, followed by a layer of muscle that is 4 mm thick and circulated around a layer of bone that is 7.5 mm thick. Two arteries, the radial, and ulnar arteries are present in the finger, and they supply the tissues with oxygenated blood and nutrients. The two arteries were placed parallel to one another with 9.5 mm spacing beneath the skin, hidden within the fat layer, on two sides of the model in order to simplify the anatomical arrangement.

In the physical experiment, we took the reading at different frequencies (100Hz, 10KHz) with different positions of electrodes top-side and then side-bottom. In the physical experiment we used 3 electrodes, the position of electrodes are side, bottom, and top. The frequencies used are 100Hz and 10kHz with a combination of a 1Mohm

resistance. Figure 4.2.4 represents the difference in impedance of imaginary electrode 1 and imaginary electrode 2 for pump and rest state. It is obtained by subtracting the data of Figure 4.2.2 from the data of Figure 4.2.3. Figure 4.2.4 documents the final data received from the simulation and serves to show the performance of the proposed technique is maximum at 100Hz and 4.0 V.

5.2 Future Work

Although the simulations showed that multiple electrode IPG can reveal more and usable signals about blood flow, the experiments were not conclusive due to the need for an impedance analyzer for more sensitive measurements. The future work will focus on repeating the characterization with an impedance analyzer once obtained, and on the application of this technique on diabetic patients to constantly monitor the blood flow through their body limbs.

REFERENCES

Articles

Álvarez, C., Lucia, A., Ramírez-Campillo, R., Martínez-Salazar, C., Delgado-Floody, P., Cadore, E. L., Alonso-Martínez, A. M., & Izquierdo, M. (2019). Low sleep time is associated with higher levels of blood pressure and fat mass in Amerindian schoolchildren. American Journal of Human Biology, 31(6), 1–11. Retrieved from https://doi.org/10.1002/ajhb.23303.

Alabdali, L. A. S., Jaeken, J., Dinant, G.-J., van den Akker, M., Winkens, B., & Ottenheijm, R. P. G. (2021). Prevalence of Upper Extremity Musculoskeletal Disorders in Patients withType 2 Diabetes in General Practice MDPI Medicines, 8(2), 8. Retrieved from https://doi.org/10.3390/medicines8020008.

Arai, M., Takeuchi, T., & Ueno, A. (2021). Cuffless continuous estimation of relative mean arterial pressure using unrestrained and noncontact ballistocardiogram and electrocardiogram: Evaluation in short time in-bed experiments. Advanced Biomedical Engineering, 10, 36–50. Retrieved from https://doi.org/10.14326/abe.10.36.

Babu, C. G., Kumar, R. S., Engineeeing, C., Krishna, S., Engineeeing, C., Engineeeing, C., Engineeeing, C., & Engineeeing, C. (2021). Determination of Cardiac Output based on Minimally Invasive Impedance Plethysmography in Various Healthy Subjects. (Vol 12, Issue 03, 2021).

Babu, J. P., Jindal, G. D., Bhuta, A. C., & Parulkar, G. B. (1990). Impedance plethysmography:basic principles. In Journal of postgraduate medicine (Vol. 36, Issue 2, pp. 57–63).

Baek, H. J., Shin, J. W., Jin, G., & Cho, J. (2017). Reliability of the Parabola ApproximationMethod in Heart Rate Variability Analysis Using Low-Sampling-Rate Photoplethysmography. Journal of Medical Systems, 41(12). Retrieved from https://doi.org/10.1007/s10916-017-0842-0.

Bejarano Monroy, M. G. (2019). A novel approach to bioelectrical impedance plethysmography for the assessment of arterial and venous circulatory problems in the forearm.

Bera, T. K. (2014). Bioelectrical Impedance Methods for Noninvasive Health Monitoring: A Review. Journal of Medical Engineering, 2014, 1–28. Retrieved from https://doi.org/10.1155/2014/381251.

Boonya-ananta, T., Rodriguez, A. J., Ajmal, A., Du Le, V. N., Hansen, A. K., Hutcheson, J. D., & Ramella-Roman, J. C. (2021). Synthetic photoplethysmography (PPG) of the radial artery through parallelized Monte Carlo and its correlation to body mass index (BMI).

Scientific Reports, 11(1), 1–11. Retrieved from https://doi.org/10.1038/s41598-021-82124-4.

Boukhechba, M., Cai, L., Wu, C., & Barnes, L. E. (2019). ActiPPG: Using deep neural networks for activity recognition from wrist-worn photoplethysmography (PPG) sensors. Smart Health, 14(November), 100082. Retrieved from https://doi.org/10.1016/j.smhl.2019.100082.

Chan, E. D., Chan, M. M., & Chan, M. M. (2013). Pulse oximetry: Understanding its basic principles facilitates appreciation of its limitations. In Respiratory Medicine (Vol. 107, Issue 6, pp. 789–799). Retrieved from https://doi.org/10.1016/j.rmed.2013.02.004.

C. Corciova, R. Ciorap, D. M. and A. S. (2012). 5th European Conference of the International Federation for Medical and Biological Engineering. 37(January). Retrieved from https://doi.org/10.1007/978-3-642-23508-5.

Corciova, C., Ciorap, R., Zaharia, D., & Matei, D. (2011). Hemodynamic monitoring using peripheral impedance plethysmography. 2011 7th International Symposium on AdvancedTopics in Electrical Engineering, ATEE 2011, I, 0–3.

Corciova, C., Ciorap, R., Zaharia, D., & Matei, D. (2011). On using impedance plethysmography for estimation of blood flow. MeMeA 2011 - 2011 IEEE International Symposium on Medical Measurements and Applications, Proceedings, May, 84–87. Retrieved from https://doi.org/10.1109/MeMeA.2011.5966672.

Corciovă, C., Turnea, M., & Sălceanu, A. (2011). A measurement system for the blood flow inperipheral territory. 2011 E-Health and Bioengineering Conference, EHB 2011, 4, 24–27.

De Pinho Ferreira, N., Gehin, C., & Massot, B. (2021). A Review of Methods for Non-Invasive Heart Rate Measurement on Wrist. Irbm, 42(1), 4–18. Retrieved from https://doi.org/10.1016/j.irbm.2020.04.001.

Dilley, A., Greening, J., Lynn, B., Leary, R., & Morris, V. (2001). The use of cross-correlation analysis between high-frequency ultrasound images to measure longitudinal median nerve movement. Ultrasound in Medicine and Biology, 27(9), 1211–1218. Retrieved from https://doi.org/10.1016/S0301-5629(01)00413-6.

Eerikäinen, L. M., Bonomi, A. G., Dekker, L. R. C., Vullings, R., & Aarts, R. M. (2020). Atrial fibrillation monitoring with wrist-worn photoplethysmography-based wearables: State-of- the-art review. Cardiovascular Digital Health Journal, 1(1), 45–51. Retrieved from https://doi.org/10.1016/j.cvdhj.2020.03.001.

Elgendi, M., Fletcher, R., Liang, Y., Howard, N., Lovell, N. H., Abbott, D., Lim, K., & Ward, R. (2019). The use of photoplethysmography for assessing hypertension. Npj Digital Medicine, 2(1), 1–11. Retrieved from https://doi.org/10.1038/s41746-019-0136-7.

Gautam Anand 1, and A. L. (2020). Investigating Electrical Impedance Spectroscopy

for Estimating Blood Flow-Induced Variations in Human Forearm, Retrieved from doi:10.3390/s20185333.

Hersek, S., Töreyin, H., & Inan, O. T. (2016). A Robust System for Longitudinal Knee Joint Edema and Blood Flow Assessment Based on Vector Bioimpedance Measurements. IEEE Transactions on Biomedical Circuits and Systems, 10(3), 545–555. Retrieved from https://doi.org/10.1109/TBCAS.2015.2487300.

Hosanee, M., Chan, G., Welykholowa, K., Cooper, R., Kyriacou, P. A., Zheng, D., Allen, J., Abbott, D., Menon, C., Lovell, N. H., Howard, N., Chan, W. S., Lim, K., Fletcher, R., Ward, R., & Elgendi, M. (2020). Cuffless single-site photoplethysmography for blood pressure monitoring. Journal of Clinical Medicine, 9(3). Retrieved from https://doi.org/10.3390/jcm9030723.

Huang, J.-J., Huang, Y.-M., & See, A. R. (2017). Studying Peripheral Vascular Pulse WaveVelocity Using Bio-impedance Plethysmography and Regression Analysis. ECTI Transactions on Computer and Information Technology (ECTI-CIT), 11(1), 63–70. Retrieved from https://doi.org/10.37936/ecti-cit.2017111.64861.

Huynh, T. H., & Chung, W.-Y. (2017). Radial Electrical Impedance: A Potential Indicator for Noninvasive Cuffless Blood Pressure Measurement. Journal of Sensor Science and Technology, 26(4), 2093–7563. Retrieved from https://doi.org/10.5369/JSST.2017.26.4.239.

Johannes Schneider, Marc Schroth, Maik Holzhey, Blöcher, Timon, W. S. (2019). Feedback control. Advances in Industrial Control, 115–141. Retrieved from https://doi.org/10.1007/978-981-13- 5770-1_7.

Kamshilin, A. A., & Margaryants, N. B. (2017). Origin of Photoplethysmographic Waveform at Green Light. Physics Procedia, 86(June 2015), 72–80. Retrieved from https://doi.org/10.1016/j.phpro.2017.01.024.

Kumar, S., Buckley, J. L., Barton, J., Pigeon, M., Newberry, R., Rodencal, M., Hajzeraj, A., Hannon, T., Rogers, K., Casey, D., O'sullivan, D., & O'flynn, B. (2020). A wristwatch- based wireless sensor platform for IoT health monitoring applications. Sensors (Switzerland), 20(6), 1–25. Retrieved from https://doi.org/10.3390/s20061675.

Lee, C., Sik Shin, H., & Lee, M. (2011). Relations between ac-dc components and optical path length in photoplethysmography. Journal of Biomedical Optics, 16(7), 077012. Retrieved from https://doi.org/10.1117/1.3600769.

Li, Y., Chen, X., Zhang, Y., & Deng, N. (2016). Noninvasive continuous blood pressure estimation with peripheral pulse transit time. Proceedings - 2016 IEEE Biomedical Circuits and Systems Conference, BioCAS 2016, 66–69. Retrieved from https://doi.org/10.1109/BioCAS.2016.7833726.

Jasaitiene, D., Valiukeviciene, S., Linkeviciute, G., Raisutis, R., Jasiuniene, E., & Kazys, R. (2011). Principles of high-frequency ultrasonography for investigation

of skin pathology. Journal of the European Academy of Dermatology and Venereology, 25(4), 375–382. Retrieved from https://doi.org/10.1111/j.1468-3083.2010.03837.x.

Le, T., Ellington, F., Lee, T. Y., Vo, K., Khine, M., Krishnan, S. K., Dutt, N., & Cao, H. (2020). Continuous Non-Invasive Blood Pressure Monitoring: A Methodological Review on Measurement Techniques. IEEE Access, 8, 212478–212498. Retrieved from https://doi.org/10.1109/ACCESS.2020.3040257.

Long, N. M. H., & Chung, W. Y. (2022). Wearable Wrist Photoplethysmography for Optimal Monitoring of Vital Signs: A Unified Perspective on Pulse Waveforms. IEEE Photonics Journal, 14(2). Retrieved from https://doi.org/10.1109/JPHOT.2022.3153506.

Martuzzi, R., van der Zwaag, W., Farthouat, J., Gruetter, R., & Blanke, O. (2014). Human finger somatotopy in areas 3b, 1, and 2: A 7T fMRI study using a natural stimulus. Human Brain Mapping, 35(1), 213–226. Retrieved from https://doi.org/10.1002/hbm.22172.

Mašanauskiene, E., Sadauskas, S., Naudžiunas, A., Unikauskas, A., & Stankevičius, E. (2014).Impedance plethysmography as an alternative method for the diagnosis of peripheral arterial disease. Medicina (Lithuania), 50(6), 334–339. Retrieved from https://doi.org/10.1016/j.medici.2014.11.007.

Mejía-Mejía, E., Allen, J., Budidha, K., El-Hajj, C., Kyriacou, P. A., & Charlton, P. H. (2021).Photoplethysmography signal processing and synthesis. In Photoplethysmography: Technology, Signal Analysis and Applications. Retrieved from https://doi.org/10.1016/B978-0-12-823374-0.00015-3.

Morales, I., & Gonz, R. (2015). Force sensing resistors used as plantar impedance plethysmography electrodes. 14(8), 1–7. Retrieved from https:// doi.org/10.1109/TIM.2022.3178961.

Morales, I., Gonzalez-Landaeta, R., & Simini, F. (2021). Pressure sensors used as bioimpedance plantar electrodes: A feasibility study. 2021 IEEE International Symposium on Medical Measurements and Applications, MeMeA 2021 - Conference Proceedings, 8–13. Retrieved from https://doi.org/10.1109/MeMeA52024.2021.9478682.

Morales, I., González-Landaeta, R., & Simini, F. (2021). Bioimpedance plethysmography with capacitive electrodes and sole force sensors: Comparative trial. Journal of Physics: Conference Series, 2008(1). Retrieved from https://doi.org/10.1088/1742-6596/2008/1/012018.

Paliakaite, B., Charlton, P. H., Rapalis, A., Plusciauskaite, V., Piartli, P., Kaniusas, E., & Marozas, V. (2021). Blood Pressure Estimation Based on Photoplethysmography: Finger Versus Wrist. Computing in Cardiology, 2021-Septe, 10–13. Retrieved from https://doi.org/10.23919/CinC53138.2021.9662716.

Piuzzi, E., Pisa, S., Pittella, E., Podestà, L., & Sangiovanni, S. (2020). Wearable belt with built- in textile electrodes for cardio—respiratory monitoring. Sensors (Switzerland), 20(16), 1– 15. Retrieved from https://doi.org/10.3390/s20164500.

Premkumar, S., & Hemanth, D. J. (2022). Intelligent Remote Photoplethysmography-Based Methods for Heart Rate Estimation from Face Videos: A Survey. Informatics, 9(3). Retrieved from https://doi.org/10.3390/informatics9030057.

Ram Kumar, M., & Ganesh Babu, C. (2019). Statistical Analysis for Non Invasive Assessment of Blood Flow Volume in the High Pressure and Low Pressure Subjects Using IPG Technique and the Stroke Volume Estimation. Proceedings of the 2019 International Conference on Advances in Computing and Communication Engineering, ICACCE 2019. Retrieved from https://doi.org/10.1109/ICACCE46606.2019.9079989.

Ramkumar, M., & Babu, C. G. (2017). A Comprehensive Analysis of Forearm Impedance Plethysmography for the Maximally Non Invasive Monitoring and Measurement of Heart Pumping Function. SSRN Electronic Journal, 1(2), 178–184. Retrieved from https://doi.org/10.2139/ssrn.2942416.

Samarawickrama, K. G., Perera, N. D., Jayasinghe, S., & De Silva, A. C. (2020). Impedance Plethysmography as an Alternative Measure of Reactive Hyperemia. Proceedings of the Annual International Conference of the IEEE Engineering in Medicine and Biology Society, EMBS, 2020-July(c), 828–831. Retrieved from https://doi.org/10.1109/EMBC44109.2020.9175899.

Sjoding, M. W., Dickson, R. P., Iwashyna, T. J., Gay, S. E., & Valley, T. S. (2020). Racial Bias in Pulse Oximetry Measurement. New England Journal of Medicine, 383(25), 2477–2478.Retrieved from https://doi.org/10.1056/nejmc2029240.

Spigulis, J., Gailite, L., Lihachev, A., & Erts, R. (2007). Simultaneous recording of skin blood pulsations at different vascular depths by multiwavelength photoplethysmography. Applied Optics, 46(10), 1754–1759. Retrieved from https://doi.org/10.1364/AO.46.001754.

Sun, Y., Sobel, E. S., & Jiang, H. (2011). First assessment of three-dimensional quantitative photoacoustic tomography for in vivo detection of osteoarthritis in the finger joints. Medical Physics, 38(7), 4009–4017. Retrieved from https://doi.org/10.1118/1.3598113.

Tahmasebpour, H. R., Buckley, A. R., Cooperberg, P. L., & Fix, C. H. (2005). Sonographic examination of the carotid arteries. In Radiographics (Vol. 25, Issue 6, pp. 1561–1575). Retrieved fromhttps://doi.org/10.1148/rg.256045013.

Wang, F., Jin, P., Feng, Y., Fu, J., Wang, P., Liu, X., Zhang, Y., Ma, Y., Yang, Y., Yang, A., & Feng, X. (2021). Flexible Doppler ultrasound device for the monitoring of blood flow velocity. Science Advances, 7(44), 1–11. Retrieved from https://doi.org/10.1126/sciadv.abi9283.

Wang, T. W., Chu, H. W., Chou, L., Sung, Y. L., Shih, Y. T., Hsu, P. C., Cheng, H. M., & Lin, S. F. (2021). Bio-impedance measurement optimization for high-resolution carotid pulse sensing. Sensors, 21(5), 1–13. Retrieved from https://doi.org/10.3390/s21051600.

Book

Ansari, S. (2013). Motion artifact reduction in impedance plethysmography signal. ProQuest Dissertations and Theses, 116. Retrieved from https://manchester.idm.oclc.org/login?url=https://search.proquest.com/docview/150146950 0?accountid=12253%0Ahttp://man-fe.hosted.exlibrisgroup.com/openurl/44MAN/44MAN_services_page?genre=dissertations+%26+theses&atitle=&author=Ansari%2C+Sardar&volume=&issu.

World Health Organization. (2016). Global Report on Diabetes. Isbn, 978, 88. Retrieved from https://doi.org/ISBN 978 92 4 156525 7.

Website

Atkielski, A. (2007). Electrocardiography - Wikipedia. Retrieved from https://en.wikipedia.org/wiki/Electrocardiography.

Dias, G. R. (2018, March 9)A Study on Sphygmomanometers _ LinkedIn. (n.d.). Retrieved from https://www.linkedin.com/pulse/study-sphygmomanometers-gaston-ravin-dias/.

Aneroid Vérnyomásmérő és Sztetoszkópkészlet Egészségügyi Kézi Otthoni VérnyomásmérőSzéria Mandzsetta és Sztetoszkóp. Wish. (n.d.). Retrieved from https://www.wish.com/hu/product/aneroid- sphygmomanometer-and-stethoscope-kit- health-manual-home-blood-pressure-monitor-with-standard-cuff-and-stethoscope- 5b6d078d59b5a176f643f010?share=web.

U.S. National Library of Medicine. (n.d.). Blood pressure check_ MedlinePlus Medical Encyclopedia Image. (n.d.). Retrieved from https://medlineplus.gov/ency/imagepages/19255.htm.

Buy Saint Health Arm Automatic Blood Pressure Monitor BP Sphygmomanometer Pressure Meter Tonometer for Measuring Arterial Pressure at affordable prices — free shipping, real reviews wi. (n.d.), Retrieved from https://www.modernheartandvascular.com/conditions- we-help-with/.

Shepes, F. (2016, May 13). Doppler Ultrasound _ The Fresh Foot Centre. (n.d.). Retrieved from https://thefreshfootcentre.com.au/service/doppler-ultrasound/.

Electrocardiogram - Modern Heart and Vascular. (n.d.). Retrieved from https://www.modernheartandvascular.com/electrocardiogram/.

Electrocardiogram | Johns Hopkins Medicine. (2021). In John Hopkins Medicine.

Retrieved from https://www.hopkinsmedicine.org/health/treatment-tests-and-therapies/electrocardiogram.

Griesmer, A. (2013). What Is COMSOL Multiphysics? In Comsol.Com. Retrieved from https://www.comsol.com/blogs/what-is-comsol-multiphysics/.

Griesmer, F. (2019). 10 Real Uses of COMSOL Multiphysics® in the Power Industry | COMSOL Blog. Retrieved from https://www.comsol.com/blogs/10-real-uses-of-comsol-multiphysics-in-the-power-industry.

Holter monitor - Wikipedia. (n.d.). Retrieved from https://en.wikipedia.org/wiki/Holter_monitor.

Holter monitoring of blood pressure _ Medicum. (n.d.). Retrieved December 23,2022, from https://www.medicum.ee/en/uuring/funktsionaaldiagnostilised-uuringud/vererohu-holter-monitooring/.

Impedance Plethysmography (IPG) - medis. (n.d.). Retrieved from https://www.medis.company/en/methods/impedance-plethysmography.

Johns Hopkins Medicine. (2019). Holter Monitor | Johns Hopkins Medicine. In The Johns Hopkins University, The Johns Hopkins Hospital, and Johns Hopkins Health System. Retrieved from https://www.hopkinsmedicine.org/health/treatment-tests-and- therapies/holter-monitor

Kuwabara, K., Higuchi, Y., Koizumi, H., & Kasahara, R. (2015). Blood flow observed with smartphone-ultracompact wearable blood flow sensor. NTT Technical Review, 13(1).

Levy, J. (2018). Plethysmography: MedlinePlus Medical Encyclopedia. Retrieved from https://medlineplus.gov/ency/article/003771.htm.

M.Sc. Cheriyedath, S. (2019). Photoplethysmography (PPG). In News Medical.

Retrieved from https://www.news-medical.net/health/Photoplethysmography-(PPG).aspx.

Model, T, & Dialog, B. (n.d.). The Model Builder Dialog Box ? Retrieved from https://doc.comsol.com/5.5/doc/com.comsol.help.comsol/comsol_ref_modeling.10.03.html.

New research backs use of pulse oximeters for assessing blood pressure - UBC Faculty of Medicine. (n.d.). Retrieved from https://www.med.ubc.ca/news/new-research-backs-use-of-pulse- oximeters-for-assessing-blood-pressure/.

Reader, R. (2022). Apple partner is developing a wearable to track blood sugar. In Fast Company. Retrieved from https://www.fastcompany.com/90730050/apple-

partner-rockley-photonics-blood-sugar.

Settings and Properties Windows for Feature Nodes. (n.d.). Retrieved from https://doc.comsol.com/5.5/doc/com.comsol.help.comsol/comsol_ref_modeling.10. 09.html.

Shrivastava, S. (2019). I-STEM-COMSOL Multiphysics. In Indian Science Technology and Engineering facilities Map. Retrieved from https://wwSSw.istem.gov.in/istem-comsol.

SPO2 Finger Pulse Oximeter fom a reputed online medical supply store _ HealthConnection. (n.d.). Retrieved from https://www.anactivelife.com/SPO2-Finger-Pulse-Oximeter-p/spo2-finger-pulse-oximeter.htm.

The Graphics Window. (n.d.). Retrieved from https://doc.comsol.com/5.5/doc/com.comsol.help.comsol/comsol_ref_visualizationselection.13.11.html#1201001.

Shrager, L. (2021, The importance of monitoring your blood pressure readings at home

- Sun Sentinel. (n.d.). Retrieved from https://www.sun-sentinel.com/health/fl-xpm-2009-10-13-sfl-blood-pressure-readings-101209-story.html.

Tissue Frequency Chart » IT'IS Foundation. (n.d.). Retrieved from https://itis.swiss/virtual-population/tissue-properties/database/tissue-frequency-chart/.

USA Medical and Surgical Supplies. (2018). EKG Machine and ECG Machine Buyer's Guide For Medical Professionals - USA Medical and Surgical Supplies. Retrieved from https://www.usamedicalsurgical.com/blog/ekg-ecg-machine-buyers-guide/.

Wearable Compact Blood Flow Sensor _ MEMS_Microfabricated Products _ NTT-AT Advanced Technology Product Introduction Site. (n.d.) Retrieved from https://keytech.ntt-at.co.jp/en/nano/prd_0050.html.

Why you need to check your blood pressure regularly - TODAY. (n.d.). Retrieved from https://www.today.com/health/why-you-need-check-your-blood-pressure-regularly-today-t235102.